POCKET ROCKET: A 1U+ PROPULSION SYSTEM DESIGN TO ENHANCE CUBESAT CAPABILITIES

A Thesis

presented to

the Faculty of California Polytechnic State University,

San Luis Obispo

In Partial Fulfillment

of the Requirements for the Degree

Master of Science in Aerospace Engineering

by

James M. Harper

June 2020

COMMITTEE MEMBERSHIP

TITLE: Pocket Rocket: A 1U+ Propulsion System Design to Enhance CubeSat Capabilities

AUTHOR: James Michael Harper

DATE SUBMITTED: June 2020

COMMITTEE CHAIR: Pauline Faure, Ph.D.
Assistant Professor of Aerospace Engineering

COMMITTEE MEMBER: Kira Abercromby, Ph.D.
Professor of Aerospace Engineering

COMMITTEE MEMBER: William C. Saucier
Lecturer, Aerospace Engineering Department

COMMITTEE MEMBER: Amelia Greig, Ph.D
The University of Texas at El Paso
Assistant Professor of Mechanical Engineering

COMMITTEE MEMBER: Jacob Fisher, Ph. D.
Aerojet Rocketdyne, Redmond, Washington
Principal Thermal Engineer

ABSTRACT

Pocket Rocket: A 1U+ Propulsion System Design

to Enhance CubeSat Capabilities

James M. Harper

The research presented provides an overview of a 1U+ form factor propulsion system design developed for the Cal Poly CubeSat Laboratory (CPCL). This design utilizes a Radiofrequency Electrothermal Thruster (RFET) called Pocket Rocket that can generate 9.30 m/s of delta-V with argon, and 20.2 ± 3 m/s of delta-V with xenon. Due to the demand for advanced mission capabilities in the CubeSat form factor, a need for micro-propulsion systems that can generate between 1 – 1500 m/s of delta-V are necessary.

By 2019, Pocket Rocket had been developed to a Technology Readiness Level (TRL) of 5 and ground tested in a 1U CubeSat form factor that incorporated propellant storage, pressure regulation, RF power and thruster control, as well as two Pocket Rocket thrusters under vacuum, and showcased a thrust of 2.4 mN at a required 10 Wdc of power with Argon propellant. The design focused on ground testing of the thruster and did not incorporate all necessary components for operation of the thruster. Therefore in 2020, a 1U+ Propulsion Module that incorporates Pocket Rocket, the RF amplification PCB, a propellant tank, propellant regulation and delivery, as well as a DC-RF conversion with a PIB, that are all attached to a 2U customer CubeSat for a 3U+ overall form factor. This design was created to increase the TRL level of Pocket Rocket from 5 to 8 by demonstrating drag compensation in a 400 km orbit with a delta-V of 20 ± 3 m/s in the flight configuration. The 1U+ Propulsion Module design included interface and requirements definition, assembly instructions, Concept of Operations (ConOps), as well as structural and thermal analysis of the system. The 1U+ design enhances the capabilities of Pocket Rocket in a 1U+ form factor propulsion system and increases future mission capabilities as well as propulsion system heritage for the CPCL.

Keywords: Micro-propulsion, Small Satellites, Space Environment, CubeSat Design Specification

ACKNOWLEDGMENTS

I would like to start off by thanking my parents, Michael, and Rina. Their unconditional support and love has allowed me to pursue my passions and achieve my goals throughout my life. Thank you both so much for everything, I would not be the same person I am today without the lessons you have taught me and I consider myself lucky to have you as parents and role models.

To Dr. Pauline Faure, I cannot thank you enough for the support you have given me throughout my thesis. You have provided me with an innumerable amount of helpful and knowledgeable advice that will only help me in my future endeavors and career.

Finally, thank you to all my committee members for all the guidance and support with my project. The help you provided along the way has been incredibly helpful in accomplishing this project.

TABLE OF CONTENTS

LIST OF TABLES

Table Page

LIST OF FIGURES

Figure Page

LIST OF NOMENCLATURE

Acronyms

ADCS = Attitude Determination and Control System

AFSPCMAN 91-710 = Air Force Space Command Manual 91-710

ANU = The Australian National University

C&DH = Command and Date Handling

CHIPS = CubeSat High Impulse Propulsion Systems

ConOps = Concept of Operations

CPCL = Cal Poly CubeSat Laboratory

CSLI = CubeSat Launch Initiative

EB = Electron Beam

FCC = Federal Communications Commission

FD = Finite Difference

GEVS = General Environmental Verification Standards

GIT = Georgia Institute of Technology

IME = Industrial and Manufacturing Engineering

ISP = Specific Impulse

ISS = International Space Station

LEO = Low Earth Orbit

MCD = Microcavity Discharge

ME = Mechanical Engineering

MEMS = Micro Electromechanical Systems

MEOP = Maximum Expected Operating Pressure

MET = Microwave Electrothermal Thrusters

MLI = Multi-Layer Insulation

NIST = National Institute of Standards and Technology

PCB = Printed Circuit Board

PIB = Payload Interface Board

PID = Piping and Instrumentation Diagram

PSU = Pennsylvania State University

PUC = Propulsion Unit for CubeSats

RF = Radio Frequency

RFET = Radiofrequency Electrothermal Thruster

SLM = Selective Laser Melting

SmallSat = Small Spacecraft

TEC = Thermal Electric Cooler

TIG = Tungsten Inert Gas

USD = United States Dollars

Symbols

- ΔV = Delta-V
- ISP = Specific Impulse
- g = Gravity
- m_0 = Initial Mass
- m_f = Final Mass
- m_{prop} = Mass of Propellant
- I_t = Total Impulse
- f_{inert} = Inert Mass Fraction
- $m_{CubeSat}$ = Dry Mass of the Overall 3U+ CubeSat
- P_{avg} = Average power
- DC = Duty Cycle
- P_{peak} = Peak Power
- $E_{eclipse}$ = Energy required during eclipse
- P_{tavg} = Total average power consumption
- $t_{eclipse}$ = Time In eclipse

- E_{sun} = Energy required outside of eclipse
- t_{sun} = time in sun
- L_L = Total line losses of discharging/charging
- A_{sp} = Total area of solar panels required
- EOL_{ef} = End of Life power generation efficiency
- α_{sun} = Heat flux at the spacecraft orbit
- E_{Batt} = Total battery capacity required
- DoD = Depth of Discharge
- Num_{batt} = Total number of batteries required
- $E_{density}$ = energy density of batteries
- $m_{battery}$ = Mass of battery

Chapter 1

INTRODUCTION

1.1 Statement of Problem

Since the beginning of the Space Age with the launch of Sputnik I in 1957, government agencies and corporations have dominated the satellite industry, due to the equipment and materials needed to build, as well as manufacturing and launch costs [1,2]. Costs to manufacture a traditional satellite start around 490 million USD for defense orientated satellites, or approximately 390 million USD for weather satellites [3]. A traditional satellite can be as large as a 3 m cube, operate for 5 – 10+ years, have a dry mass of around 1 ton and provide power of 2 – 20 kW, with the assumption that the mass of the power system is 10% of the dry mass, and deployable solar panels are utilized [4,5]. However, with advancements in the miniaturization of components, the Small Spacecraft (SmallSat) platform has re-emerged as a form factor in demand, while preserving technical capabilities. SmallSats typically operate for 2 – 5 years, have a mass of less than 180 kg [6] and can range in power from a few hundred of watts to less than 5 kW, with the assumption that the mass of the solar panels is 10% of the dry mass and deployable solar panels are utilized. Nano-satellites are a subset of SmallSats that ranges in mass from 1-10 kg, and available power ranges of up to 20 W for a spacecraft equipped with deployable solar panels and the assumption that the mass of the solar panels is 10% of the dry mass of the spacecraft [5,6]. One type of nano-satellite is a CubeSat, which is a standardized platform of 10 cm cubic form factor that is designed to increase the accessibility of space by decreasing the cost as well as development time of a satellite [6]. CubeSats come in various sizes based around a standard “1U” that utilize a 10 cm cube form factor with mass of up to 1.33 kg, and which can generates approximately 1.5 W per 1U with body mounted solar panels [7]. CubeSat missions costs can vary from less than 100,000 dollars for university educational based CubeSats to 20 million dollars or more for scientific missions, with the mission type and workforce that design, manufacture, and integrate the spacecraft driving the overall cost [8,9]. There are larger CubeSat sizes available that stack multiple 1Us into form factors of 3U, 6U, etc. as shown in Figure 1.1

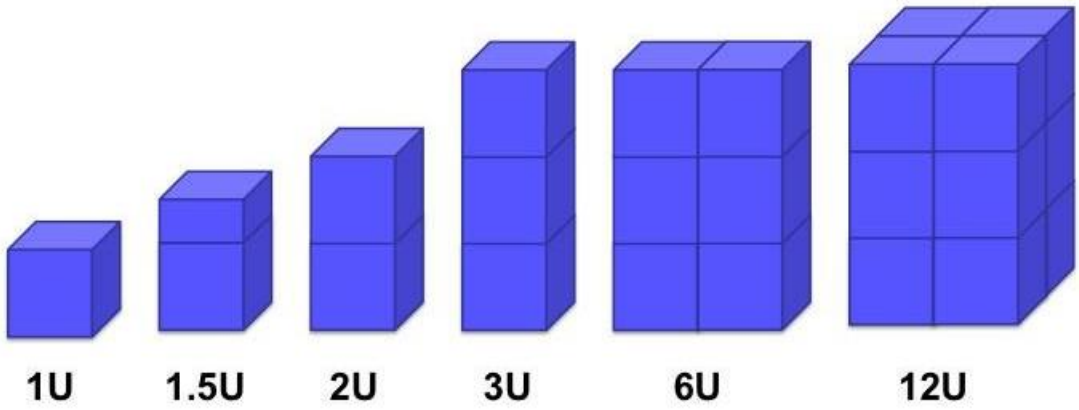

Figure 1.1: CubeSat Configuration Options [6]

The CubeSat platform allows for an increase in mission applications such as experimental missions with high science and commercial benefit [10]. Due to the increase in accessibility of resources to develop CubeSats, universities, high schools and commercial entities have started to create new innovations, business models and missions concepts that utilize the CubeSat platform [11]. With the increase in development and demand of CubeSats, additional mission capabilities are desired for the platform such as: drag compensation, formation flight, constellation deployment, as well as orbital maneuvers and corrections [12–16]. A specific breakdown of performance needs for each maneuver type is shown in Table 1.1. The ranges presented in Table 1.1, utilize the assumption of a Hohmann transfer that ignores the effects of plane changes, specific details about the altitudes utilizesd are showcased in Appendix A. The increased demand for a variety of mission maneuvers necessitates the need for propulsion systems that can generate between 1 – 1500 m/s of delta-V [12,17].

Propulsion systems can be broken into two main categories, chemical and electric propulsion. Each system consists of a variety of components that are necessary to propel the spacecraft forward such as: propellant storage, propellant feed systems, power systems as well as the thruster [18]. There are a variety of heritage propulsion systems that have accomplish many different mission capabilities, however traditional propulsion systems in production today require power greater than 8 Wdc just to operate valves of the propellant feed systems, as well as

propulsion system components that encompass envelopes larger than what is available to CubeSats [19–21]. Therefore, direct application of heritage thrusters in the CubeSat form factor can be limiting, with CubeSat systems constrained by weight of 1.33 kg, 1.5 W of power generation without deployable solar arrays and 1,000 cm^3 per 1U [7].

Safety regulations are also a limitation, due to the inability to use pyrotechnics, need for at least three inhibits to activation, safety regulations related to propellant choice and hazardous materials, as well as inability to store chemical energy that exceeds 100 Wh [7,22]. Further, range safety limitations from the Air Force Space Command Manual 91-710 (AFSPCMAN 91-710) drive the design, testing, analysis, and integration, for any pressurized structure or vessel, which can be prohibitively expensive [22].

Therefore, due to the limitations present of the CubeSat form factor, micro-propulsion systems have only been utilized in a few applications, with solar sails as well as cold gas, electrospray, and vacuum arc thrusters having been flown onboard a CubeSat [23]. Therefore, there is a demand for micro-propulsion systems that fit within the constraints of the CubeSat form factor to be developed and flown that adhere to the limitations present.

Table 1.1: delta-V needs for different mission maneuvers [5,12]

Maneuver Type	**delta-V range (m/s)**	**Calculated 3U delta-V needs* (m/s)**
Drag Compensation	10 – 100s	3
Formation Flight	1 – 100s	10 - 30
Constellation Deployment	1 – 100s	10 - 30
Change of Orbit Altitude / Corrections	50 – 1500	20 – 55

*Refer to Appendix A for assumptions and details regarding delta-V calculated

1.2 Problem Solution

Due to the limitations of the CubeSat form factor, a comparison between different micro-propulsion systems must be accomplished to ensure the correct application for the desired mission. Each micro-propulsion system can be compared using separate performance parameters such as thrust, specific impulse (ISP) , and possible delta-V [17]. ISP is a measure of total impulse delivered per unit of propellant consumed, which allows for comparison between different types of micro-propulsion systems. However, ISP does not incorporate any measure of the total impulse within a system or how quickly the system can achieve the impulse [23]. ISP of a chemical system varies between 40 – 300 s, whereas an electric system has an ISP that varies between 40 – 8,000 s, but the speed at which the impulse is delivered varies widely, with a chemical system able to deliver impulse at a faster rate [17,23]. The rate of impulse delivery affects the mission timeline and potential application of the CubeSat mission, which is an important factor in comparison between micro-propulsion systems. Thrust of a propulsion system is a combination of momentum thrust as well as pressure thrust and creates a force to propel the spacecraft forward that is directly related to how quickly a system can deliver an impulse to the spacecraft as shown in Figure 1.1.

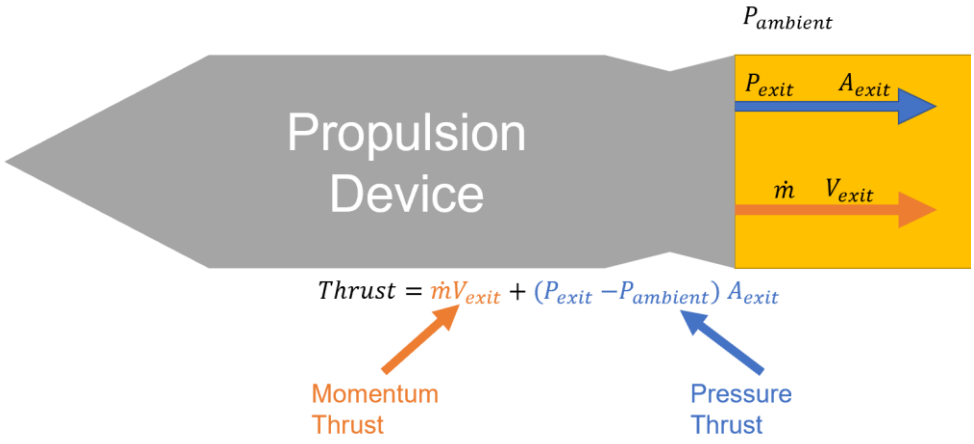

Figure 1.1: Pressure Thrust vs Momentum Thrust

Thrust is generated by four main components, exhaust velocity, mass flow rate, exit pressure, and exit area [23,24]. These four factors vary by micro-propulsion system type with chemical systems typically producing thrusts between 1 – 1,100 mN of thrust for mono-propellant and bi-propellant options and 13 – 76 N for solid propellant options. Whereas, electric micro-propulsion systems generate between 0.001 – 500 mN of thrust [17,23]. A summary of the different thrust and ISP ranges is presented in Figure 1.2.

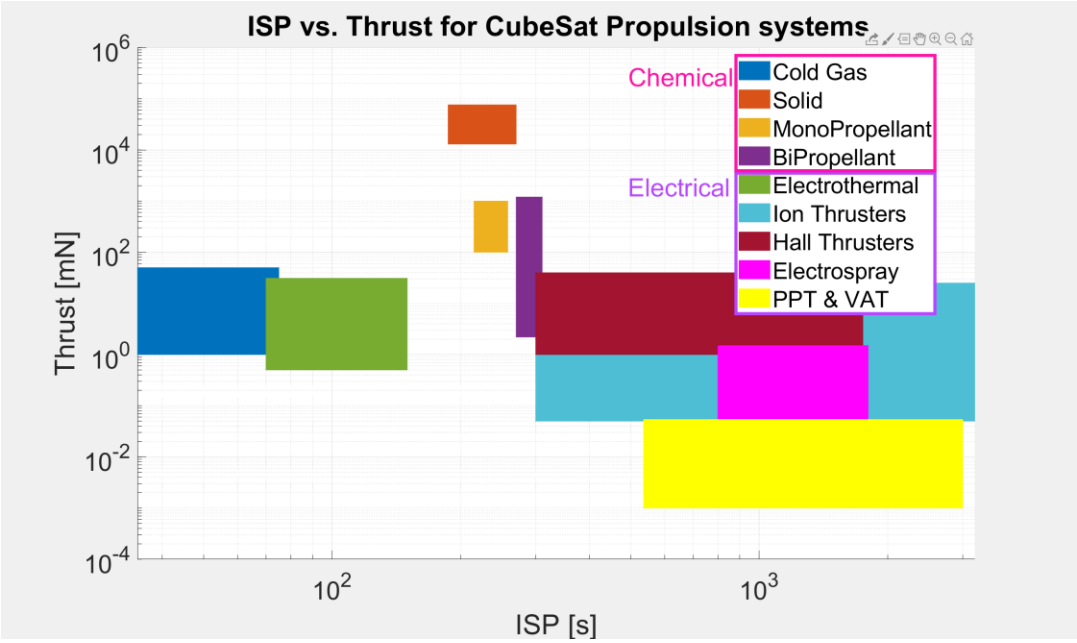

Figure 1.2 Summary of ISP and Thrust ranges of CubeSat propulsion systems [24]

Chemical and electrical systems vary widely between each mission objective and are applicable to a variety of different types of applications and thrust or ISP are not the only comparison needed between the two types of propulsion options. Delta-V is a performance parameter that characterizes the total change of speed a micro-propulsion system can generate and is a key part of providing comparison metrics. The delta-V (ΔV) of the micro-propulsion system is able to define what types of maneuvers are achievable to accomplish specific tasks within the mission concept [23].

$$\Delta V = (ISP) g \ln \frac{m_0}{m_f} \quad 1.1$$

Delta-V is calculated by combing the ISP(ISP) of the system in seconds, gravity (g) in m/s^2, initial mass (m_0), and final mass (m_f) in kg as shown in Equation 1.1 where m_0 and m_f are directly related to the amount of storage within the propellant storage volume [18].

CubeSat propulsion can be broken up into three key sections: existing, new, and emerging micro-propulsion system technologies. Existing technologies can encompass cold gas butane systems, pulsed plasma thrusters, and vacuum arc thrusters that have commercial options readily available that are able to adhere to the CubeSat form factor limitations [17,24–28]. New technology such as hydrazine monopropellant systems, ion engines, electrothermal thrusters, or colloid thrusters, necessitates miniaturization development effort into feed systems, power processing units, or power generation before application to CubeSats can be achieved. Finally, emerging technology that have TRL levels from 1 – 4 , such as micro-electrospray or micro-cavity discharge arrays, require development, to a majority of micro-propulsion system components such as: feed systems, power processing units, power generation units, and thruster technology, before application within the CubeSat platform [24].

A key area of interest with CubeSat propulsion systems is the development of electrothermal or warm-gas thruster technologies, due to an increase of up to double the ISP of cold gas systems, traditional satellite and CubeSat flight heritage, lack of pyrotechnics, and the ability to use inert, storable propellant [23,29]. Cold gas thrusters need only three components for operation, a propellant feed system, a thruster nozzle, and a propellant volume. Electrothermal thrusters in contrast have all the same components, but also incorporate a heating element before the thruster nozzle that accelerates propellant to provide additional ISP [17,24]. Due to the simplicity of the system, lack of need for pyrotechnics, and the non-hazardous propellants available, electrothermal propulsion systems are a good choice for university projects that follow the criteria laid out by AFSPCMAN 91-710. Electrothermal systems have one documented flight with the TW-1 CubeSat mission from China, which flew the CubeSat micro electromechanical systems (MEMS) Propulsion Module onboard STU-2A, on September 25th, 2015. This mission

successfully utilized a micro-propulsion electrothermal module to raise the satellites orbit 600 meters, as well as de-tumble the satellite when spin-rate were over the limit of the Attitude Determination and Control System (ADCS) [30]. Therefore, electrothermal systems remain a promising technology with flight heritage on the CubeSat platform, as well as flight heritage on traditionally sized satellites [23]. Furthermore, an electrothermal thruster named Pocket Rocket is available for use at Cal Poly CubeSat Laboratory (CPCL) [29]. Unfortunately, electrothermal thrusters carry important limitations when applied to the CubeSat standard such as power that is consumed when operating, which can vary between 2 – 30 W of DC power depending on the thruster and its components [17,23,24]. Another limitation that is present on electrothermal propulsion as well as other micro-propulsion systems is the amount of propellant that can be carried in order to ensure the needed delta-V for mission maneuvers [29]. This latter limitation is also driven by AFSPCMAN 91-710 that dictates structural and design decisions to ensure safe integration, as well as storage and operation [22]. Due to the lack of space available within the CubeSat form factor, CubeSat developers have to maximize available space within a deployer system to achieve required delta-V. One potential solution to maximizing the space available is a 1U+ CubeSat that utilizes the space between the spring of a CubeSat deployer referred to as a "Tuna Can", and increases available volume of a 1U from 1,000 to 1,116 cm^3 in a 1U+ CubeSat as shown in Figure 1.3 [7]. Currently, CPCL does not have a flight heritage Tuna Can structure, however the Tuna Can has been utilized before. ELFIN is a spin-stablizied 3U+ CubeSat, that was developed by UCLA, and laucnhed September 15th, 2018. ELFIN is currently operational in a 455 km, 93 degree inclination orbit [31].

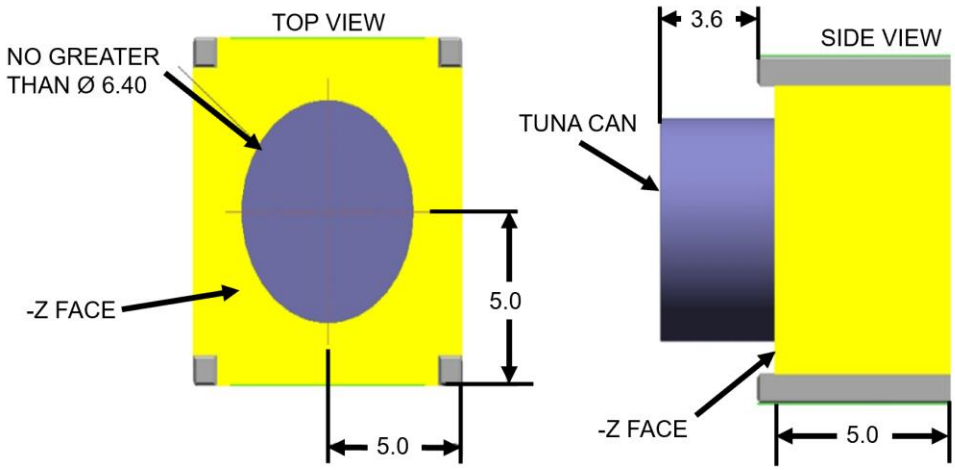

Figure 1.3: 1U+ CubeSat design, with dimensions in centimeters [7]

In each 1U block of a CubeSat, there is limited size (1,000 cm^3), weight (1.33 kg) and power (1.5 W) available, therefore CubeSats developers prioritize optimization of propulsion systems and propellant storage to minimize the volume, weight, and power of the propulsion subsystem while maximizing the performance [7,32]. Commercial propulsion systems are typically targeted for 2 – 6U+ overall form factors to enable enough space for other CubeSat subsystems such as: ADCS, power, thermal, command and data handling (C&DH), thermal and a payload [33]. In a 3U CubeSat form factor, commercial propulsion systems generally encompass 1-1U+ of the CubeSat which enables an estimated performance of 50 – 60 m/s of delta-V for the entire system [33–36]. However, all but one electrothermal micro-propulsion system, the CubeSat MEMS device from the Chinese TW-1 mission has flight heritage, therefore development must continue to advance TRL levels of thruster systems from 3 – 5 to 7 – 9 [30]. At the CPCL, micro-propulsion system development has been focused on integration of a 1 – 1U+ electrothermal system, called Pocket Rocket, capable of 5 – 50 m/s of delta-V into a generic 3U CubeSat design, utilizing manufacturing means currently available at the university [37]. As presented in Table 1.1, the performance target of 5 – 50 m/s of delta-V can potentially allow for mission applications of: drag compensation, formation flight, constellation deployment, as well as orbital maneuvers and corrections. Pocket Rocket would help mature propulsion technologies that align with NASA's

strategic goals 2 and 4 [38]. Alignment with NASA's strategic goals opens up the opportunity for programs such as the NASA CubeSat Launch Initiative (CSLI), that can provide a free launch into a Lower Earth Orbit (LEO), deep space or interplanetary orbit, to conduct scientific investigations as well as technology demonstrations in space. A free launch can offset upwards of 300,000 dollars [39] for a deployment in Low Earth Orbit (LEO), that commonly ranges from 400 – 700 km [36,40]. Finally, small satellite licensing with the Federal Communications Commission (FCC), now requires a propulsion system whenever a SmallSat, is deployed above 600 km, to limit chance of debris creation or collision with other objects in an orbit.

1.3 Thesis Scope

This research focuses on the Pocket Rocket thruster, an RFET micro-propulsion system that is readily available for use by CPCL and is capable of expanding CubeSat mission opportunities. The Pocket Rocket thruster has been ground tested and manufactured at CPCL, with traditional manufacturing techniques to create a cost-effective design that complies with the CubeSat standard and helps to enable opportunities for access to space [29,37]. As of 2019, Pocket Rocket has yet to fly onboard any spacecraft, but it has been incorporated into a preliminary design of a 1U+ micro-propulsion system that could be integrated into a 3U+ CubeSat form factor and is capable of 5 m/s of delta-V.

This thesis focuses on furthering the conceptual design and analysis of the Pocket Rocket 1U+ system. In addition, the creation of a propellant storage cavity design, system components, routing and electrical diagrams and overall 1U+ layout are developed to reach a target delta-V potential for the system, while following guidelines maintained by the CubeSat Standard as well as AFSPCMAN 91-710. The target of this thesis is to design Pocket Rocket such as to increase its delta-V capability to between 17 – 23 m/s, which will enable the use of the Pocket Rocket system for: drag compensation, formation flight, constellation deployment, or orbital maneuvers and corrections [5]. Then, estimated performance was calculated for a 3U+ form factor technology demonstration mission to showcase that the CubeSat can compensate for the drag

force in LEO with 17 – 23 m/s of delta-V. A simulated transient as well as steady state thermal analysis is performed to ensure survivability of electrical components when exposed to the LEO environment during thruster demonstration mission phases. Pressure vessel static structural analysis is simulated at Maximum Expected Operating Pressure (MEOP) to ensure adherence to AFSPCMAN 91-710 with a minimum safety factor of 1.5. Finally, random vibrational analysis of the entire 1U+ system is carried out at qualification as well as acceptance levels to showcase design validity and adherence to AFSPCMAN 91-710. Finally, recommendations for further advancement of the design as well as lessons learned during the design process are presented.

This thesis does not cover the manufacturing, integration or testing of the design, and is solely focused on the 1U+ Propulsion Module system, with assumptions for inputs/outputs from a 2U spacecraft. Assembly instructions, interface control documentation, requirements as well as recommended plumbing and electrical components are included to showcase the feasibility of the design. The 3U+ system vibrational analysis is not carried out due to the variability of attaching the 1U+ propulsion system to a 2U CubeSat design. The 2U CubeSat design is not developed, and different placement of components within the structure will affect the results of the vibrational study.

Chapter 2

BACKGROUND

2.1 Prior Research

2.1.1 Electrothermal Propulsion Systems for CubeSats

Electric propulsion for CubeSat applications in general utilizes external power sources to increase the exit velocity of a propellant and create thrust [12]. One type of electric propulsion is the electrothermal thruster, sometimes referred to as a warm-gas thruster, that uses electrical power to heat up a propellant, before it is expelled through the nozzle [23]. This heating mechanism allows for improvement in ISP of the system of up to double, by increasing the exit velocity of the propellant as compared to cold gas thrusters [23,24]. The four main types of electrothermal propulsion are; Radio Frequency (RF) heating, micro cavity discharges, microwave heating, as well as resistojets, the most common [17,24].

Resistojets have flight heritage for traditionally sized spacecraft; however there has yet to be a flight of a resistojet on a CubeSat [19,23]. Resistojet technology is currently being developed and miniaturized for flight on CubeSats to meet their SWaP limitations. Currently under development, CubeSat High Impulse Propulsion Systems (CHIPS) created by CU Aerospace and VACCO, is designed to allow for CubeSat operations such as: altitude changes, formation flying, and rendezvous or docking. The 3D printed aluminum design integrates the thruster, feed system, power processing unit, and propellant volume into a 1U+ design that is capable of 82 seconds of ISP, a maximum thrust of 30.2 mN with 1 W of DC power, and R134-a as non-toxic propellant. However, to achieve this performance, an additional battery pack that makes the overall propulsion system size 1.5U+ must be integrated, which further limits the space available as the in a 3U, as well as have the capability to 3D print the entirety of the aluminum structure, which is unavailable at CPCL [33]. Busek is developing a micro-resistojet propulsion system that stays true to the 1U size, with a mass of less than 1.25kg, maximum DC power draw of 15 W,

with 10 mN thrust, and 150 seconds ISP, and is capable of 60 m/s of delta-V for a 4kg CubeSat [28]. The 60 m/s of delta-V could be utilized for mission applications of: change of orbital altitude or corrections, drag compensation, formation flight, constellation deployment, as well as attitude control but currently has not yet been scheduled on a mission [5,12,28]. This system utilizes aluminum 3D printing, a capability currently unavailable to the CPCL, and does not maximize the dead space inside a CubeSat deployer, with a 1U+ design [28]. RAMPART is a 2U CubeSat mission that utilizes a resistojet propulsion system that encompasses 1U and is designed and manufactured using rapid prototyping 3D printing and MEMS technologies to utilize R-134a propellant and produce 90 seconds of ISP [34]. The propulsion system for RAMPART will be utilized in a 2U configuration for altitude raising, as well as orbit maintenance for a radiation analysis mission electing to not include the additional volume capacity of a 2U+ system [34], that does not have an expected launch date currently. CPCL does not have the ability to 3D print with aluminum necessary for RAMPART but has a similar applicable capability with SS 316L that has not been demonstrated in a CubeSat application yet. Further, MEMS manufacturing techniques are not available at Cal Poly [34].

Microcavity Discharge (MCD) is another type of electrothermal thruster that is designed for use on less than 10 kg satellites. Microcavity discharge works by heating up the propellant through containment of plasma, before being expelled through a micronozzle [41]. The primary goal of MCD thrusters is to achieve performance levels of 1 mN per cavity with number of cavities varying from 4 – 9+ by heating the temperature of the propellant by 1,000+ K with a 60 % efficiency and an ISP of 160 seconds for utilization in orbit transfer and maneuvers, as well as attitude and position or acceleration control within LEO [41,42]. The Propulsion Unit for CubeSats (PUC) developed by CU Aerospace and Vacco Industries is an MCD thruster designed for orbital maneuvering, formation flight as well as rendezvous [35]. PUC is configured in a 0.25U+ design and produces 5 mN of total thrust, with 70 seconds of ISP, providing 48 m/s of delta-V for a 4 kg CubeSat, and draws 15 Wdc of power[35,43]. Compared to resistojets, the PUC was able to achieve constant lifetime operations over a 19 hr test. The PUC is also capable of expansion of the 0.25U+ form factor, by changing the propellant tank size to incorporate a larger delta-V of up

to 148 m/s in warm gas mode [35]. PUC is a commercial thruster with nine flight systems delivered [44].

Microwave Electrothermal thrusters (MET) operate by injecting microwave power into a resonant cavity that turns the propellant into plasma that is then ejected through the nozzle [45]. METs have been tested in varying frequency levels, that correspond to different power applications on small satellites, however due to the design of the microwave cavity chamber, a commercially ready design has yet to flourish that maintains the limitations on SWaP of a 3U CubeSat design [45]. Georgia Institute of Technology (GIT) and Pennsylvania State University (PSU), are designing a propulsion system that takes between 1 – 1.5U of space, less than 2 kg of mass, and operates with 30 – 50 W of DC power, but is able to produce more than 500 m/s of delta-V [46]. A delta-V of more than 500 m/s would be an improvement over current capabilities of 40 – 60 m/s for the form factor and allow for additional mission maneuvers such as deorbit, in addition to change of orbital altitude or corrections, drag compensation, formation flight, constellation deployment, as well as attitude control [5]. The concept is still undergoing design of the thermal and fluid flow parameters but incorporates water as propellant at a frequency of 17.8 GHz [47].

Radio frequency electrothermal thrusters (RFET) , incorporates RF power to produce a plasma within the propellant, causing gas expansion and acceleration through charge exchange, producing thrust as seen in Figure 2.1[29]. RFET thrusters are desirable due to their ability to generate ISP from 75 -158 s, as well as thrust between 1 – 5 mN [37,48]. PSU has been developing a RFET that draws 100 W of power and has shown during ground testing an ISP between 128 – 158 seconds and thrust levels for attitude adjustment, station keeping as well as deep space missions but has not yet provided performance metrics [48]. The PSU RFET would be hard to apply to a 3U CubeSat form factor, due to the 100 W of DC power draw currently needed but could be equipped for small spacecraft. However, Pocket Rocket, which started development at the Space Plasma, Power and Propulsion Laboratory at The Australian National University (ANU), solves this issue with a nominal DC power of 10 W and thrust of 2.4 mN [37]. Pocket Rocket utilizes argon or xenon gas, and RF energy to generate a plasma and increase the

exit velocity of gas leaving the outlet [49,50]. Pocket Rocket development at CPCL, is centered around obtaining new thrust measurements, as well as development of a Propulsion Module [29,37].

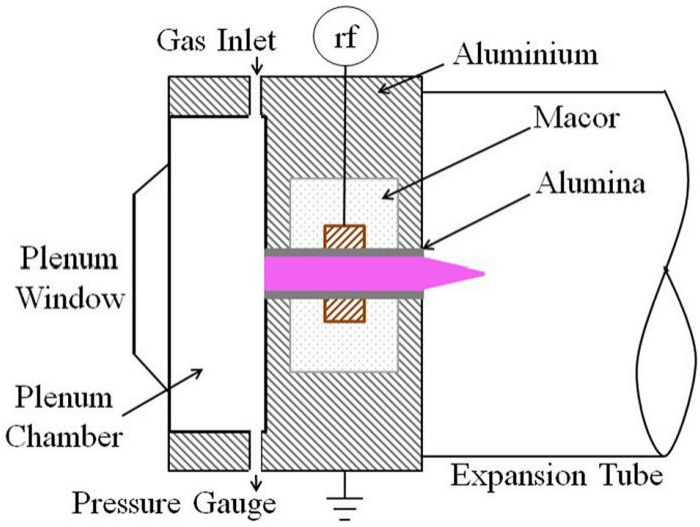

Figure 2.1: RFET Diagram of Pocket Rocket [48]

A table of performance parameters alongside system constraints for all the electrothermal systems mentioned in this section is shown in Table 2.1.

Table 2.1: Summary of Current Electrothermal Thruster Performance

Thruster	Manufacturer	Thrust (mN)	ISP (s)	Size	Weight (kg)	DC Power (W)	Ref.
CHIPS *(resistojet)*	CU Aerospace /VACCO	31.0	76	1U+	1.4	25	[33,43]
Micro-Resistojet	Busek	2.0 – 10.0	150	<1U	<1.3	3-15	[28]
RAMPART *(resistojet)*	University of Arkanas	0.5	90	1U+	1.1	-	[34,51]
PUC *(MCD)*	CU Aerospace /VACCO	5.0	70	1U	1.5	15	[35,43]
Water-Propellant MET	PSU/GIT	-	-	0.1U (Thruster only)	-	30	[47]
Low-Power RFET	PSU	3.7	140	N/A	-	100	[48,52]
Pocket Rocket *(RFET)*	ANU	2.4 mN	100	1U	1.4	10	[29,37,49]

2.1.2 Thermal Design of CubeSat Propulsion Platforms

To ensure operational temperatures of a spacecraft, its propulsion system and all other subsystems encompassed within the satellite, the external and internal thermal environments must be considered. Externally, the driving types of radiative heat transfer in LEO are Solar, Albedo, and earth radiation, as well as radiation to space and other surfaces of the satellite. Internally, heat is generated by radiation and conduction through equipment, components, and payloads, such as the propulsion system, batteries, solar panels, and other electronics within the spacecraft [53].

To ensure operational temperatures of all spacecraft subsystems, thermal management must be incorporated into the spacecraft to adapt to the changing external and internal environments. A CubeSat mission has a variety of thermal management techniques that can be utilized to ensure adherence to required operational temperatures, that can be broken down into passive and active management [54].

Passive thermal management does not use power input from an electrical system, and incorporates techniques such as materials and coatings, multi-layer insulation (MLI), heat sinks as well as heat pipes and sun shades to help regulate temperature within the spacecraft [53,55]. Due to the SWaP constraints, passive management is the most commonly utilized method to maintain required operating temperature limits of the CubeSat platform [56]. Within the CubeSat form factor, MLI is difficult to handle and integrate into a CubeSat deployer therefore, surface coatings are utilized as an alternative and are one of the most common types of passive thermal management [54,56]. At the CPCL, black anodized aluminum is the most common form of passive management utilized on spacecraft currently under development, to help manage the thermal environment.

Active thermal management, utilizes electrical input to manage the operating temperature limits, with techniques such as heaters or thermal electric coolers (TECs) [53]. Active systems are usually incorporated into the thermal management of CubeSat missions, when passive systems are unable to maintain required temperature limits of subsystems [54]. Active heaters

have been successfully utilized on small satellites on missions such as Compass-1, MASAT-1, and OUTFI-1 [55].

Thermal analysis is a technique utilized to estimate the thermal environment that will be experienced by the spacecraft on orbit, and allow for the planning of the implementation of management techniques to ensure operational temperature limits are maintained throughout the life of the spacecraft, if required [57]. Thermal management is especially important when considering designs of a CubeSat propulsion system, as the heat generated from different types of propulsion systems has an effect on the operational temperatures within the spacecraft as well as the performance of the propulsion system [54]. For an electrothermal propulsion system, excess heat is generated and conducted or radiated through the spacecraft due to system inefficiencies. System inefficiencies can affect other CubeSat subsystems as components inside the bus operational temperatures nominally range between between 220 – 350 K, with batteries requiring a stringent range at 293-290 K for Li-Ion. Electrothermal thrusters are designed to heat propellant to temperatures between 500-1200 K, which can introduce excessive heat throughout the CubeSat system and must be managed by the thermal control system [23,24]. Therefore, to ensure operational temperature limits of the propulsion system as well as the other subsystems present within the CubeSat, it is important to develop a thermal model to simulate the expected thermal environment experienced.

2.2 Safety Regulations

CubeSats must adhere to requirements in the CubeSat standard as well as AFSPCMAN 91-710 to operate a propulsion system as a secondary payload on a US rocket launch. Chapter 3 of AFSPCMAN 91-710 specifies design criteria and hazard mitigation of non-traditional systems or CubeSats and identifies the number of inhibits depending on the hazard and its severity. Chapter 10 discusses hazardous materials, and selection criteria to ensure that your system carries the lowest potential hazard given your mission criteria and design constraints. Finally, Chapter 11 and 12, discuss topics related to pressurized structures and their design factors, testing criteria,

manufacturing criteria, as well as identification of varying failure modes. In addition to pressurized structures chapter 11 and 12 go into detail about the entire pressurized system and criteria required to mitigate the potential hazards. Some of the standards regarding integration from AFSPCMAN 91-710 do not apply to CubeSat applications, as limitations once integrated with a deployer can limit handling of spacecraft [22].

AFSPCMAN 91-710 stated that there will be a Wing Safety officer assigned to each operation whose duty is to review and approve design, inspection, and testing of all hazardous materials, as well as review and approval of all requirements and documents specified in AFSPCMAN 91-710. Hazardous materials utilized must comply with data and environmental requirements and have a process safety and risk management plan, as well as be the least flammable material that can meet design requirements. When hazards are not well understood, the Wing Safety may require testing of any materials. These tests can incorporate the following: toxicity reactivity, compatibility, flammability and combustibility.

Operational pressures are regulated as well, with no designated upper limits, but pressure vessels must remain below maximum design pressure of the propellant tank. Additionally, once a system has an operating pressure above 100 Psig, it is deemed hazardous flight hardware, and must undergo testing, inspection and certification prior to wing safety approval [22]. In order to launch as a payload for the NASA CubeSat Launch initiative, safety requirements that come from the AFSPCMAN 91-710 must be adhered to [58].

The requirements specified in this section must be followed to ensure a launch opportunity for American launches [22]. Therefore, this research follows all standards introduced by CDS as well as AFSPCMAN 91-710 that are applicable for the CubeSat form factor to ensure launch.

2.3 Environmental Testing & Simulation

Due to the requirements laid out in AFSCMAN91-710, environmental testing must be accomplished to ensure the system operates as intended before allowing the design to launch. Structurally, AFSCMAN91-710 requires an acceptance test at a minimum of 1.25 the MEOP to test the pressure vessel. After the acceptance test, qualification must be completed

with a random vibrational test, cycle test, as well as burst test [22]. The random vibrational test is designated by NASA General Environmental Verification Standard (GEVS), that specifies requirements as well as guidelines for environmental verification programs of payloads, subsystems, or components [59]. After random vibration, cycle testing is accomplished, where the pressure load is cycled through the system four times more than the expected number of operating cycles for the pressure vessel or system. Finally, burst testing is accomplished, where the test article is pressurized to the design burst pressure, and maximum external load is applied concurrently, and held for a sufficient period of time [22]. The verification approach for pressure vessels as specified by AFSCMAN91-710 is shown in Figure 2.2.

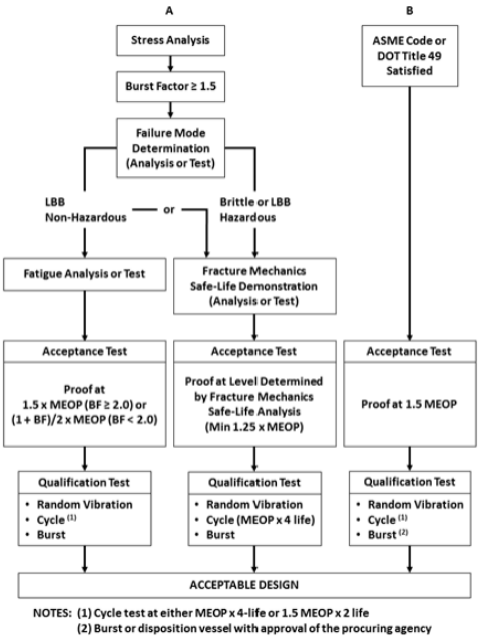

Figure 2.2: Pressure Vessel Design Verification Approach [22]

In addition to structural testing, thermal testing is also outlined in NASA GEVS. The purpose of this testing is to show that the payload is able to perform nominally within the vacuum and thermal mission limits. Additionally, the thermal design must be shown to maintain the affected hardware within thermal limits during all mission phases, including survival/safe hold, when applicable. The materials and quality of the workmanship must also

be able to pass thermal cycle test screening in vacuum or under ambient pressure if the hardware is determined to not be sensitive to vacuum effects [59].

2.4 Prior Pocket Rocket Development

2.4.1 Pocket Rocket Testing Iteration

Pocket Rocket has been ground tested for performance characterization at California Polytechnic State University: San Luis Obispo. The purpose of this testing was to ensure operation in a vacuum environment, and enable future plans to compete a space mission that demonstrates the capability of the Pocket Rocket thruster [29]. This test specifically demonstrated spin maneuver testing in a 1U form factor; incorporating argon propellant storage, pressure regulation, RF power and thruster control, and a modular support structure, the test article layout is presented in Figure 2.3, and incorporates two Pocket Rocket thrusters. The major drawback of this design is a lack of integration of RF generation and amplification into the test article, as well as lack of propellant storage. To further development of Pocket Rocket, a flight specific layout must be designed and manufactured.

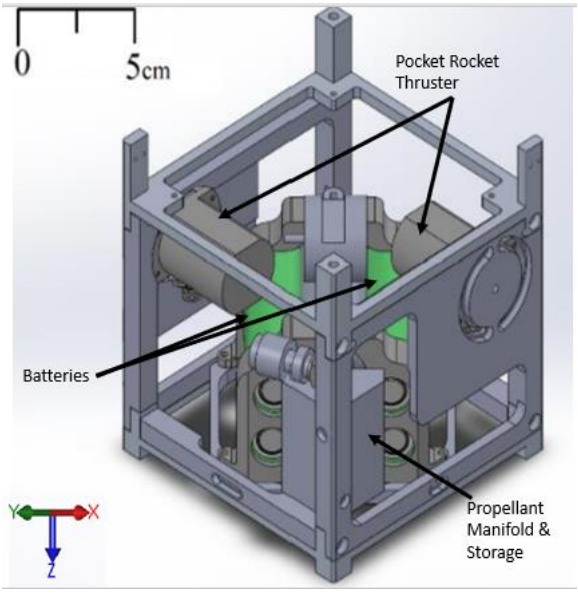

Figure 2.3: Pocket Rocket System Testing Configuration [29]

2.4.2 Conceptual Flight Iteration

The initial flight system design iterated upon the developments made during performance characterization using a testing article. The new design incorporates the Pocket Rocket Thruster, pressure regulation components, propellant storage, as well as RF generation, amplification, and control. The components were placed within a 1U+ CubeSat form factor that is attached to either a 1 or 2U CubeSat as seen in Figure 2.4. The new design operated under the assumptions that power would come from the spacecraft bus, and the MEOP would be 8.27 MPa (1200 PSI). The improved aspects of this design were incorporation of additional propellant storage that allowed for an estimated delta-V of 5 m/s, first order thermal and structural analysis, and integration of RF generation and other critical components to allow for thruster operation with the 1U+ system [60]. However, this design did not define mechanical or electrical interfaces, follow necessary guidelines outlined by AFSCMAN91-710, implement routing and assembly instructions, or define system inputs and outputs. Therefore, there is a need to develop the design further, to allow for assembly and integration of the Pocket Rocket thruster into the Propulsion Module system.

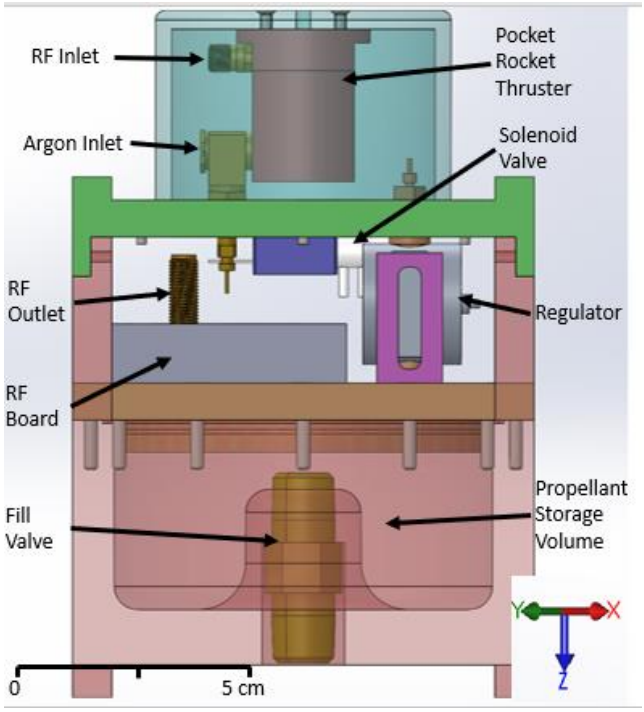

Figure 2.4: Conceptual Flight Design of Pocket Rocket [60]

Chapter 3

DESIGN OVERVIEW AND DEVELOPMENT

3.1 Mission Objectives and Overview

To improve upon previous Pocket Rocket development, mission objectives as well as requirements were established to highlight what needs to be achieved for mission success. The mission objectives shown below, showcase the goals of the project, as well as Pocket Rocket development. Fully defining mission objectives as shown below as well as operational objectives, allows for decomposition of mission requirements, bus requirements and development of the overall system architecture.

- Develop a Propulsion Module that will demonstrate CubeSat propulsion in the LEO environment
- Further development and demonstration of Pocket Rocket thruster capabilities in a space-based demonstration mission
- Cal Poly CubeSat Laboratory demonstrates operation of a CubeSat propulsion system

After the objectives of the project were defined, mission requirements were derived and can be seen in Appendix B. Preliminary constraints were also defined, one of which is mission cost. Pocket Rocket is an internal research and development project: therefore, funding must be acquired from internal or external sources. In particular, the mission concept was designed to align with NASA strategic goals 2 and 4 [38] to allow for launch opportunities through the CubeSat Launch Initiative. Additionally, to limit development costs, the propulsion system components are intended to be manufactured and integrated, whenever possible, within the capabilities of the machine shops within the College of Engineering and within CPCL's mechanical engineering (ME) team skill set.

CubeSats are commonly launched into a LEO orbit through NASA's CSLI, with the most common deployment points constituting a rideshare to Sun synchronous orbit (~500 km), or deployment from the International Space Station (ISS) (~400 km) [36]. Consequently, this mission baselines operations in LEO. Out of the two most available LEO orbits for rideshare, the

deployment from the ISS is the most common for CubeSat deployment. Therefore, this research assumes that the 3U+ system will launch from the ISS.

The form factor of the mission was selected by leveraging CPCL's heritage capabilities with current trends in commercial thrusters, as well as maximizing performance capabilities of the system. A 3U+ form factor was decided on, due to the prevalence of the form factors used for technology demonstration missions, manufacturing capabilities at CPCL, and prevalence of launch opportunities as shown in Figure 3.1 [10,36]. The 3U+ CubeSat was assumed to have 2Us devoted to the customer CubeSat and relevant non-propulsive subsystems, while the remaining 1U+ would be reserved for the propulsion system. 3U+ CubeSats are allowed 4 kg per the CDS Rev 13 [7], therefore the initial assumption for the maximum allowable mass of the Propulsion Module was assumed to be ~2 kg, leaving another 2 kg reserved for the 2U CubeSat.

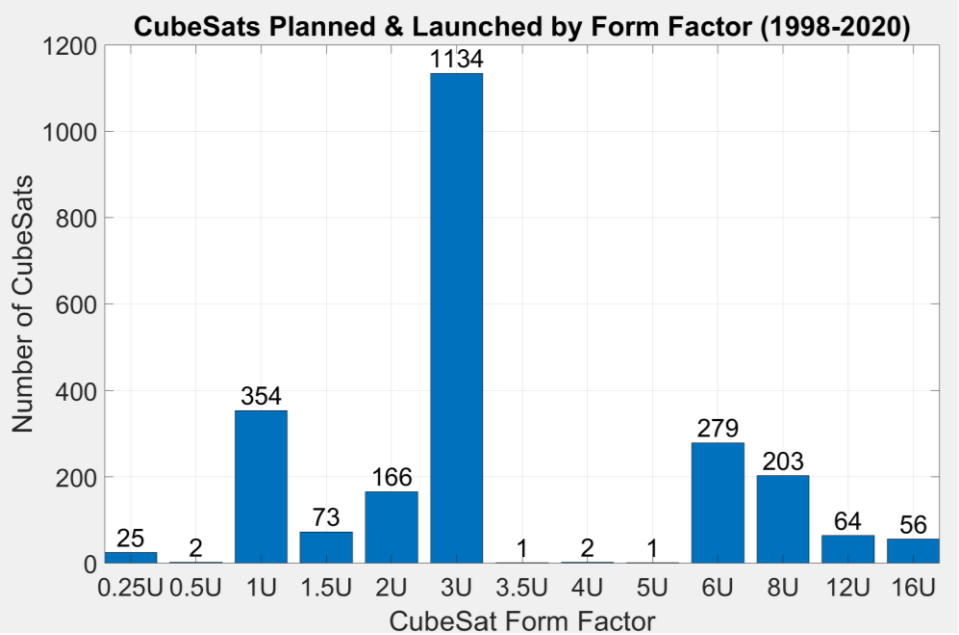

Figure 3.1: Breakdown of CubeSats launched by form factor [36]

The DC power sources available to CPCL include: commercially available deployable solar panels that generate between 28 – 42 W [61], CPCL deployable solar panels under development, or body mounted solar panels which generate about 5 W per 3U spacecraft. The total average power consumption of the Propulsion Module is 6.3 W per orbit, assuming only the propulsion

system portion of the mission is operated. A total solar cell area of about 340 cm^2 was determined necessary to generate and store the energy needed for operation of the Propulsion Module with xenon propellant. The Propulsion Module was assumed to receive power from the 2U spacecraft bus, and not have an independent power generation or storage system. The assumptions to not include an independent power source for the Propulsion Module, was due to the limited SWaP available in the 1U+ system because of necessary functional components for Pocket Rocket. Therefore, due to the power constraints of the Propulsion Module as well as the needs of the customer 2U CubeSat, a deployable solar cell architecture is proposed for this research. The overall system requirements for the 3U+ system as well as the Propulsion Module are shown in Table 3.1.

Table 3.1: CubeSat system level constraints and limitations

	3U+ CubeSat	1U+ Propulsion Module
Maximum Mass	4.0 kg	2.0 kg
Maximum Dimensions	34 x 10 x 10 cm	14 x 10 x 10 cm
Power Source	Deployable Solar Panels	Power from bus
Operational Orbit	~ 400 km, ISS deployed	~ 400 km, ISS deployed

3.1.1 System Overview

An overview of the 3U+ CubeSat, 2U CubeSat and 1U+ Propulsion Modules system breakdown are shown in Figure 3.2. The 1U+ Propulsion Module is designed to incorporate only the necessary components for operation of Pocket Rocket. Therefore, the 1U+ Propulsion Module interfaces with a variety of 2U CubeSat systems through mechanical, electrical, and data interfaces, to allow for flexibility in the design of the overall 3U+ CubeSat technology demonstration mission.

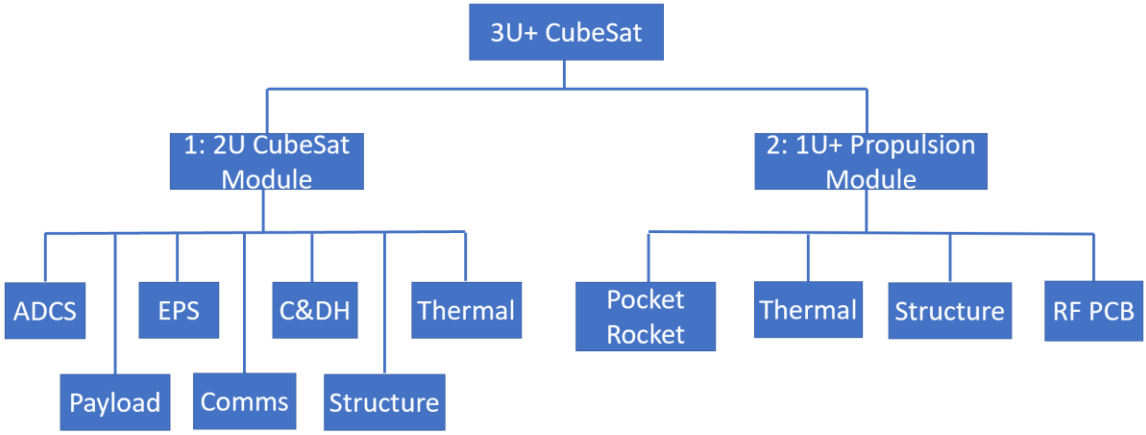

Figure 3.2: 3U+ CubeSat Product Breakdown Structure

The 1U+ Propulsion Module will operate based on assumed inputs from the 2U CubeSat to limit impact on the design and operations. The 2U CubeSat shall provide regulated and unregulated DC power between 1 – 61 W, alongside RF power between 0 – 12 W. The software communication protocol will be I2C, between each of the boards. The overall inputs and outputs for each system and the electrical, software, and plumbing interfaces necessary for the Propulsion Module to operate are shown in Figure 3.3.

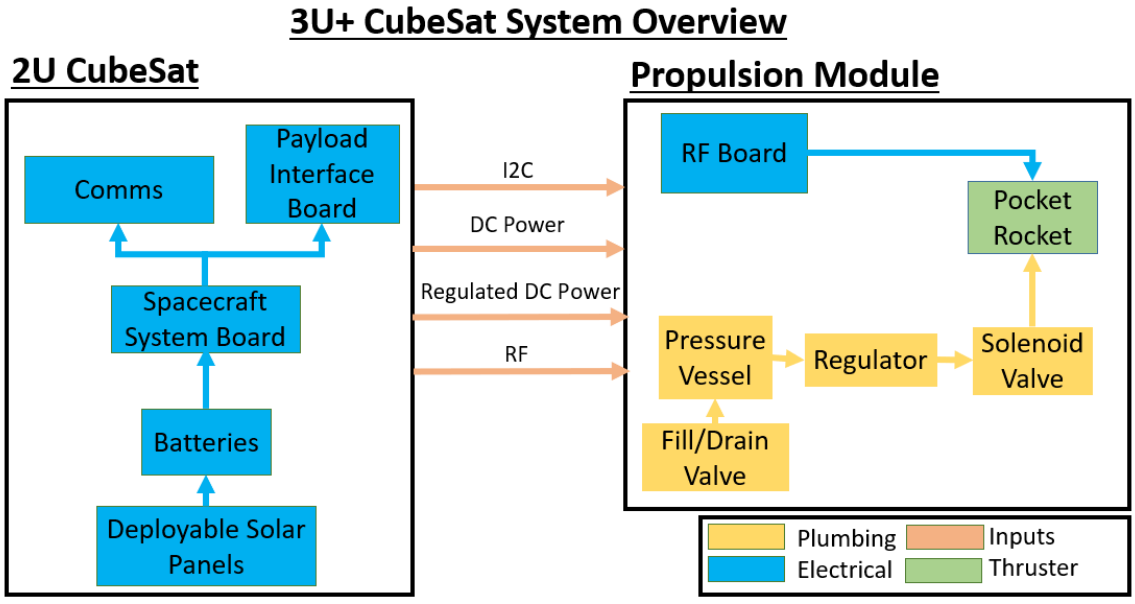

Figure 3.3: 3U+ System Interconnections Overview

3.1.2 Concept of Operation

Pocket Rocket necessitates extended duration burns to generate the delta-V required for mission maneuvers. The 3U+ CubeSat baselined in the research is limited in burn duration by the power generation from the deployable solar arrays, as well as thermal loads from extended burn durations. Power draw from the 1U+ Propulsion Module must not interfere with the 2U CubeSats nominal operations as defined in the overall mission concept of operations (ConOps) shown in Figure 3.4. Therefore, a burn time of 10 minutes was selected, that balances power draw with a delta-V generation of ~0.5 m/s per burn. The ConOps (Figure 3.4) of the Propulsion Module system demonstration constitutes three separate phases: 1) thruster checkout, 2) thruster nominal operation, and 3) thruster standby.

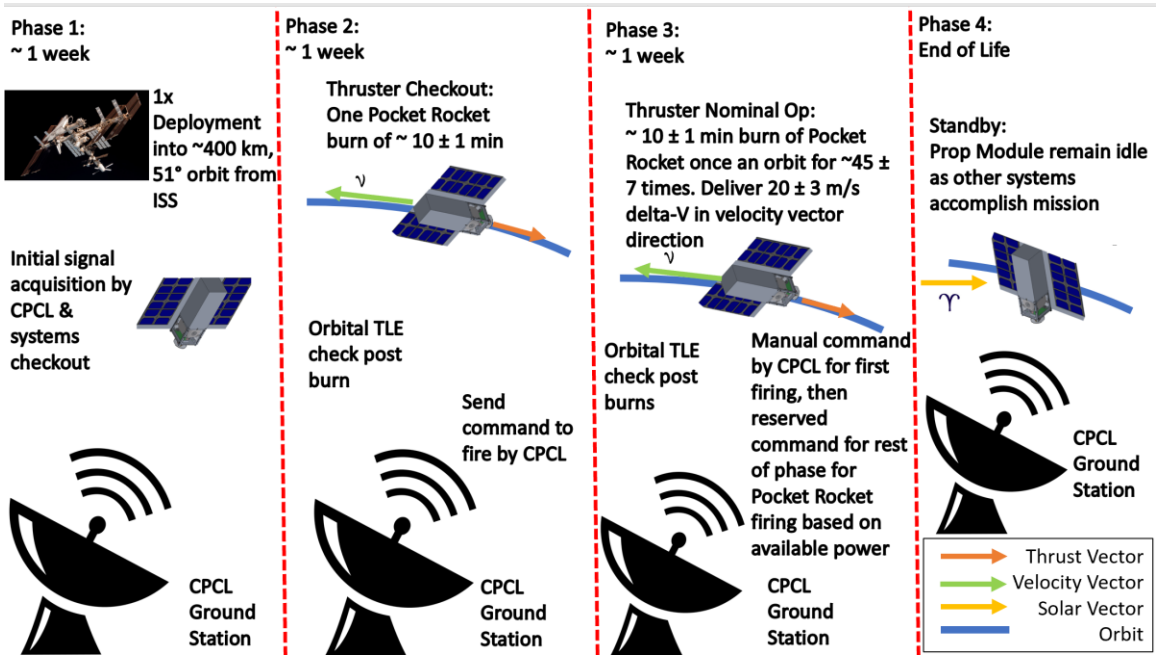

Figure 3.4: Overview of phases of them mission for the Propulsion Module

Initially the Propulsion Module will be in thruster standby mode, during the overall 3U+ system acquisition. Afterwards, the 1U+ Propulsion Module will begin its thruster checkout phase, as specified in the overall 3U+ CubeSat ConOps. The thruster checkout phase involves actuating the thruster electrical and plumbing components to verify Propulsion Module operation before

moving forward into the thruster nominal operation phase. Thruster checkout ends after the ground station operators have been able to compare, via NORAD orbital information, the 3U+ CubeSats orbit altitude prior to thruster checkout with the post-firing orbit altitude. The second phase of the ConOps is the thruster nominal operation phase, which focuses on the technology demonstration of Pocket Rocket. Upon command reception from CPCL ground station and if outside of eclipse, the 1U+ Propulsion Module will begin thrusting once per orbit for a duration of ~ 10 minutes if the system has generated and stored enough power. The reserve command checks the status of energy storage and generation once an orbit to ensure that the system has stored and generated the expected amount of energy. Thrusting will occur for a total of 45 ± 7 orbits and take a total time of approximately 4 days if the thruster can fire every orbit. This phase will impart approximately 20 ± 3 m/s of delta-V that will overcome orbital perturbations such as atmospheric drag, and raise the orbit altitude by a maximum of 70 km. After accomplishing the thruster nominal operation, the third phase of the ConOps thruster standby, starts. During the standby phase, the thruster will not operate and will sit idle for the remainder of the 3U+ CubeSat mission, until the eventual deorbit of the spacecraft.

The firing of the Pocket Rocket thruster requires interaction between the plumbing, electrical, ADCS, C&DH, communications, as well as EPS of both the 2U CubeSat and the 1U+ Propulsion Module. An overview of the step by step operations of the Propulsion Module is shown in Figure 3.5. The first thrusting burn will begin with a command received from CPCL at the start of the thruster nominal operation. This command will also enable the automatic scheduling of the subsequent burns at a rate of once per orbit if the spacecraft is outside of eclipse and if enough power has been generated and stored for the duration of the nominal operation phase. The thruster checkout has a single phase, for which a single thrusting command is sent from the CPCL ground station, with no automatic scheduling afterwards. Thruster expected performance is quantified via comparison of expected orbit vs. NORAD orbital data, before moving into the thruster operation phase. The ADCS system will then be commanded to point the -Z face of the 3U+ CubeSat in the velocity vector direction. After the – Z face is pointed towards the velocity vector, the 3U+ system will supply power to the Payload Interface Board (PIB) which will begin

RF signal generation as well as DC-DC regulation. The RF signal as well as regulated DC power, and unregulated DC power will then be distributed to the Propulsion Module through ribbon and coaxial cabling. The RF PCB onboard the Propulsion Module will perform RF final amplification as well as utilize I2C communication protocols to actuate the Solenoid valve. The amplified RF energy will then be distributed to the Pocket Rocket thruster via coaxial cabling, as pressure pushes the xenon propellant into the thruster chamber. For the first 30 seconds of actuation, the DC power distributed to the system will be 61 W to allow for generation of initial plasma breakdown that initiates Pocket Rocket. After the initial 30 seconds, the power draw will be reduced to 31 W to maintain plasma breakdown for nominal thrusting operations. The 30 second initiation time is a worst-case scenario based on maximum expected time for electronics actuation, plasma ignition and inductance matching that will depend on ambient conditions. During both system checkout and nominal thrusting, Pocket Rocket will operate for 30 seconds at start-up and 10 minutes for nominal operation to ensure operation of the propulsion system.

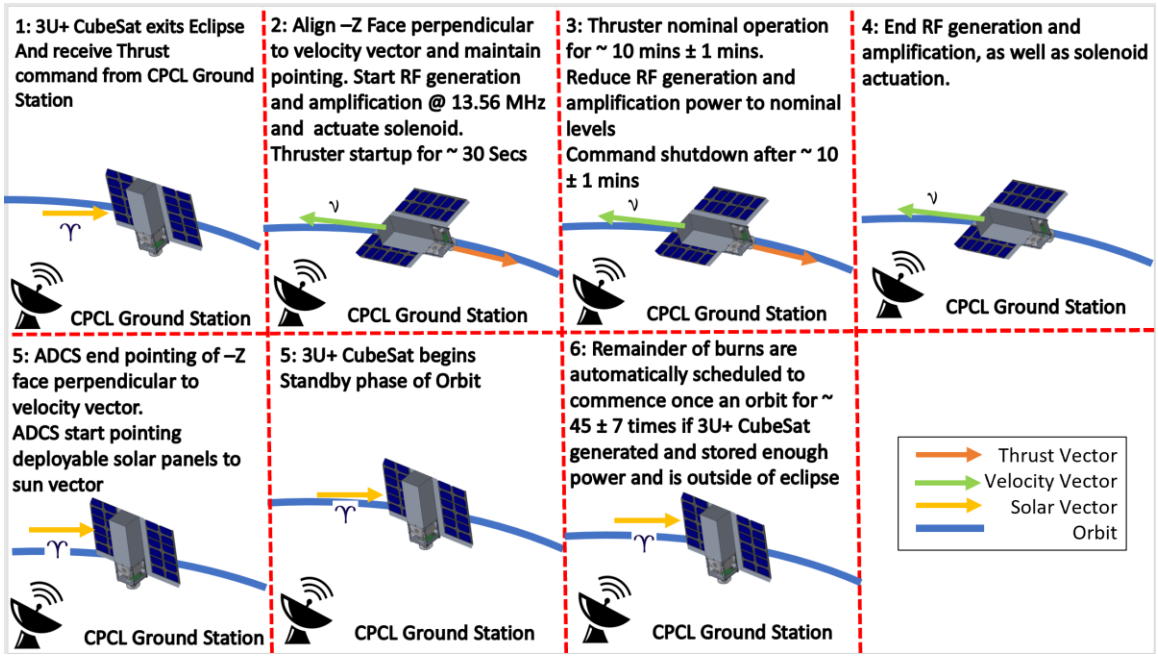

Figure 3.5: Operation of the Propulsion Module

3.1.3 System Budgets

During the Pocket Rocket system demonstration phases, the Propulsion Module is designed to fire once an orbit for ~10 minutes, if power generation and storage requirements are met. The subsystems that must be powered on to accomplish this are the ADCS, C&DH, communications, and propulsion system. The ADCS, C&DH, and communications subsystems are part of the 2U CubeSat under development. Therefore, assumptions for the power draw of these subsystems are based on available CPCL in-house components as well as commercial options to baseline the DC power generation and usage of the spacecraft. The ADCS system was assumed be the BCT XACT-15 that draws a maximum of 5.5 W, during pointing, and 0.5 W when on standby [62]. The BCT XACT-15 is assumed to be at maximum power draw during ignition and nominal operation of Pocket Rocket. The communications system was assumed to be the CPCL in house radio, which requires 0.1 Wdc for Rx, 4 W for Tx, and 0.2 Wdc for standby power [63]. The CPCL radio was assumed to be receiving during Pocket Rocket ignition as well as nominal operation, and then on standby for the remainder of the orbit. The C&DH system was assumed to be a CPCL in-house system board that draws 0.3 Wdc for operation. The system board was assumed to be operating during all phases of the mission. Finally, the Propulsion Module power draw was broken up into three phases, ignition, nominal operation, and standby. Pocket Rocket ignition is required to warm-up the thruster and initiate plasma breakdown. The RF PCB requires 61 Wdc to initiate plasma breakdown of xenon for about 30 seconds and 0.85 Wdc to actuate the Solenoid valve and allow xenon to flow into the chamber. Initiation of plasma breakdown was assumed to be 30 seconds for a worst-case power draw scenario based on inductance matching, electronics actuation, and plasma breakdown in ambient conditions. After the plasma breakdown is started, nominal Pocket Rocket burns will be conducted for about 10 minutes and require 30 Wdc supplied to the RF PCB to maintain plasma breakdown and 0.85 Wdc to maintain actuation of the Solenoid valve. In the standby phase, the propulsion system will require 0.01 Wdc to maintain the RF PCB components. The total average DC power consumption with the addition of a 20%

margin is 6.30 W, which requires about 337.4 cm^2 of solar panel area, and one Li-ion battery to operate the Propulsion Module, as well as defined 2U components, as seen in Table 3.2.

Table 3.2: Power Budget for operation with xenon

Total Average DC Power Consumption + 20 % margin (W)	6.3
Peak DC Power Consumption (W)	66.8
Energy Required During Eclipse (Wh)	3.1
Energy Require During Sun (Wh)	10.1
Total Solar Cell Area (cm^2)	340.0
Total Number of Li-Ion Batteries Required	1.0

The solar cell area and number of lithium ion batteries required was calculated by breaking the power drawn into three separate phases of an orbit by duty cycle. The three phases were the thruster nominal operation, thruster ignition, and standby phases, and constituted 10.8, 0.5, and 89.7 % of an orbit, respectively. The peak power draw was calculated by totaling the overall DC power draw of all functional components by phase. The average power P_{avg} was calculated by multiplying the duty cycle DC (%) by the peak power P_{peak} (W) as shown in Equation 3.1, and multiplied by 1.20 to incorporate a 20% margin.

$$P_{avg} = 1.20 * DC * P_{peak} \quad (3.1)$$

Afterwards all average power consumptions were summed to solve for the total average power consumption with a 20% margin of 6.3 W as shown in Table 3.2. The energy required during eclipse $E_{eclipse}$ (Wh) was then calculated from the total average power consumption P_{tavg}(W) by multiplying with time in eclipse $t_{eclipse}$ (s) as shown in Equation 3.2.

$$E_{eclipse} = t_{eclipse} * P_{tavg} \quad (3.2)$$

Energy required during sun E_{sun} (Wh) was calculated utilizing the time in the sun t_{sun} (s), total average power consumption P_{tavg} (W), total line losses of charging and discharging L_L (%), and energy required during eclipse $E_{eclipse}$ (Wh) as shown in Equation 3.3

$$E_{sun} = t_{sun} * P_{tavg} + \frac{E_{eclipse}}{(1 - \left(\frac{L_L}{100}\right)} \quad 3.3$$

Solar cell total area needed A_{sp} (cm^2) was then calculated with energy required during the sun E_{sun} (Wh), end of life power generation efficiency EOL_{ef} (%), heat flux at the spacecraft orbit c (W/m^2), and time in sun t_{sun} (s) as shown in Equation 3.4.

$$A_{sp} = \frac{E_{sun}}{\left(\left(\frac{EOL_{ef}}{100}\right) * \alpha_{sun} * t_{sun}\right)} \quad 3.4$$

The total battery capacity,E_{Batt}, (Wh) was calculated utilizing the maximum depth of discharge DoD (%), total line losses of charging and discharging L_L (%), and energy required during eclipse $E_{eclipse}$ (Wh), as shown in Equation 3.5.

$$E_{Batt} = \frac{E_{eclipse}}{\left(1 - \frac{L_L}{100}\right) * \frac{DoD}{100}} \quad 3.5$$

Finally, the total number of batteries required, Num_{batt}, was calculated using the total battery capacity required E_{Batt} (Wh), energy density of the batteries $E_{density}$ (Wh/kg), and battery mass $m_{battery}$ (kg) as shown in Equation 3.6. The number of batteries required was rounded up to the nearest whole number. For specific breakdowns of calculations and assumptions made see Appendix C.

$$Num_{batt} = \frac{E_{batt}}{E_{density} m_{battery}} \quad 3.6$$

To demonstrate drag compensation, the system must be able to counteract the lowering of the orbit altitude caused by atmospheric drag. Therefore, the overall 3U+ system must be able to maintain pointing of the -Z face of the CubeSat towards the velocity vector for periods of about 10 min to enable Pocket Rocket to impart delta-V in the intended direction. In addition to pointing the ADCS system must also be able to identify the current orientation of the CubeSat, to align the thrust vector in the velocity vector direction. The Pocket Rocket force vector is assumed to be aligned along the center of mass of the Propulsion Module to limit torque on the 3U+ CubeSat during pointing operations. Additionally, a minimum of 17 m/s of delta-V must be impart in the

velocity vector direction to satisfy mission requirement 1. Therefore, for the purposes of this research, the pointing budget of the ADCS system is dominated by the need to impart the 17 m/s in the intended direction, which corresponds to a pointing budget of ± 43 degrees. The pointing budget limitations highlight that the Propulsion Module is not the driving factor for the 3U+ CubeSat ADCS system, therefor commercial or CPCL in-house designed ADCS systems should be able to meet the necessary performance (Figure 3.6).

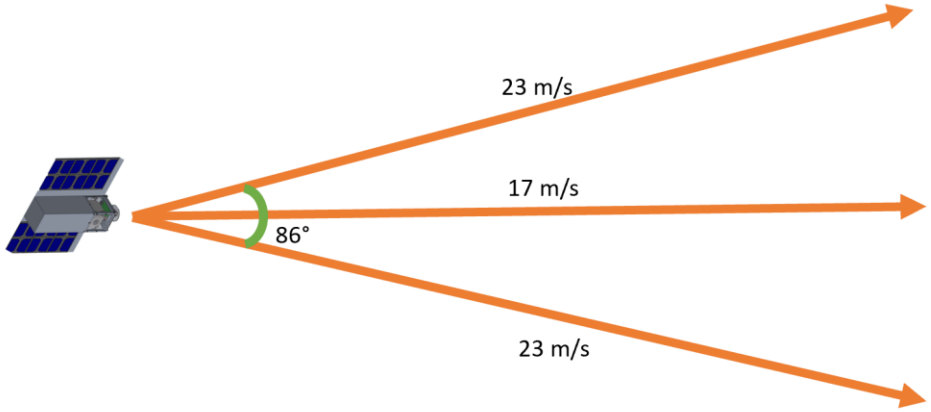

Figure 3.6: 3U+ CubeSat pointing limitations

For this research, the pointing budget was calculated utilizing the geometry of an isosceles triangle, Pythagorean theorem and the law of cosines. The isosceles triangle was assumed to have 23 m/s for the equal side lengths, labeled c, and 17 m/s for the height, labeled b as shown in Figure 3.7.

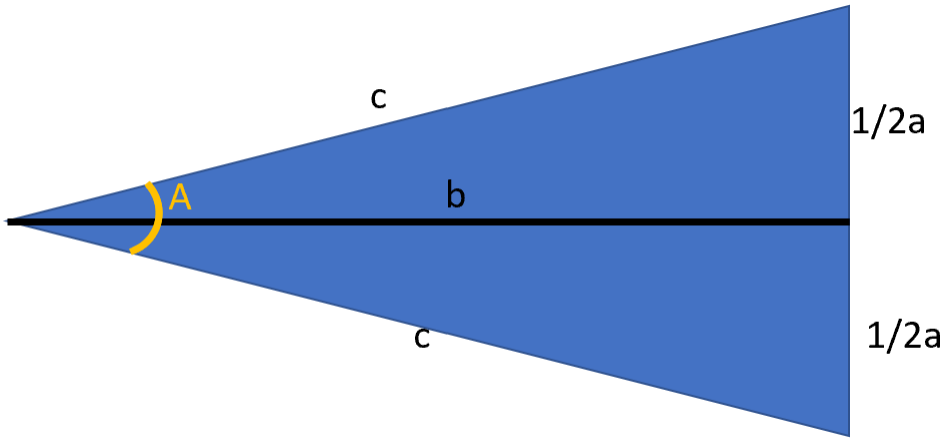

Figure 3.7: Pointing budget geometry calculations

Pythagorean theorem (Equation 3.7) was utilized to calculate one half of side a. Afterwards angle A was calculated utilizing the law of cosines shown in Equation 3.8, which gave a total angle of 86 degrees, and a ± 43 degree pointing budget. Further breakdown of the pointing budget is shown in Appendix C.

$$\left(\frac{1}{2}a\right)^2 + b^2 = c^2 \tag{3.7}$$

$$a^2 = c^2 + c^2 - 2 * c * c * \cos(A) \tag{3.8}$$

3.1.4 Propulsion Module Overview

The flight configuration of the 1U+ Propulsion Module is shown below in Figure 3.8 with transparent side paneling as a reference point for subsequent sections of the research that touch on specific aspects of the design. The Propulsion Module system can impart an estimated 20 ± 3 m/s of delta-V with xenon when integrated into an overall 3U+ CubeSat form factor. The Propulsion Module specifications are shown in Table 3.3**Error! Reference source not found.**. The system incorporates RF amplification, electrical components, propellant storage, pressure

regulation, but cannot incorporate the PIB, which is assumed to be integrated into the 2U CubeSat.

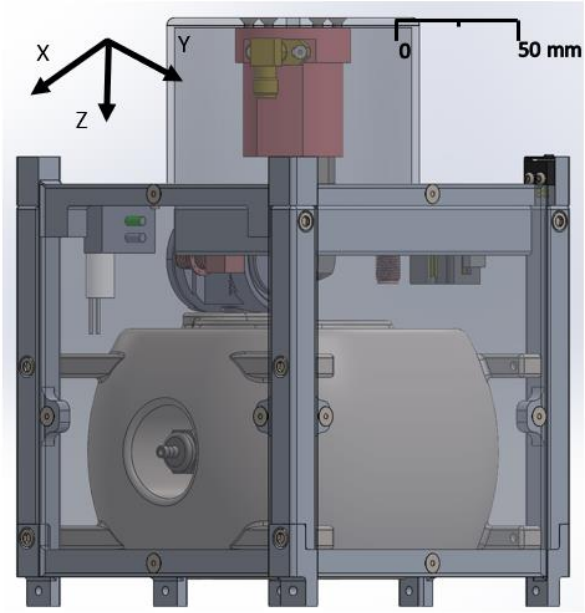

Figure 3.8: Propulsion Module Isometric CAD View

Table 3.3: Propulsion Module Size Weight and Power

Envelope (cm)	15.0 x 10.0 x 10.0
Total Mass (kg)	2.3
Average Power Consumption (Wdc)	6.3
Estimated delta-V (m/s)	20.0 ± 3

Pocket Rocket is a RFET thruster assumed to operate at a thrust of 2.4 mN, and an ISP of 70 seconds with argon propellant [49]. Pocket Rocket requires the usage of an RF PCB that has a maximum DC power draw of 60 Wdc and an electrical efficiency of 50 %. The propellant storage volume will have a MEOP of approximately 21 MPa. The propellant storage volume safety factor must be larger than 1.5 as defined by AFSCMAN91-710. The system will be able to support Pocket Rocket continuously thrusting for 10 ± 1 min for a total of 45 ± 7 operations. A general overview of the system with the definition of its key parameters is presented in

subsequent sections alongside the internal layout, propellant volume design, component selection, as well as mechanical and electrical interfaces.

3.1.5 3U+ CubeSat Overview & Recommendations

The overall 3U+ CubeSat integrates the Propulsion Module on the -Z face of the 2U. The Propulsion Module is mounted to the 2U railing and boot through six #4-40 socket head cap screws. The mass of the Propulsion Module is 2.31 kg, with a center of mass that is 61 cm from the -Z face of the Propulsions Module. The 3U+ CubeSat system mass is expected to be between 4 – 6 kg depending on the on the components within the 2U spacecraft, with a center of mass that is within ± 7 cm of the geometric center as specified by the CDS rev. 13 [7]. The power required to operate the Propulsion Module necessitates approximately 340 cm^2 of solar paneling, therefore it is recommended that the 3U+ system have deployable solar panels with cells on both sides of the paneling as shown in Figure 3.9. The overall envelope of the 3U+ system shall be 39.5 cm x 10.0 cm x 10.0 cm. An example of the deployed configuration the 3U+ system is shown in Figure 3.9.

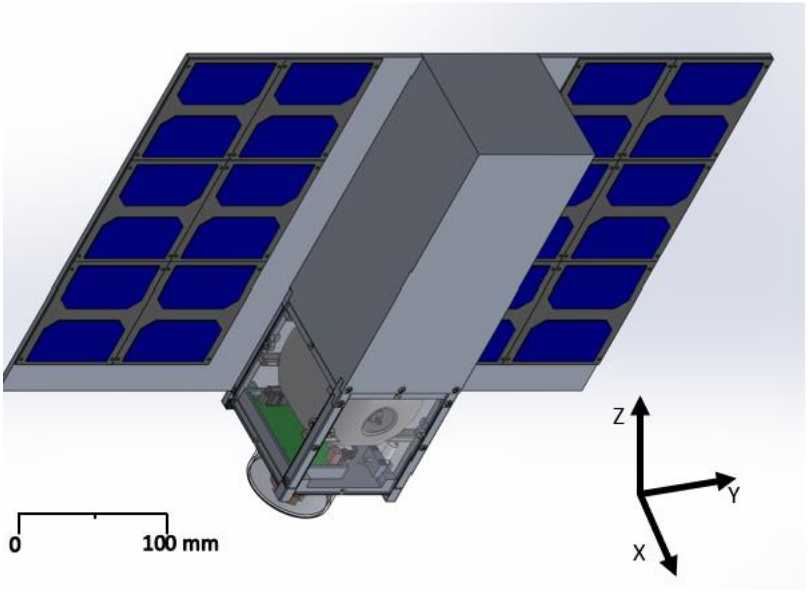

Figure 3.9: 3U+ Overall System w/ Solar Panel deployed

3.2 Design Development

The Propulsion Module detailed design is presented in this section, showcasing SWaP as well as key design decisions. This section will cover, the Propulsion Module structure, propellant choice for Pocket Rocket, an overview of Pocket Rocket, the plumbing and electrical system designs, and pressure vessel design.

3.2.1 Propulsion Module Structure

The first step in designing the Propulsion Module was to create an overall structure that houses all the Propulsion Module components, as well as mechanically interfaces with the 2U CubeSat. The Propulsion Module was designed to adhere to the dimensions of a 1U+ CubeSat, with a Tuna Can attached on the -Z face. Therefore, the overall volume was baselined at 100 mm x 100 mm x 149 mm. The previous design of the Propulsion Module had a dry mass of 1.9 kg, added system mass negatively affects the overall delta-V, therefore a target dry mass of about 1.5 kg was selected to increase the overall delta-V by 0.4 m/s as shown in Figure 3.10.

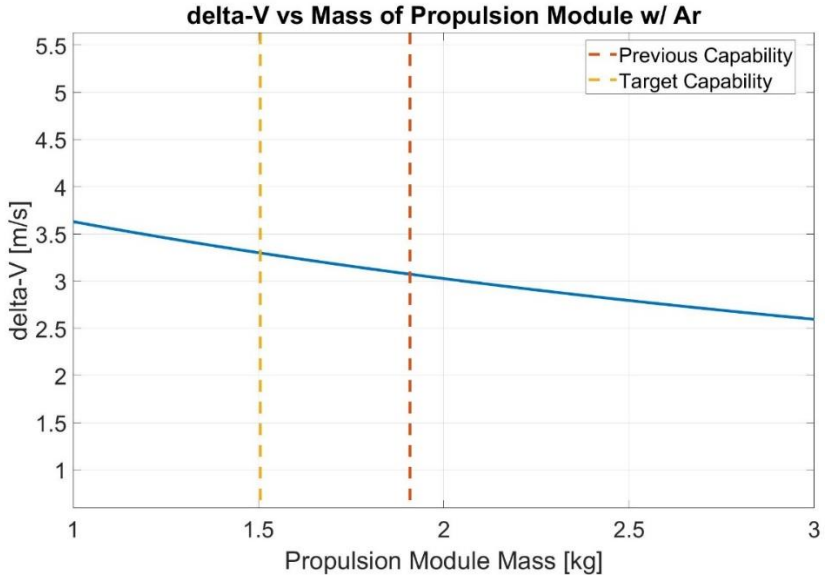

Figure 3.10: delta-V values with increasing overall mass of the Propulsion Module

The design of the Propulsion Module structure incorporates five main components, the Side Rails, Boot, Top Hat, Tuna Can, and Side Panels. The main structural components as well as side rails of the CubeSat must be made from Aluminum 7075, 6061, 5005, and/or 5052, as per the CDS Rev. 13 [7]. This research will utilize Aluminum 7075-T6 for the main structural components as well as Side Rails, due to the CPCL ME teams manufacturing and design experience with the material. The Tuna Can, as specified by the CDS Rev. 13 is allowed a maximum height of 36 mm past the Side Railing, with a diameter no greater than 64 mm, centered on the -Z face of the 3U+ CubeSat [7]. Therefore, the Propulsion Module Tuna Can has an external diameter of 64 mm centered on the Top Hat -Z face, an internal diameter of 60 mm height of 35.5 mm from the railing and weighs 73 grams. The Tuna Can is attached to both Pocket Rocket and the Top Hat as shown in Figure 3.12. Pocket Rocket is attached on the internal side with four #2-56 Flat Hex Screws, with the outlet of Pocket Rocket pointing in the -Z direction. The Tuna Can is also attached to the Top Hat with four #2-56 Flat Hex Screws on the -Z face of the CubeSat.

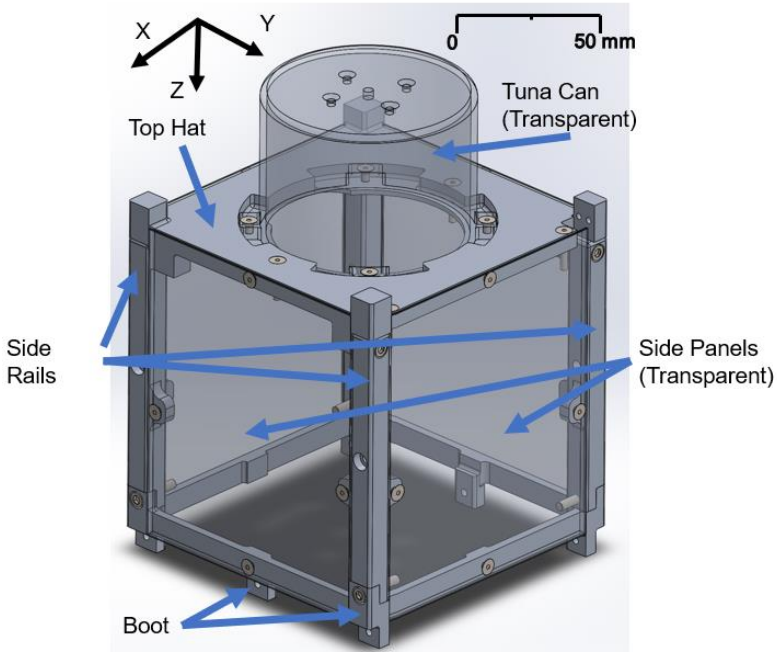

Figure 3.11: Propulsion Module components

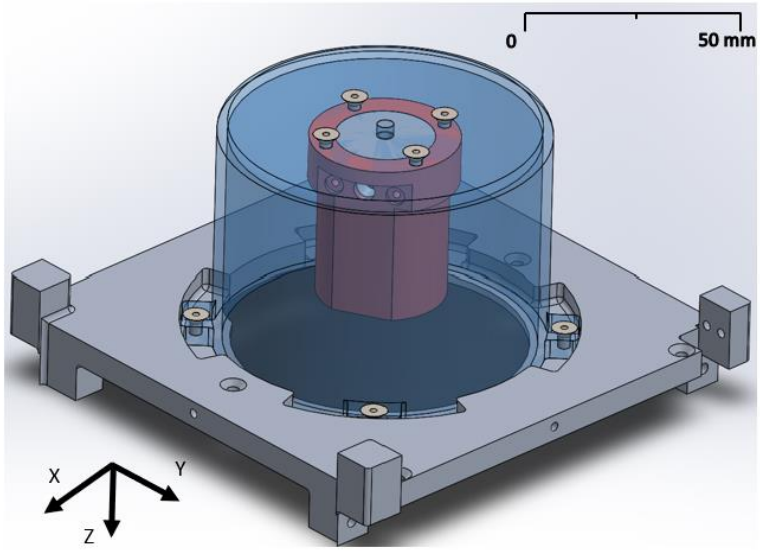

Figure 3.12: Pocket Rocket Tuna Can highlighted in blue attached to the Top Hat, as well as Pocket Rocket

The Top Hat is another key structural aspect of the Propulsion Module and attaches to the Tuna Can, Side Paneling, Side Railing in addition to various Pocket Rocket functional components. The Top Hat has an overall envelope of 100 mm x 100 mm x 2.5 mm as seen in Figure 3.13 and has a total weight of 99.4 grams. To satisfy the Side Railing requirements of the CDS Rev. 13, the aluminum railing on the Top Hats -Z face extend out 7 mm to allow for interfacing with the CubeSat deployer. The Top Hat attaches to the Tuna Can with four #2-56 thru holes on the -Z face, the Side Railing attachment is accomplished via four #4-40 tapped holes on the ±Y faces of the Top Hat. Finally, the Top Hat attaches to the Side Paneling via four #2-56 tapped holes in the ±X as well as ±Y directions.

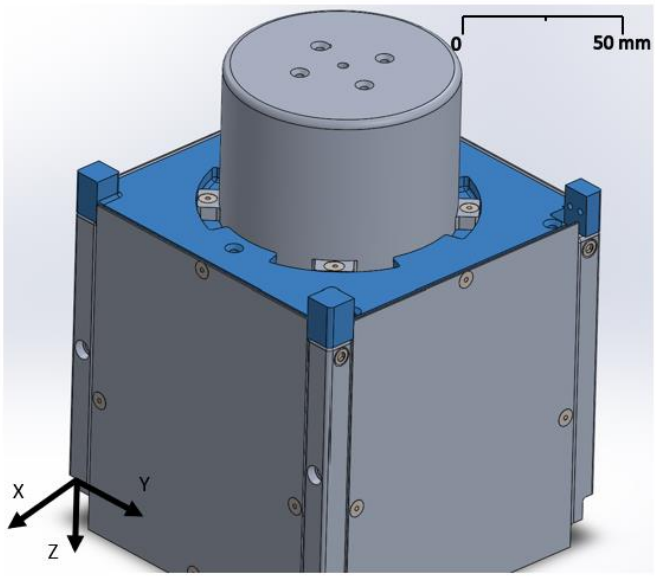

Figure 3.13: Propulsion Module Top Hat highlighted in blue attached to the Side Paneling, Side Rails, as well as Tuna Can

The Side Rails are the primary structural component that attach structural as well as Pocket Rocket functional components together. The Side Railing must maintain a 75% surface contact with the deployer railing, a minimum width of 8.5 mm, a surface roughness of less than 1.6 μm, and have 1 mm filleted corners. There are four Side Rails included in the Propulsion Module design, each of which connect to the Top Hat, Side Paneling, and Boot. As shown in Figure 3.14, the overall envelope of each individual Side Rail is 8.5 mm x 8.5 mm x 87.5 mm with 1 mm fileted external corners and each Side Rail weighs 34.4 grams. The connection to the Top Hat incorporates four #4-40 socket head cap screw thru holes on the ±X faces of the CubeSat structure. Connection to the Boot is accomplished with four #4-40 thru holes on the ±Y faces of the CubeSat structure, that also connect to the thru #4-40 thru holes of the pressure vessel. Side Paneling is attached by two #2-56 flat hex screw thru holes on the corners of each Side Rail.

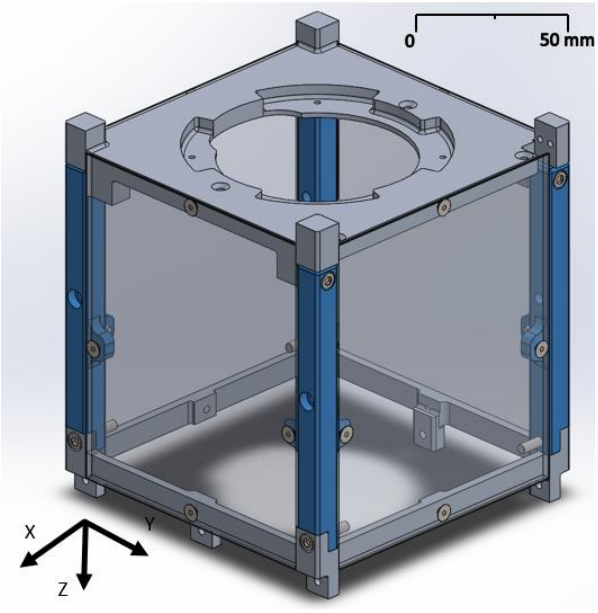

Figure 3.14: Propulsion Module Side Railing, highlighted in blue, connected to the Top Hat Boot, and Side Paneling

The Boot of the CubeSat is designed to connect the Side Rails, Side Paneling, as well as the 2U CubeSat rails that mate with the Propulsion Module. The overall envelope of the Boot is 100 mm x 100 mm x 21 mm as shown in Figure 3.15, and weighs a total of 31.4 grams. The Boot has four #4-40 thru holes on the ±X face of the CubeSat that allow for attachment to the Side Rails as well as the pressure vessel. The Side Paneling is attached on the ±X as well as ±Y face via four #2-56 thru holes. Finally, the Boot is designed to mechanically interface with the 2U CubeSat by six #4-40 thru holes attached to the 2U structure.

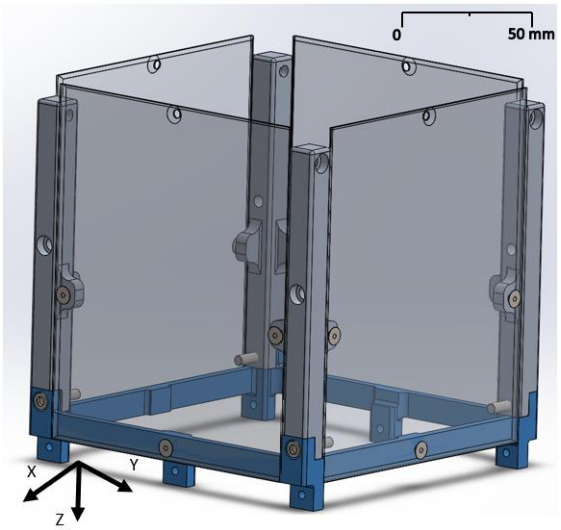

Figure 3.15: CubeSat Boot highlighted in blue, attached to the Side Rails as well as Side Paneling

The final part of the CubeSat structure are the four Side Panels designed to reduce thermal stresses on internal subsystems, as well as act as staking areas for securing the plumbing tubing, and electrical cabling. As shown in Figure 3.16, the four Side Panels have an overall envelope of 83 mm x 1.5 mm x 100 mm and weigh 34.8 grams each. The Side Panels attach to the Top Hat, Side Rails, and Boot with four #2-56 thru holes on the ±X, and ±Y faces of the CubeSat structure.

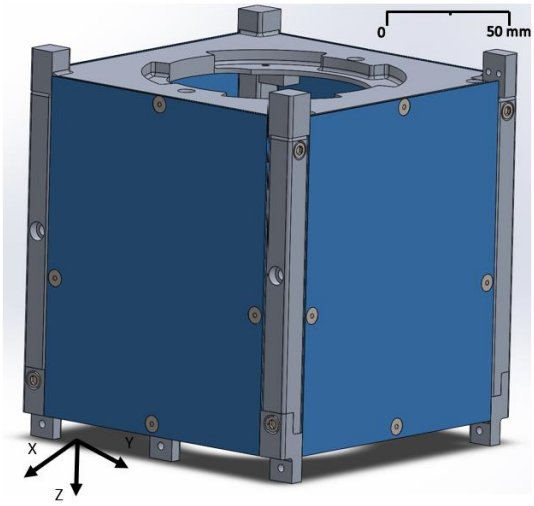

Figure 3.16: CubeSat Side Paneling highlighted in blue, and attached to the Boot, Top Hat, Side Railing

The overall mass of the structure is 480.6 grams and adheres to the specifications laid out within the CDS Rev. 13, while also providing a mechanical interface for the Propulsion Module to attach with the 2U CubeSat. The overall envelopes and mass estimates for each structural component is shown below in Table 3.4. The mechanical connections between components are showcased further in Appendix D.

Table 3.4: Overall Size and Weight of the Propulsion Module Structure

Component Name	Quantity Required	Envelope (mm)	Weight (grams)
Tuna Can	1	L: 35.5 Ø: 64.0	73.0
Top Hat	1	100.0 x 100.0 x 2.5	99.4
Side Rails	4	8.5 x 8.5 x 87.5	34.4
Boot	1	100.0 x 100.0 x 21.0	31.4
Side Paneling	4	83.0 x 1.5 x 100.0	34.8

3.2.2 Pocket Rocket Propellant Choice

To improve the usefulness of the Propulsion Module in orbit, the choice of propellant that will be utilized by Pocket Rocket is critical. Pocket Rocket's thruster performance has been characterized with three separate propellants: argon, nitrogen and xenon [49,64]. Therefore, a trade study that compared the delta V, thrust, input RF power, and estimated cost per liter information was used to determine the best propellant choice for the considered mission. Delta-V is weighted the highest as, a larger delta-V will allow for additional mission capabilities. Propellant price per liter is weighted as the second most important criteria, as this is an internal development project, so mission cost is critical. Finally, thrust is weighted as the least important alongside Power input, as the Propulsion Module is not forced to impart a large amount of momentum in a

short amount of time, a lower thrust can be substituted with longer operational times. Power input is weighted as the lowest because the mission timeline is not time critical and waiting longer for the appropriate power generation and/or storage is not an issue. However, power generation for a CubeSat is limited by power generation options, therefore power input still carries some weight in this trade study. The weighting criteria of the propellant trade study is shown below in Figure 3.17.

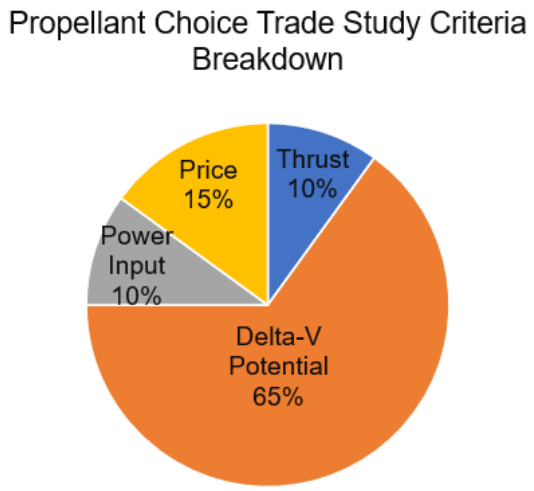

Figure 3.17: Propellant choice trade study criteria

The most important parameter for this research was achieving a delta-V larger than 15 m/s as this allows the technology demonstration mission the flexibility to target multiple different mission maneuvers as shown in Table 1.1. Delta-V was calculated by assuming a constant storage temperature and pressure of 285 K and 8.27 MPa (1200 PSI), for the approximation of storage density for each propellant based on National Institute of Standards and Technology (NIST) data. The mass of the propellant was then calculated using a constant storage volume of 180 cm^3 based on the previous version of the Propulsion Module design and the storage density of each propellant considered in the trade study. The ISP, (ISP), (s) mass of propellant, m_{prop}, (kg) and gravity, g, (m/s^2) was used to calculate total impulse, I_t, (Ns) of each propellant with Equation 3.9.

$$I_t = ISPm_{prop}g \tag{3.9}$$

Then, the inert mass fraction ,f_{inert}, of the overall 3U+ CubeSat was calculated for each propellant mass with Equation 3.10. The dry mass of the overall 3U+ CubeSat, $m_{CubeSat}$, (kg) was assumed to be 4.32 kg, 2.32 kg for the Propulsion Module and 2 kg for the remainder of the CubeSat.

$$f_{inert} = \frac{m_{CubeSat}}{m_{CubeSat} + m_{prop}} \tag{3.10}$$

Finally, the total impulse, ISP and inert mass fraction of each propellant were utilized alongside gravity, and dry mass of the CubeSat, to calculate the total achievable delta-V ,ΔV, (m/s) as shown by Equation 3.11. This delta-V value was then compared between each propellant type to weigh them within the trade study.

$$\Delta V = I_{sp} g ln\left(\frac{\left(I_t + I_{sp} g m_{CubeSat}(1 - f_{inert})\right)}{I_t f_{inert} + I_{sp} g m_{CubeSat}\,(1 - f_{inert})}\right) \tag{3.11}$$

Thrust as well as input RF power were obtained from relevant publications by A. Greig, C. Charles, and R. W. Boswell [49,65]. Estimated costs per liter of High Purity (>99%) concentration propellant in a Dewar for each gas were received from AirGas.

Thrust, delta-V, input RF power, and cost estimates that were utilized in the trade study are shown in Table 3.5. The overall results of the trade study shown in Figure 3.18, indicate that xenon is the ideal propellant to focus on for the purposes of this research. Utilizing xenon as a propellant increases the delta-V from previous iterations of the Propulsion Module by upwards of 500 %. As a backup for xenon, if cost is determined to be prohibitive, argon is a good alternative choice due to decreased cost and input power, alongside increase thrust, however, the decrease in delta-V generated will negatively impact the capabilities of the proposed mission. An overview of the propellant trade study can be seen in Appendix E

Table 3.5: Pocket Rocket propellant performance parameters

	Thrust (mN)	Delta-V (m/s)	ISP value utilized for Delta-V calculations	Input RF Power (Wr)	Estimated Cost per liter (USD)
Argon	2.4	2.9	70.0	10.0	0.2
Nitrogen	3.0	1.5	55.0	10.0	0.2
Xenon	1.0	15.7	30.0	32.5	6.4

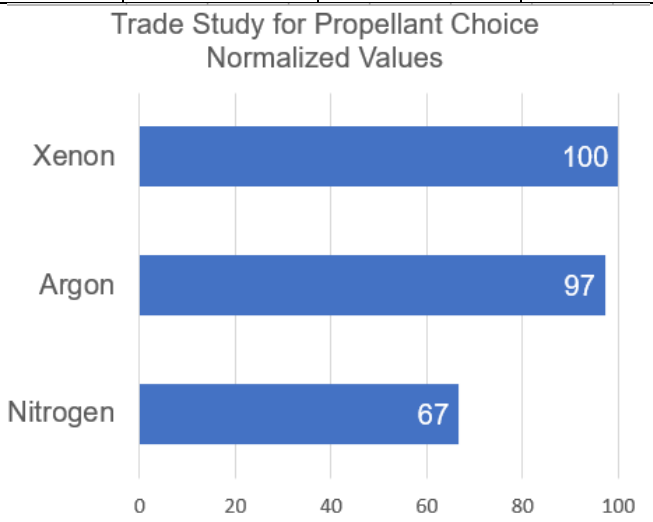

Figure 3.18: Propellant trade study results, with normalized values

3.2.3 Pocket Rocket Overview

The Pocket Rocket thruster has a length of 33 mm, and a diameter of 29 mm as shown in Figure 3.19, with an overall mass of 36 grams [29]. The Pocket Rocket thruster has four #2-56 tapped holes to attach to the Tuna Can, as well as two #0-80 tapped holes for attaching the RF antenna shown in bronze color in Figure 3.19. On the -X side of Pocket Rocket, a 10-32 thru hole is highlighted in blue, which serves as the propellant inlet.

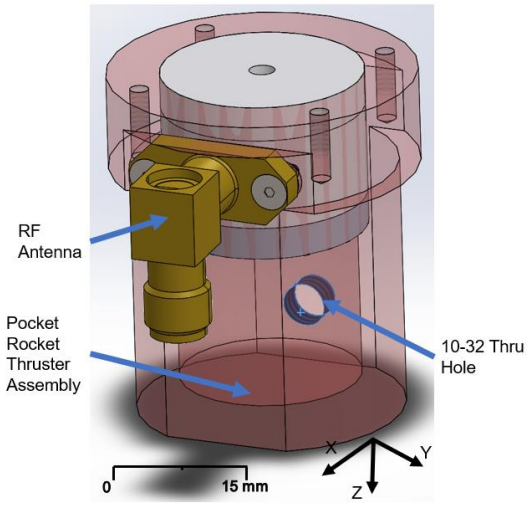

Figure 3.19: Pocket Rocket Thruster, with internal disks and SMA-Antenna right angle connection

There are four internal disks shown in Figure 3.20, that are made of Aluminum, Copper and two from Macor. The Aluminum disk serves as the interface between the propellant inlet area, and the insolated Macor area. The Copper disk receives energy from the RF antenna inlet area shown on the right image of Figure 3.20 and conducts RF energy and heat into the central excitation area allowing for the generation of a plasma. The External Macor disk act as an insulator, slowing the rate at which the RF energy and heat is expelled from the Pocket Rocket housing. The Internal Macor disk, surrounds the Copper disk as shown in Figure 3.20, and further helps to insulate the RF energy and heat generated in the formation of plasma. The Macor disks are important to ensure that heat remains internal to the Pocket Rocket thrust chamber to increase the exhaust velocity of the propellant.

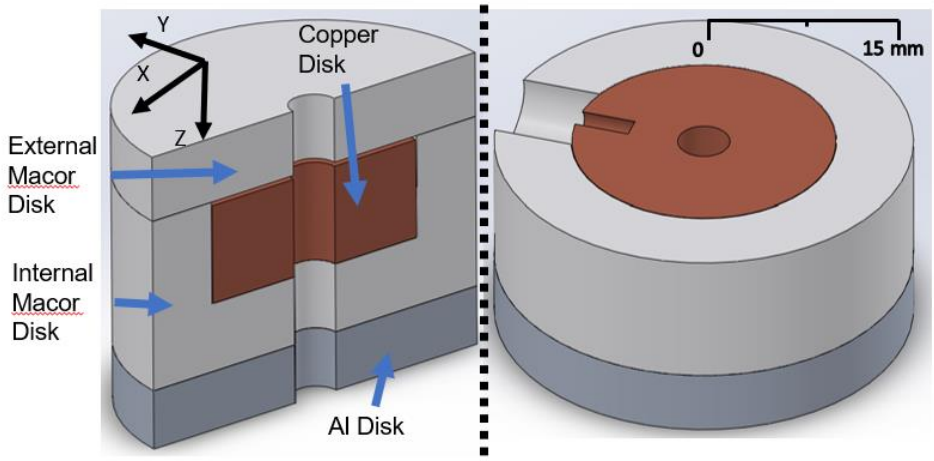

Figure 3.20: a) Sectioned view of Internal Disks of Pocket Rocket and b) Internal Disks of Pocket Rocket

3.2.4 Pressure Vessel Design & Plumbing Component Selection

After xenon was selected as the propellant, the pressure vessel storage capacity and the storage pressure were investigated. The initial storage pressure of the previous flight iteration was designed to be around 8.27 MPa (1200 PSI), with a volume of approximately 180 cm^3 available for propellant. The storage volume and pressure would allow for a maximum estimated delta-V of 15.67 m/s with xenon as calculated with Equation 3.11. In order to improve upon the capabilities of Pocket Rocket and increase the delta-V of the Propulsion Module, three driving parameters were investigated: 1) the mass of the system, 2) the storage pressure of the system, and 3) the storage volume of the system. The storage pressure of the pressure vessel was the first aspect to be investigated from the prior Propulsion Module design. In prior Propulsion Module iterations, the pressure vessel design was designed to store 8.27 MPa (1200 PSI) at a non-justified factor of safety of 4, whereas a factor of safety of 1.5 is the minimum requirement [22]. The new pressure vessel targets a MEOP of 20.68 MPa (3000 PSI) to increase the estimated delta-V of the Propulsion Module system by about 3 m/s to a total theoretical delta-V of 18 m/s, as seen in Figure 3.22. The target of 20.68 MPa (3000 PSI) was chosen as most commercial plumbing systems that are applicable to CubeSat SWaP limitations have a MEOP of 20.68 MPa

(3000 PSI), and CPCL does not currently have the capability to manufacture high pressure plumbing components.

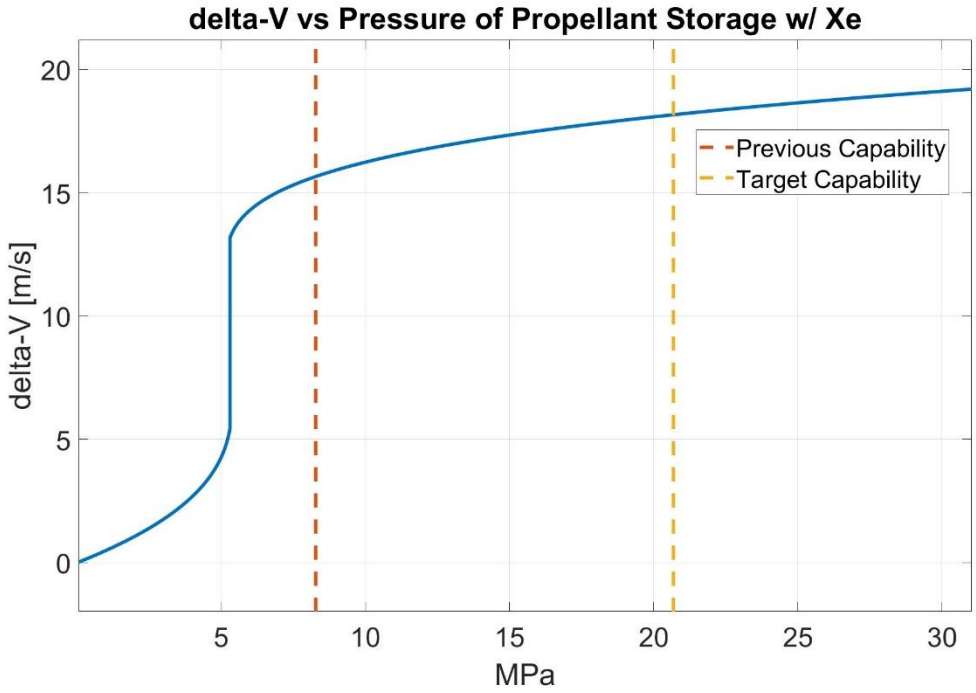

Figure 3.21: Delta-V values with increasing propellant storage pressure

After the pressure of the pressure vessel was increased, the storage volume was the next parameter to be investigated. As seen in Figure 3.22, increasing the storage volume increases the delta-V of the Propulsion Module system at a faster pace than increasing the MEOP. However, the size available within the 1U+ Propulsion Module is limited, with the plumbing components, electrical components, Pocket Rocket, as well as structural components all needing to fit into the 1,116 cm^3 structural envelope. A target to increase the internal area by 40 cm^3 was established to increase the estimated delta-V by approximately 3 m/s from 16 m/s to 19 m/s. The 40 cm^3 target was chosen based on the overall internal space available in the structure of the previous pressure vessel design, as well as changes to the overall shape of the pressure vessel design.

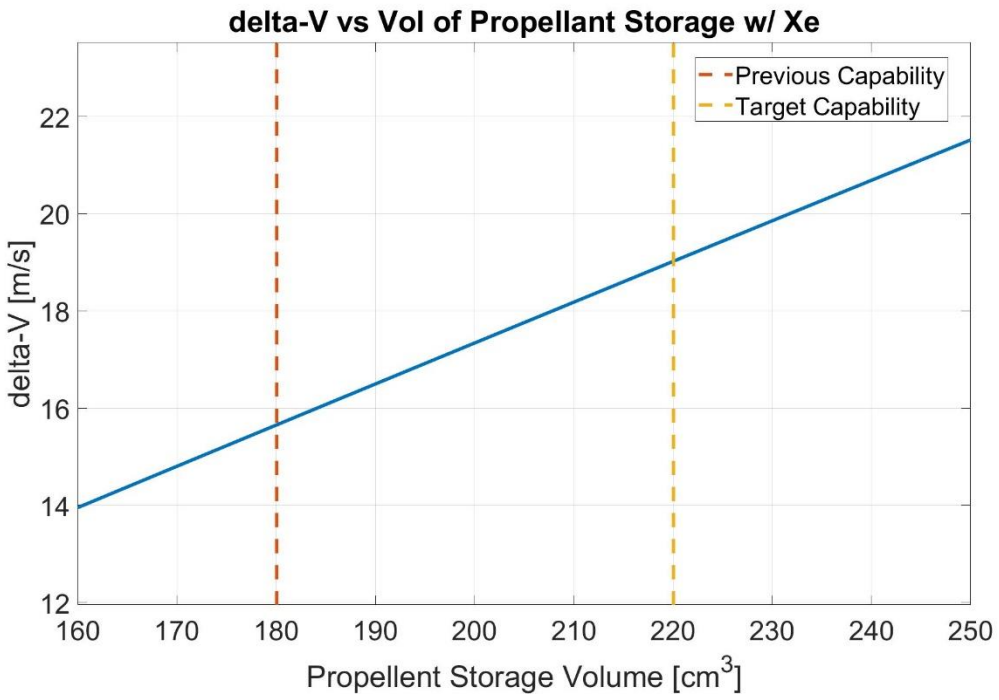

Figure 3.22: Delta-V values with increasing internal storage volume

Combining, increases in the storage pressure and storage volume enables a total theoretical delta-V of the system to about 20 ± 3 m/s. After target values for the key performance parameters of the pressure vessel were established, the physical design had to be developed. The primary driving parameters for the physical design, were the space available, plumbing, and structural interfaces, manufacturing method, as well as material selection.

Pocket Rocket operates between 0.27 - 0.62 kPa, therefore the plumbing system must be able to start at 20.68 MPa (3000 PSI) and regulate the pressure to operational ranges, control the flow of propellant, and allow for the pressure vessel to be filled or vented manually. A Piping and Instrumentation Diagram (P&ID) is shown in Figure 3.23 to highlight the solution proposed for this research that accounts for the SWaP available to CubeSats while ensuring key characteristics needed for operation of Pocket Rocket.

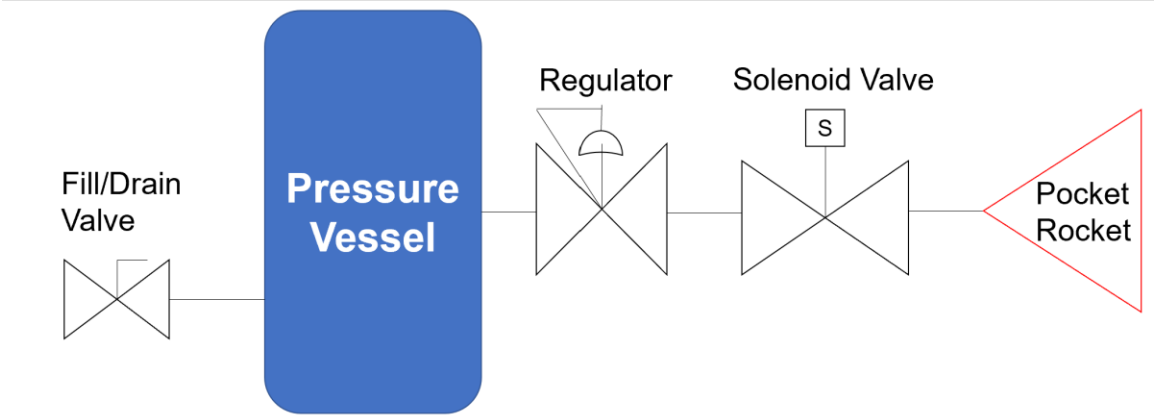

Figure 3.23: P&ID of the Propulsion Module

To manage inlet pressures for Pocket Rocket, the approach chosen was the utilization of a regulator that reduces inlet pressures from the pressure vessel of 20.68 MPa (3000 PSI) to a lower outlet pressure between 0 – 0.3 MPa (0 – 40 PSI). The regulator must fit within the size and weight limitations of the 1U+ Propulsion Module as well as be able to handle 20.68 MPa (3000 PSI) inlet pressure. The Beswick PRD3HP Three-Stage High Pressure Diaphragm Regulator is one component that can solve this problem. The PRD3HP has a maximum inlet pressure of 20.68 MPa (3000 PSI) and is ideal for applications where the regulator is directly connected to the pressure vessel. Additionally, due to the frictionless design of Beswick's diaphragm style regulators, this component is well suited for low pressure regulation around 3.45 kPa [66] with constant outlet pressure despite changes in the inlet pressure. Finally, the PRD3HP shown in Figure 3.24 further fulfills size and weight limitations, with an overall envelope of 27 mm in diameter and 35 mm in length as well as an overall mass of 76 grams. The regulator has a ¼-28 threaded inlet port, as well as a 10-32 threaded outlet port to connect to other components [66]. To connect the regulator to the pressure vessel, MN-1414, a ¼-28 male thread to ¼-28 male thread adaptor was attached to the inlet of the regulator, as well as the outlet of the pressure vessel.

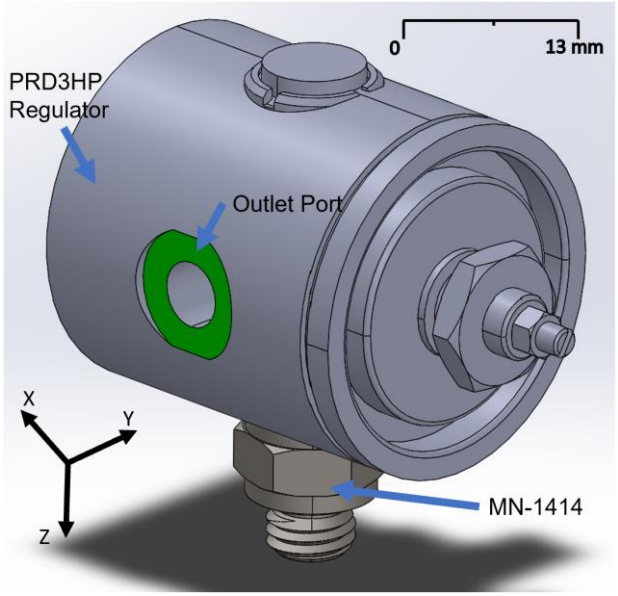

Figure 3.24: Beswick PRD3HP Regulator with outlet port highlighted in green attached to the MN-1414 male-male thread adaptor

To enable commanded actuation of the Pocket Rocket thruster, a valve must also be incorporated into the design that can be shut on and off remotely. A Solenoid valve was chosen for this application as it allows the valve to be electrically commanded to open during operation of the Pocket Rocket and remain closed during standby phases. The Solenoid valve that was chosen for this design is a Lee Co. LHDB0352115H two-port face mount valve. This valve pulls a maximum of 0.85 W of DC power during actuation and is nominally closed until power is activated [67]. The Solenoid valve attaches to a two-port manifold, which has an inlet and outlet port to allow for the propellant to come in and then be expelled from the system to the Pocket Rocket thruster. The overall envelope of the Solenoid assembly is 20.2 mm x 19.1 mm x 32.4 mm with an overall mass of 6 grams (Figure 3.25).

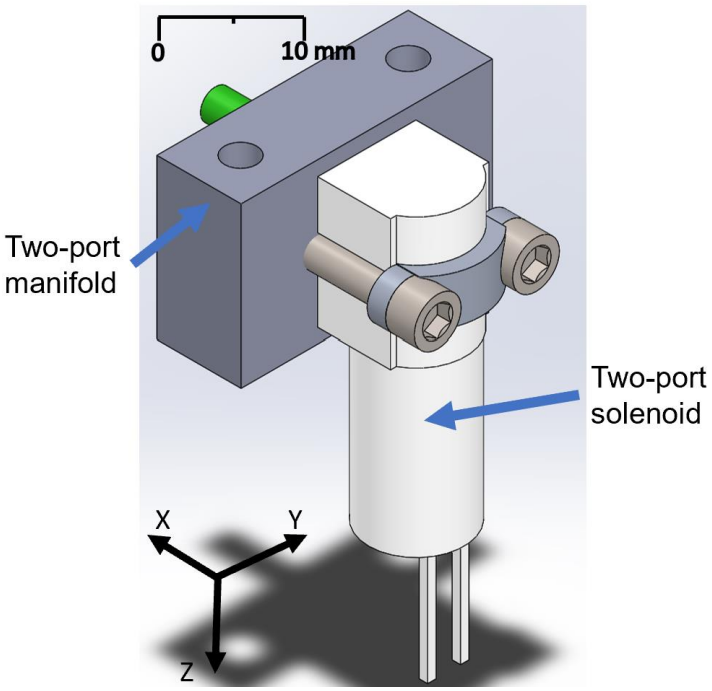

Figure 3.25: Lee Co. Two-port Face Solenoid Valve pictured with outlet highlighted in green

The fill & drain valve is the final functional component that will need to be incorporated into the Propulsion Module. This valve will interface directly with the propulsion tank to allow for the manual loading, venting, and propellant draining from the tank without operation of the thruster. The valve selected for this design is the Cobham miniature service valve that is tailored for small satellite propulsion systems where SWaP and cost are limited. The overall envelope of this valve is 41.3 mm in length and 19.1 mm in diameter as shown in Figure 3.26, with an overall mass of 32 grams. The valve has a 9/16 – 18 threaded inlet to interface with the propellant tank and has a maximum leak rate of 1E-5 cm^3/s [68].

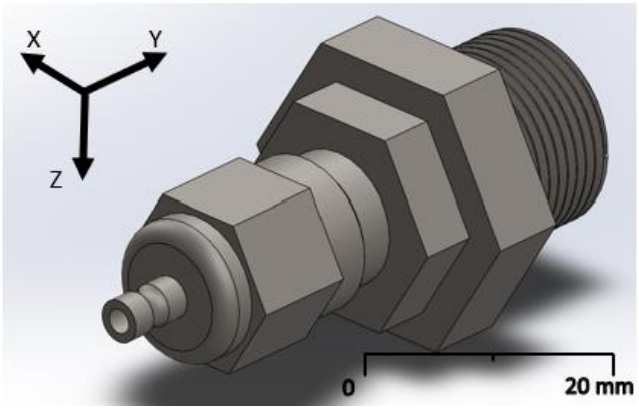

Figure 3.26: Cobham Miniature Service Valve

Connections between each of the plumbing components are accomplished by MTT-1018 Teflon tubing that is secured using compressive fittings and tubing inserts that maintain the structure of the tubing while compressed to not choke the flow of propellant. The estimated overall length of tubing needed is approximately 270 mm to ensure no restrictions in flow and secure attachment to the structure of the Propulsion Module. The compression fittings that were chosen for the Propulsion Module are the Beswick MCB-1018 and MCBL-1018, both of which are designed to interface with the MTT tubing. The MCB is a straight compression tubing component that has a 10-32 thread to allows its attachment to the regulator on one side and have the MTT tubing attached on the other side. The envelope of the MCB-1018 is 19.4 mm in length and 10.8 mm in diameter as shown in Figure 3.27, and weighs a maximum of 7.8 grams. The MCBL-1018 is the elbow joint version of the MCB-1018 and has an overall envelope of 42.3 mm in length and 12 mm in diameter as shown in Figure 3.28 and weighs a maximum of 11.2 grams. The MCBL connects to Pocket Rocket's propellant inlet with a 10-32 thread, and provides a compression fit to the MTT tubing on the opposite side.

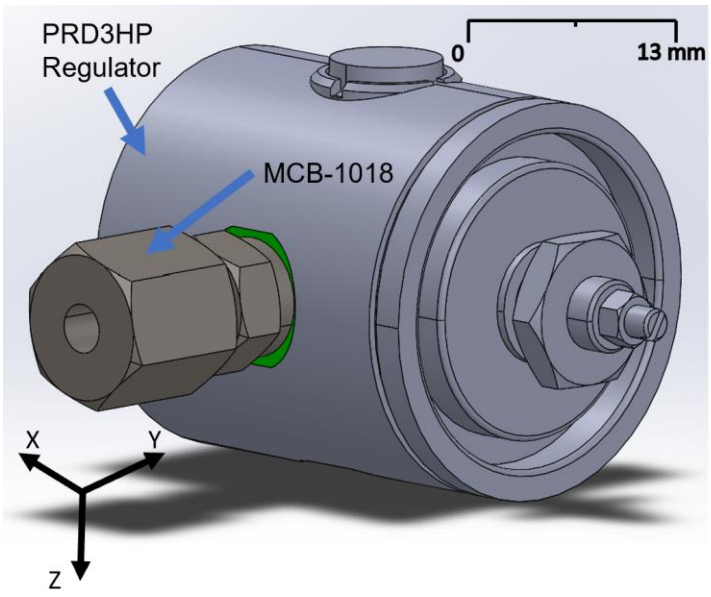

Figure 3.27: MCB-1018 attached to the PRD3HP regulators green outlet face

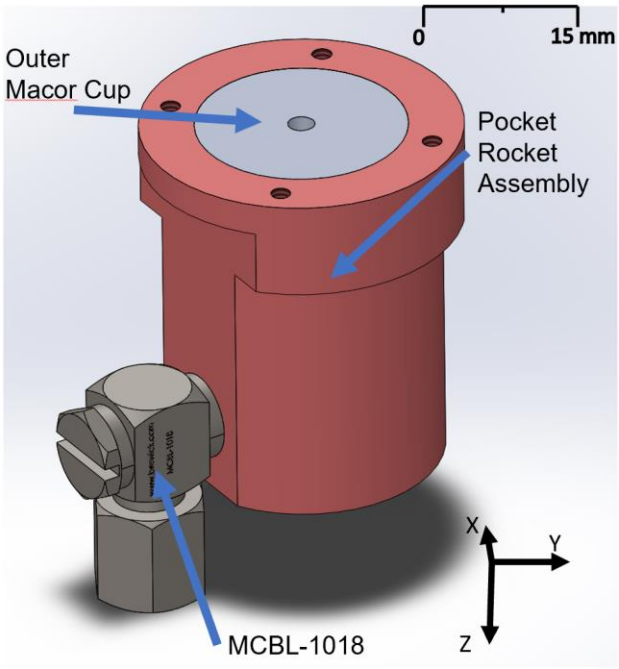

Figure 3.28: MCBL-1018 attached to the Pocket Rocket thruster propellant inlet

After the plumbing components and layout were established, an estimated maximum envelope of the pressure vessel of 88 mm x 88 mm x 58 mm was established as shown in Figure 3.29. Additionally, the pressure vessel must be able to be filled, vented, and drained without

major de-integration of the Propulsion Module. Therefore, for the purposes of this design, it is assumed that the pressure vessel shall fill, vent, and drain from the + X side.

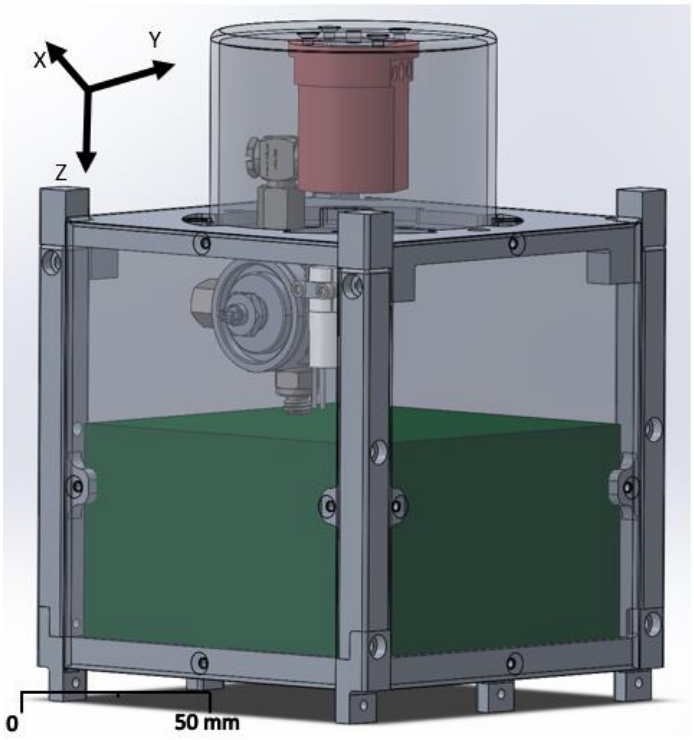

Figure 3.29: Pressure Vessel maximum size (highlighted in green)

To allow for geometry that maximizes the space available for the pressure vessel and demonstrates an alternative manufacturing capability for the CPCL, 3D printing of the pressure vessel was explored. At Cal Poly, the Industrial & Manufacturing Engineering (IME) department has access to a Stainless Steel 316L 3D printer that is capable of printing structures with overall envelopes that can range up to 100 mm x 100 mm x 200 mm. Therefore, the design of the pressure vessel baselined SS316L as the material that would be utilized. An issue that occurs in 3D printed metal selected laser melting (SLM) assemblies is the need to print additional support structures that can conduct away heat generated during printing. The IME department's printer prints the thermal support structures in 316L SS; therefore, after 3D printing they must be removed through traditional manufacturing techniques available at Cal Poly. An example of the support structures is shown in Figure 3.30. The support structures would severely limit the

amount of propellant available to the pressure vessel, which would decrease the delta-V of the system.

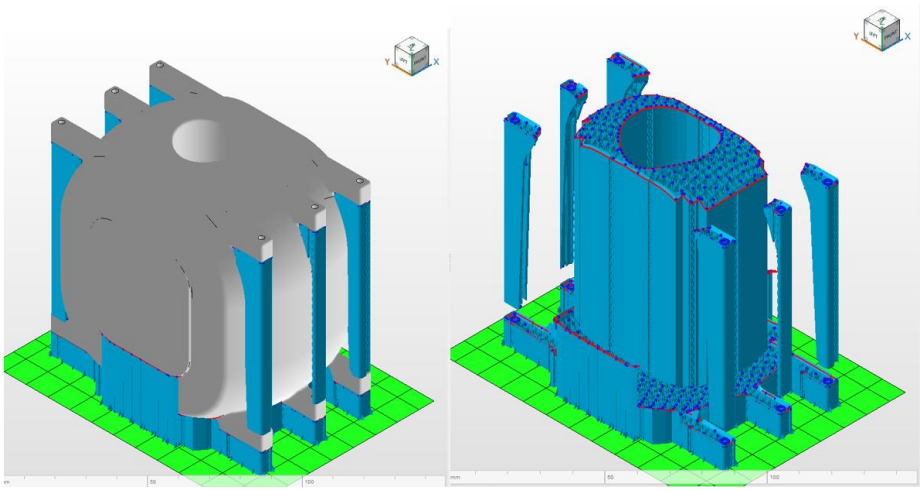

Figure 3.30: a) Example of thermal support structures in 3D printed SS316L part with part included and b) Example of thermal support structures in 3D printed SS316L part without part included

Therefore, this research proposes printing the pressure vessel in two separate parts and then welding the components together. The part would be split 16 mm below the top of the part as shown in Figure 3.31 and Figure 3.32. Printing of the part in two pieces would allow for the machining as well as finishing of each component to remove the support structures, and ensure desired propellant capacity is reached. The stainless-steel components would be welded together with an Electron Beam (EB) or Tungsten Inert Gas (TIG) welding process to mitigate the leakage of xenon from the weld.

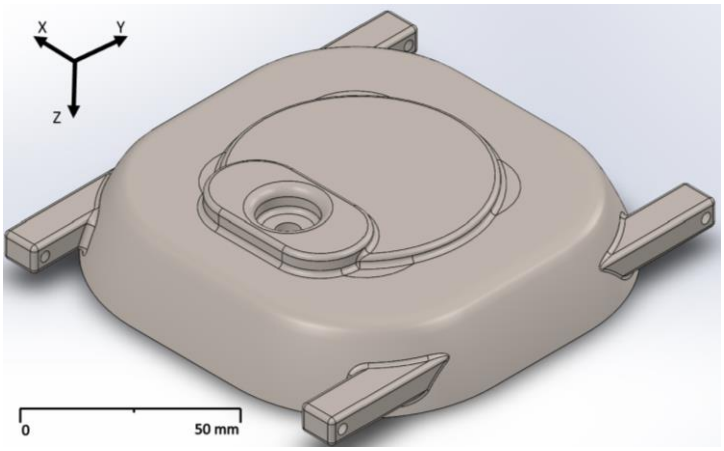

Figure 3.31: Top of Pressure Vessel

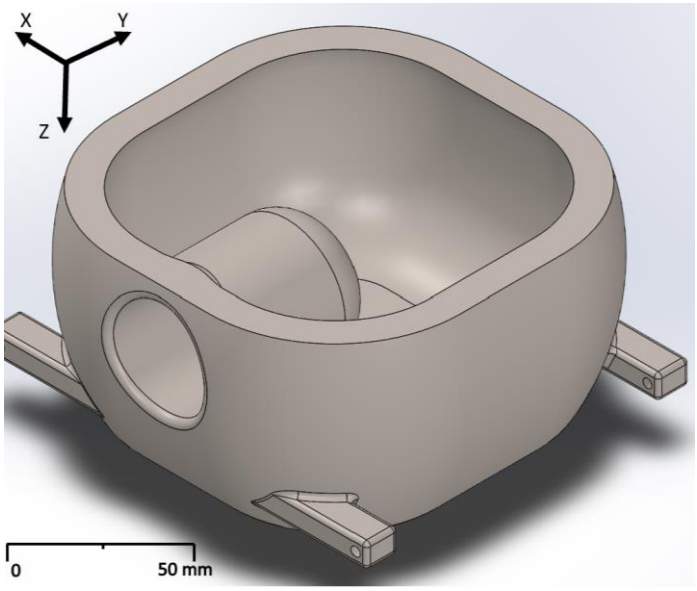

Figure 3.32: Bottom part of Pressure Vessel

Finally, the pressure vessel must be able to attach to the overall structural of the Propulsion Module. To reduce weight of the overall Propulsion Module, the pressure vessel was designed to attach to the Side Rails with eight separate attachment points that would be 3D printed alongside the structure of the pressure vessel. The eight separate attachment points are all connected via #4-40 Socket Head Cap Screws and help to hold together the railing of the Propulsion Module as seen in Figure 3.33. This allows for a portion of the Propulsion Module structure to be supported by the pressure vessel and reduce the amount of material needed in

the pressure vessel design. The envelope of the pressure vessel is 97 mm x 97 mm x 68 mm with a mass of 1,628 grams, due to the increased density of using SS316L.

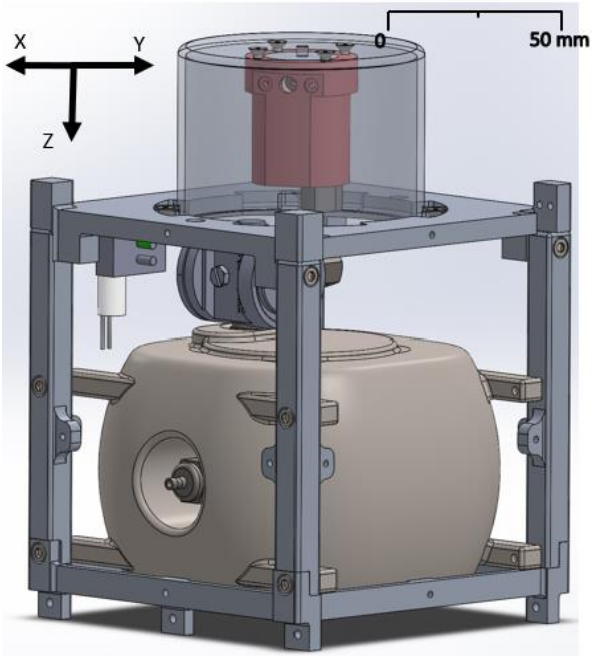

Figure 3.33: Pressure Vessel Design integrated into overall Propulsion Module Structure

The overall mass of all the plumbing system components is approximately 1,763 grams, excluding the Pocket Rocket thruster. The summary of the plumbing system components SWaP is shown in Table 3.6.

Table 3.6: Plumbing System Overall SWaP

Component Name	Envelope (mm)	Weight (grams)	Maximum DC Power (W)
Pressure Vessel	97.0 x 97.0 x 68.0	1,628.0	N/A
Cobham Miniature Service Valve	L: 41.3 Ø: 19.1	32.0	N/A
PRD3HP Regulator	L :135.0 Ø: 27.0	75.0	N/A
Solenoid Assembly	20.2 x 19.1 x 32.4	6.0	0.85
MCB-1018	L :19.4 Ø: 10.8	7.8	N/A
MCBL-1018	L :42.3 Ø: 12.0	11.2	N/A
MTT-1018 Teflon Tubing	L: 270.0	10.0	N/A

3.2.5 Electrical System Overview

For Pocket Rocket to operate, a steady flow of xenon to the propellant inlet, as well as amplified RF energy must be delivered to the thruster's excitation area. The first stage of RF energy generation happens on the 2U spacecraft PIB. The PIB will incorporate DC/DC power regulation and RF signal generation circuitry. RF signal is generated initially on the PIB before being transferred to the Propulsion Module, alongside regulated DC power and non-regulated DC power. Then, the RF PCB onboard the Propulsion Module amplifies the RF power to operational levels for Pocket Rocket and controls actuation of the Solenoid valve. An overview of the Electrical system for the Propulsion Module is shown in Figure 3.34. To prevent inadvertent actuation of any RF generating portions of the RF PCB or 2U PIB during launch, a deployment switch is installed in the Propulsion Module in addition to two deployment switches in the 2U spacecraft.

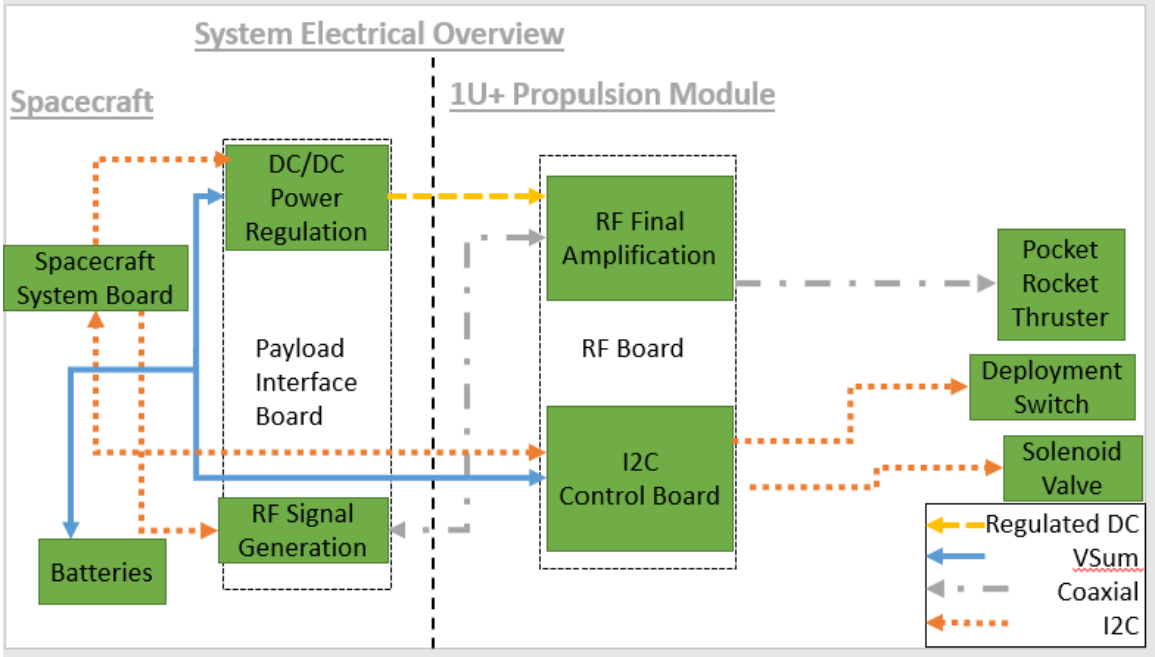

Figure 3.34: Propulsion Module electrical system overview

The RF PCB has an overall envelope of 72.8 mm x 56.6 mm x 17.6 mm as shown in Figure 3.35, and an overall weight of 23 grams. The RF PCB has four #1-80 Flat Hex Screws to attach it to the RF PCB enclosure. The PCB receives RF power at the inlet highlighted in blue on Figure 3.35. RF energy is supplied to Pocket Rocket via the RF outlet highlighted in black on Figure 3.35. The 2-pin connector highlighted in yellow on Figure 3.35 connects to the deployment switch and ensures that while inside the CubeSat deployer the Propulsion Module will not be able to be powered. An additional 2-pin connector highlighted in orange, connects with the Solenoid valve to control actuation when commanded. Finally, regulated and unregulated DC power is received via the ribbon cable attachment point between the orange and yellow highlighted 2-pin connectors shown in Figure 3.35 [60]. The RF PCB utilizes a peak DC power of about 61 W for startup of the Pocket Rocket thruster that takes less than 30 seconds. DC power draw during nominal operation of Pocket Rocket is approximately 31 W to provide RF power of 15 W due to the 50% electrical efficiency.

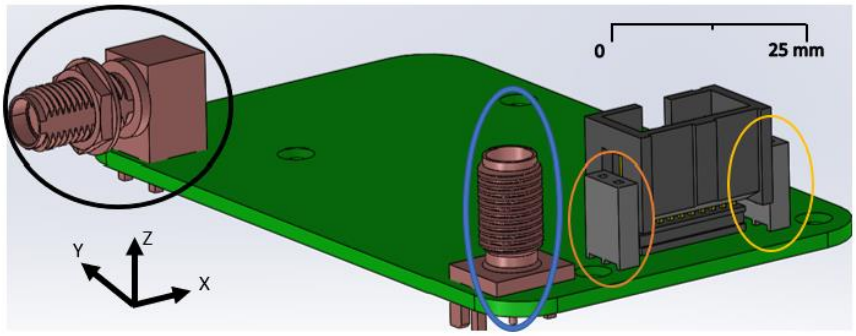

Figure 3.35: Propulsion Module RF PCB with components attached and highlighted

The RF PCB Board enclosure is an aluminum component that attaches the RF PCB assembly to the Top Hat and acts as a heat sink for the 15 – 30 W of heat generated due to the 50 % efficiency of the board. The overall envelope of the enclosure is 79.8 mm x 50.8 mm x 12.7 mm as shown in Figure 3.36 and weighs 52 grams. The board enclosure has four #1-80 tapped holes to attach the PCB on the inside, and four #2-56 tapped holes on the -Z face that mates with the underside of the Top Hat. The internals of the board enclosure are machined out to allow for the PCB to rest flush due to the PCB components on both ± Z faces. Additionally, the board enclosure is filled with conductive paste to draw excess heat away from the PCB generated during operation and assist in RF energy amplification.

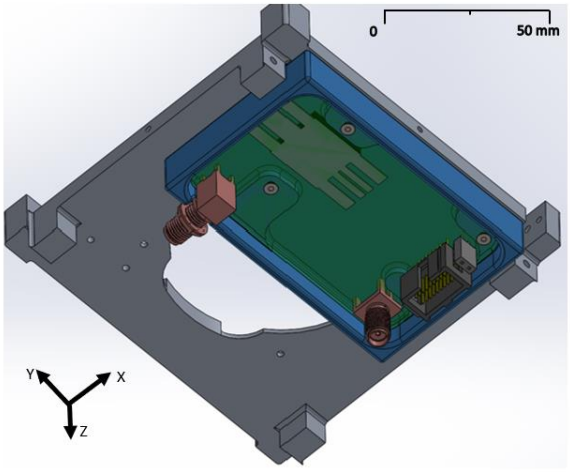

Figure 3.36: RF PCB Enclosure highlighted in blue, and attached to the underside of the Top Hat

The final electrical component of the Propulsion Module is the deployment switch. The deployment switch has an envelope of 8.23 mm x 2.7 mm x 10.7 mm as shown in Figure 3.37, and a mass of 0.5 grams. The purpose of the deployment switch is to be electrically connected to the RF PCB and ensure that while contacting the inside of the CubeSat deployer, no power can be utilized by the Propulsion Module system. The switch has two #1-80 thru holes and attaches to two #1-80 tapped holes on the Top Hat.

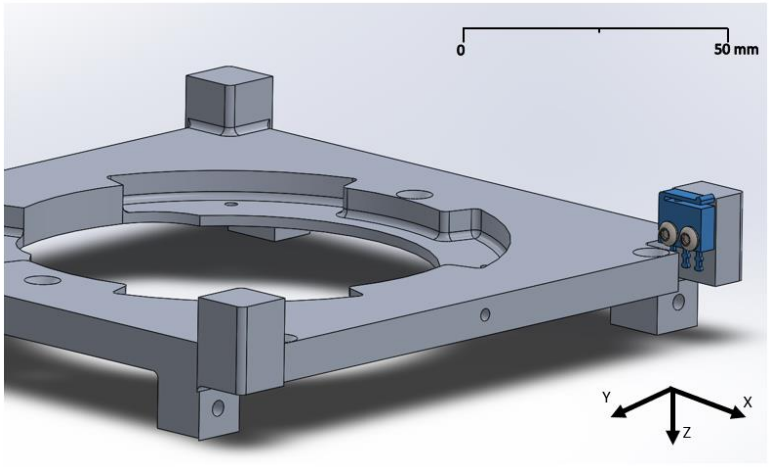

Figure 3.37: Deployment Switch highlighted in blue, and attached to the Top Hat

The electrical system has an overall mass of 74.6 grams, a peak DC power usage of 60.85 W and a nominal power usage of 30.85 W. Table 3.7 showcases the SWaP of the electrical system components

Table 3.7: Electrical System Overall SWaP

Component Name	Envelope (mm)	Weight (g)	Maximum DC Power (W)
RF PCB	72.8 x 56.6 x 17.6	23.0	60.9
PCB Enclosure	79.8 x 50.8 x 12.7	52.0	N/A
Deployment Switch	8.2 x 2.7 x 10.7	0.5	N/A

3.2.6 Overall System SWaP

After finalizing the mechanical and electrical designs of the Propulsion Module, a system dry mass was established at 2.35 g, and a wet mass of 2.85 kg. The peak DC power draw for the system is 66.75 W, and the total average DC power consumption is 6.28 W with a 20 % margin. The total envelope of the 3U+ system is 10 cm x 10 cm x 37.7 cm stowed, and 10 cm x 50 cm x 37.7 cm deployed. A summary of the system SWaP is shown in Table 3.8 alongside CDS Rev. 13 limitations. Overall assembly as well as routing instructions are expanded upon in Appendixes F and G.

Table 3.8: Overall SWaP of 3U+ System with CDS Rev. 13 Requirements

	1U+ Propulsion Module	3U+ CubeSat	CDS Rev 13. Limitations
Envelope - Stowed (cm)	10.0 x 10.0 x 15.0	10.0 x 10.0 x 37.7	10.0 x 10.0 x 37.7
Envelope – Deployed (cm)	10.0 x 10.0 x 15.0	10.0 x 50.0 x 37.7	N/A
Mass (kg)	2.8	5.0	4.0*
Center of Mass (From -Z Tuna Can Face)	6.1	163.3	163.3 – 177.3
Peak DC Power (W)	66.8	66.8	N/A
Average DC Power Consumption + 20 % Margin (W)	6.3	6.3	N/A

**Larger masses may be evaluated on a mission to mission basis*

Chapter 4

DESIGN VERIFICATION

4.1 Pressure Vessel Structural Verification

As a secondary payload, a CubeSat must demonstrate it will not cause issues to the deployment of the primary payload. CubeSats with propulsive systems must also follow additional requirements defined by the CDS Rev. 13 and AFSCMAN91-710, which ensure the safety of integrators, and the primary payload. One specific requirement that relates to the propulsion system and must be verified by testing and analysis is the need to have a minimum burst factor of 1.5. Burst Factor is the ratio between maximum pressure that a pressure vessel can handle before rupturing or “bursting” and the MEOP of the pressure vessel. This research will focus on the structural analysis necessary to verify the safety requirements are met. After the analysis is completed and the system manufactured, burst factor testing that determines the absolute maximum pressure a given component will “burst” at must also be accomplished before the system can be cleared for flight.

4.1.1 Simulation Setup

To verify the burst factor of the pressure vessel a simulation that utilizes Ansys Workbench 18.1 was performed. The simulation used the assumptions f a linear static structural test to solve for the displacements within the materials, with statically applied forces, small deflection theory, and linear elastic material behavior, while assuming internal and time varying forces are negligible. This assumption is valid, as the pressure within the pressure vessel under nominal operations will not drastically change or spike, and instead change slowly over time, which can be assumed to be negligible.

The simulation incorporated the geometry of the top and bottom parts of the pressure vessel assembly, as well as a 2 mm thick weld that connects the top and bottom together as shown in Figure 4.1. The material utilized for each half of the pressure vessel and the weld joint was CT

PowderRange 316L E powder from Carpenter Additive, as it is the material utilized in Cal Poly's IME labs for 3D printing of metals. The Material properties for the stainless steel are shown in Table 4.1.

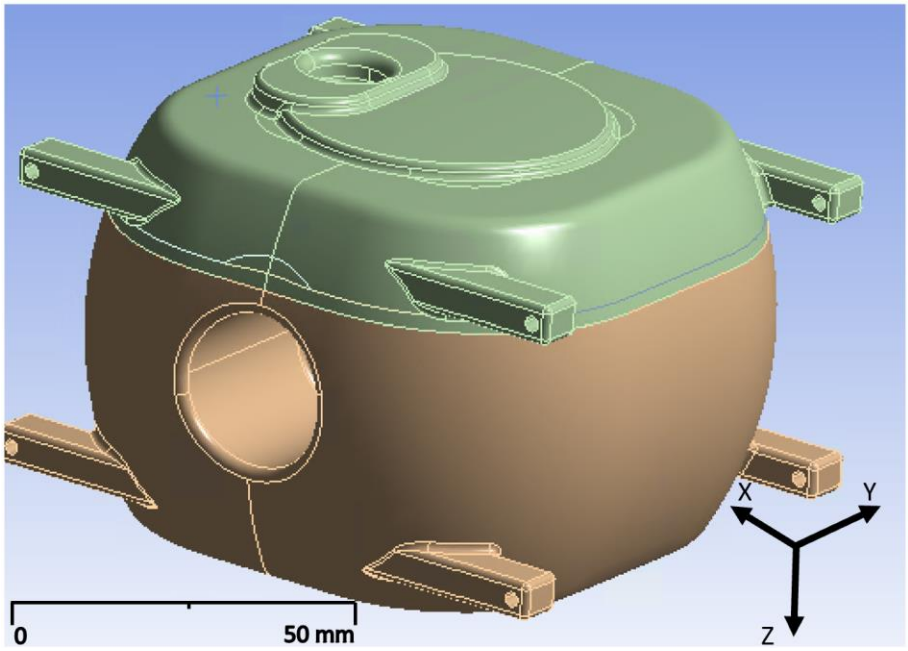

Figure 4.1: Pressure Vessel model in Ansys Workbench 18.1,

Table 4.1: Material properties utilized for Pressure Vessel Simulation [69,70]

Density (g/cm^3)	7.9
Poisson's Ratio	0.27
Youngs Modulus (GPa)	165
Tensile Yield Strength (MPa)	550
Compressive Yield Strength (MPa)	520
Tensile Ultimate Strength (MPa)	650
Compressive Ultimate Strength (MPa)	560

After the model was imported, a mesh was created as shown in Figure 4.2. The mesh was program controlled with an adaptive size, and a minimum element size of 1 mm to reflect the

smallest feature in the pressure vessel design. The reference center of each mesh was coarse alongside the span angle center. In total there are 279,100 nodes and 162,291 elements used within the model.

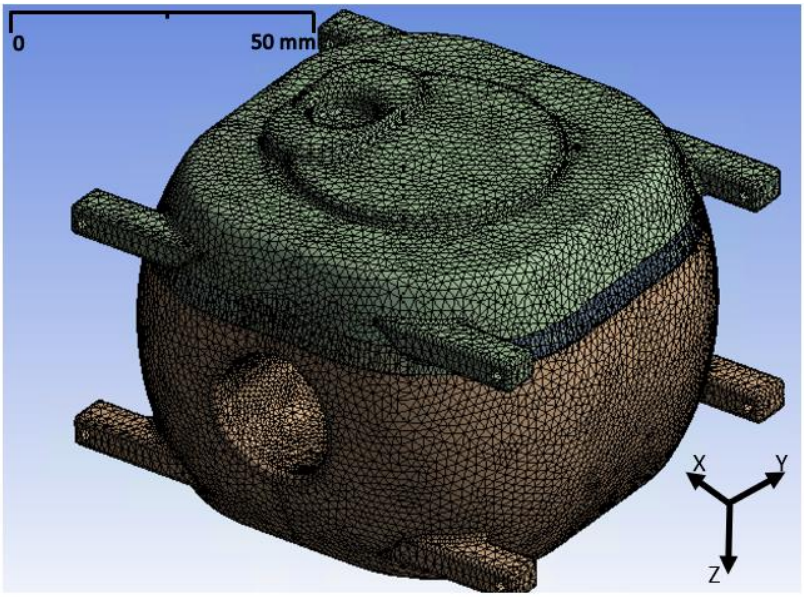

Figure 4.2: Pressure Vessel simulation generated mesh

A constant pressure of 20.7 MPa was applied to the internal faces of the pressure vessel to simulate the expected internal force if loaded with a maximum of 500 grams of xenon. The geometries of the plumbing system components that connect to the pressure vessel were not modeled. However, to simulate the effects of the plumbing interface on the structure of the pressure vessel, pressure was applied up to the point at which the interface would be mated with the as shown in neon green on Figure 4.3.

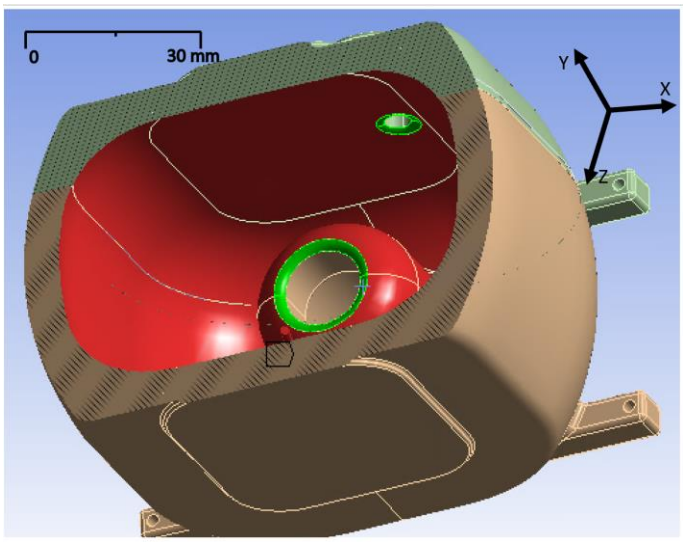

Figure 4.3: Pressure Vessel simulation section view with plumbing component interfaces highlighted in neon green

To model the mechanical interfaces to the Side Rails, boundary conditions were applied to mimic the flight design and the structural impacts that attachment points such as fasteners and contact with other structures would produce. Fixed supports that constrain all degree of freedom were applied on the thru holes of the attachment points as shown in Figure 4.4. The locations chosen for the fixed supports reflect where #4-40 fasteners would attach the pressure vessel to the rest of the Propulsion Module.

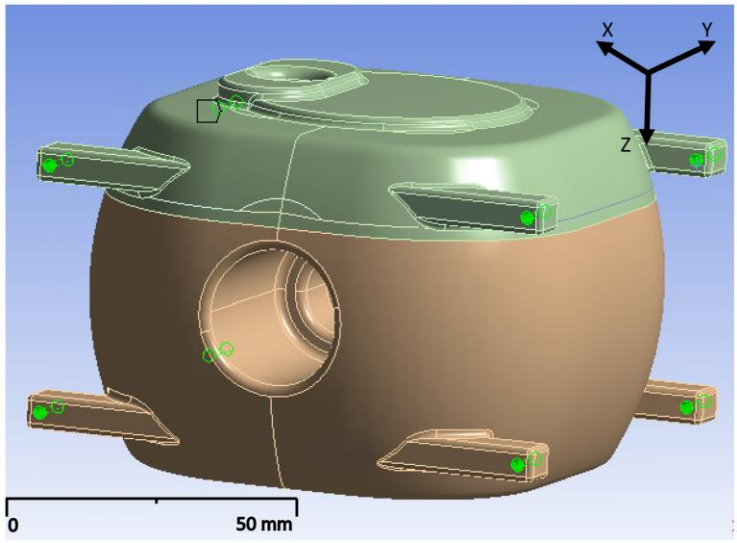

Figure 4.4: Pressure Vessel simulation, fixed support boundary conditions highlighted in green

In addition to fixed displacements, remote displacements were applied to the simulation that help to further replicate the interface with the Side Rails. Remote displacements are similar to fixed supports except that there is a choice in which axis you can limit translation, as well as an option to allow for a rotation about an axis on the part. The remote displacements were applied on the edges of the pressure vessel that were compressed against the Side Rails due to the torque applied on the #4-40 socket head cap screw. Translation in the X, Y, and Z axis was limited, but moments could be generated in the X, Y and Z directions. Together, fixed supports and remote displacement boundary conditions applied will simulate the mechanical environment experienced by the pressure vessel when attached to the Propulsion Module.

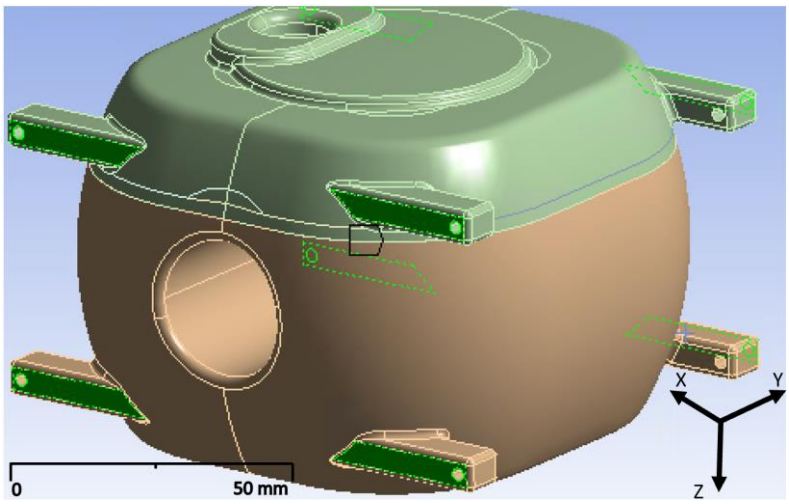

Figure 4.5 Pressure Vessel simulation, remote displacement boundary conditions highlighted in green

Finally, the simulation was assumed to be a thick wall pressure vessel, as the wall thickness of the pressure vessel is 7.5 mm which is greater than 1/10 of the mean radius of 44 mm. This means that the stresses between the inside and outside surfaces can vary significantly and shear stress of the cross-sectional area cannot be ignored [71].

4.1.2 Static Structural Results

The simulation was executed, and maximum equivalent stress theory was utilized alongside tensile yield per material to calculate the safety factors of every node within the model. The maximum safety factor was 15 located on the support rails, with most of the pressure vessel at a safety factor of larger than 2. The minimum safety factor of the pressure vessel was 1.51, localized around the location of the regulator connection. The location of the minimum safety factor makes sense as on a cylinder the highest stress location are created by the hoop stress, and the location of the lowest safety factor, is where hoop stress would likely be highest in the structure. The value of 1.51 is acceptable as the material properties of stainless steel were conservatively selected from the data sheets available, to mimic an imperfect print. The maximum safety factor occurs on the external spherical sections of the pressure vessel and pressure vessel support rails. This makes sense, as the support railing is not directly affected by the internal stresses of the pressure vessel, and a spherical geometry should limit stress concentrations that produce lower safety factors. Internally, the range of safety factors showcased in the data is between 1.5 – 2.0. This range makes sense, as internal geometry has lower safety factors in thinner sections of the pressure vessel or where there are geometry transitions. The geometry transitions are meant to limit stress concentrations and are mitigated by filets or similar technique. The overall view of the safety factor results are presented in Figure 4.6 through Figure 4.10.

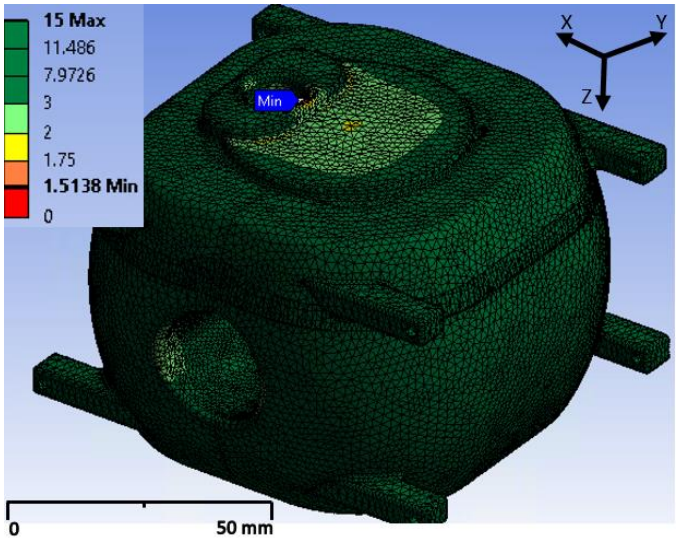

Figure 4.6: Safety factor results of Pressure Vessel simulation (+Y isometric view)

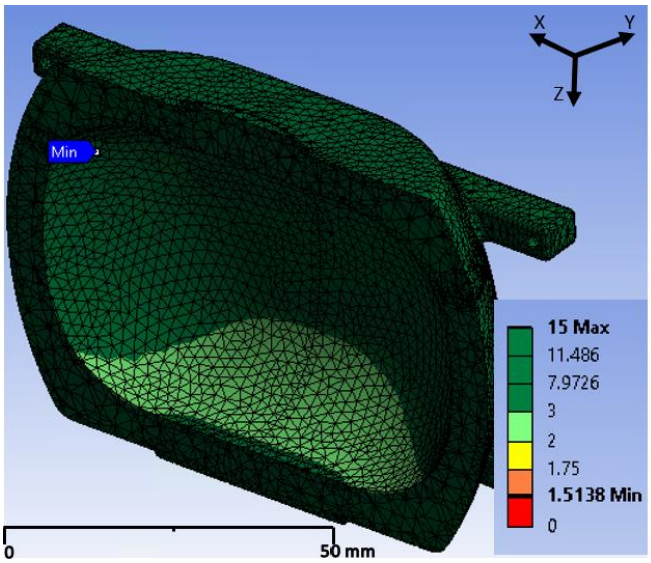

Figure 4.7: Safety factor results of Pressure Vessel simulation (+Y isometric view sectioned)

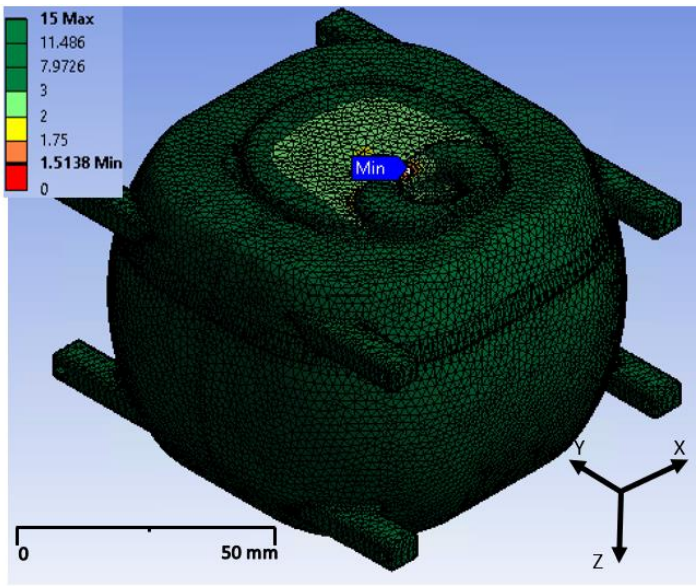

Figure 4.8: Safety factor results of Pressure Vessel simulation (+X isometric view)

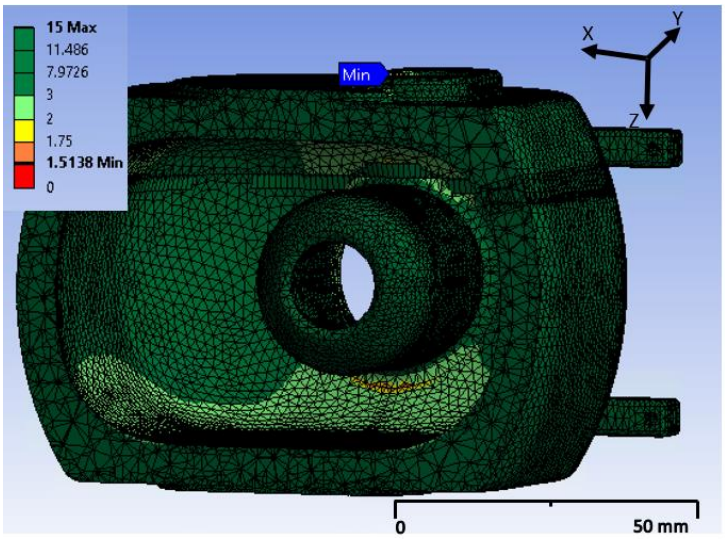

Figure 4.9 Safety factor results of Pressure Vessel simulation (+X isometric view sectioned)

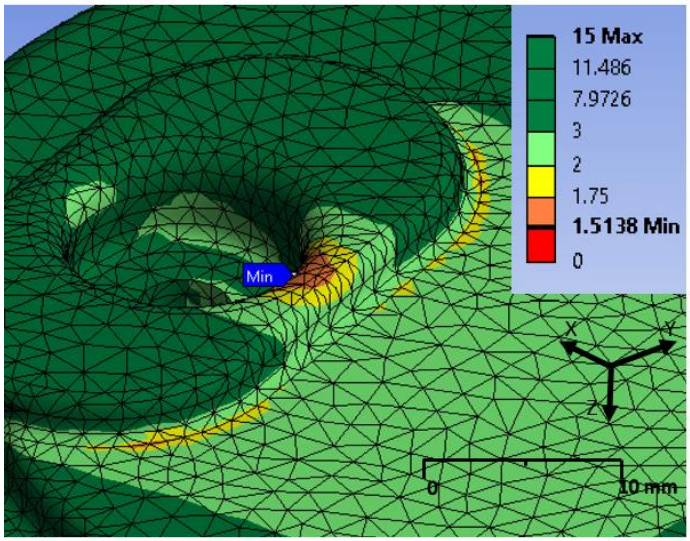

Figure 4.10: Area view of the minimum safety factor from the Pressure Vessel simulation

4.2 Propulsion Module Vibrational Verification

In order to demonstrate that flight hardware is qualified for the mission environment, and the hardware utilized in the design is structurally reliable without workmanship errors, a Vibrational simulation that incorporates random vibration and modal analysis was carried out to characterize the system response. The Random vibration analysis was carried out to verify that the flight design would be capable of handling the launch environment, whereas the modal analysis was carried out to identify potential resonant conditions within the design.

Due to the continued development of the 2U CubeSat that will interface with the Propulsion Module, the vibrational analysis was conducted on the Propulsion Module individually. To verify compliance for the flight unit, vibrational analysis must be completed on the entire 3U+ system after development of the 2U is completed.

4.2.1 Simulation Setup

The vibrational simulation utilized two separate simulations, a modal analysis and random vibration analysis. Modal analysis imparts no load on the system to generate the natural

frequencies that the mechanical system is likely to resonate at. The natural frequencies are where the design is likely to be damaged during vibration and therefore the most dangerous and destructive areas when additional force is applied. The modal analysis was used as a baseline that was then imported into the random vibration simulations to represent the mechanical response the system would have.

The random vibrational analysist was based around NASA GEVS testing standards that provide environmental verification programs for payloads, subsystems, and components, as well as methods for implementing the testing requirements. A random vibration test was performed in the X, Y, and Z axis at specific frequency and qualification ASD levels shown in Table 4.2

The values specified relate to qualification test levels, that demonstrate the system could function within performance specifications under simulated conditions that are more severe than those experienced during launch, handling, and mission ops [72].

A damping factor of 0.05 for the structure was utilized throughout simulation as a first order baseline assumption for the design. The damping factor represents how the oscillations in a system decay after the disturbance and would need to be updated once vibrational testing was accomplished. A damping factor of 0.05, corresponds to a initial quality factor approximation of 10 defined by NASA GEVS [59], due to the relationship between damping and quality factor shown in Equation 4.1. After mechanical testing and greater definition of the 2U system is established, approximations for quality and damping factor can be iterated upon.

$$\boldsymbol{Damping\ Ratio} = \frac{\mathbf{1}}{\mathbf{2} * \boldsymbol{Quality\ Factor}} \tag{4.1}$$

Table 4.2: Generalized Random Vibration Test Levels [59]

Frequency (Hz)	Qualification ASD Level (g^2 / Hz)
20	0.026
50	0.160
800	0.160
2000	0.026

The geometry of the Propulsion Module was imported into Ansys Workbench 18.1 from a STEP file. The STEP file was simplified to remove the PCB board components before import into the software as shown in Figure 4.11. The simplification was accomplished to reduce the number of elements within the mesh. The electrical components removed in the simulation would be attached to both the RF PCB, as well as cemented in conductive paste, thus vibrations would not be a large concern.

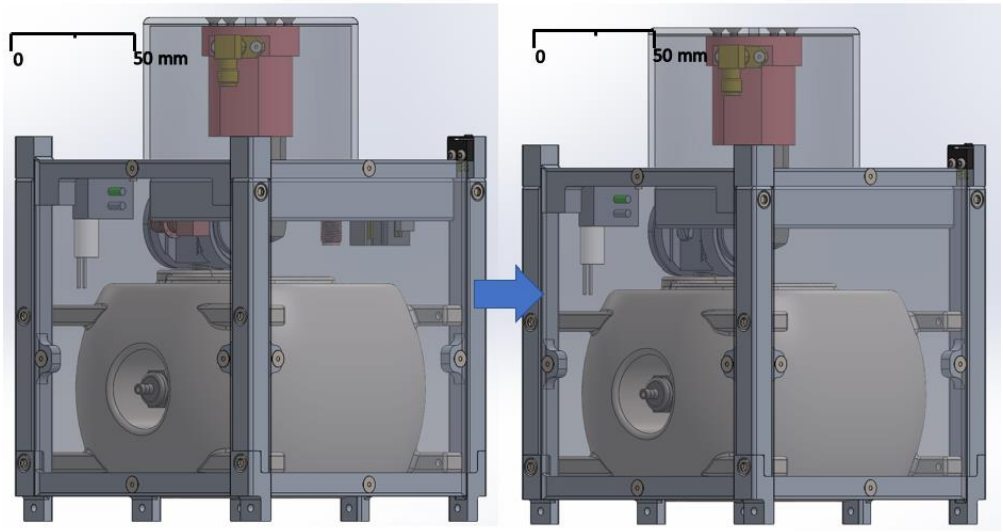

Figure 4.11: a) Nominal geometry of Propulsion Module and b) Vibrational Simulation simplified geometry of Propulsion Module

The materials of each components were then selected to model the flight design in the vibrational simulation. A list of materials utilized and the associated components for each material was applied to can be found in Table 4.3 and Table 4.4.

Table 4.3: Materials utilized in vibrational simulation [70,73–77]

Material Type	Density (g/mm^3)	Youngs Modulus (GPa)	Poisson's Ratio
Al 7075-T6	2.81E-3	71.70	0.33
Beryllium Copper	8.26E-3	131.00	0.30
FR4	1.80E-3	16.50	0.39
Macor	2.52E-3	66.90	0.29
Stainless Steel 304	7.99E-3	193.00	0.29
Stainless Steel 316L	7.90E-3	165.00	0.27

Table 4.4: Material type by component for vibrational simulation

Material Type	Components Utilized
Al 7075-T6	Tuna Can, Top Hat, Side Panels, Side Rails, Pocket Rocket, RF PCB Enclosure, Boot, PR Aluminum Disk, Solenoid Manifold
Beryllium Copper	SMA-F right angle connector, PR Copper disk
PCB	Deployment Switch, RF PCB, Solenoid Valve
Macor	Macor Inner Cup, Macor Outer Cup
Stainless Steel 304	Screws, MCB-1018, MCBL-1018, MN-1414, Cobham service valve, PRD3HP
Stainless Steel 316L	Pressure Vessel

After the model was imported into the simulation and materials were assigned, the boundary conditions for the vibrational study were chosen. The testing fixture for a 3U+ CubeSat mimics a CubeSat deployer and provides a press fit on the railing of the CubeSat during vibrational testing. Therefore, while a model of the test fixture was not included in the simulation due to limitations in computational resources, boundary conditions were utilized to mimic the mechanical interactions of the fixture on the CubeSat.

The boundary conditions utilized for the 1U+ propulsion system assumed that the bottom railings would be fixed to a 2U CubeSat via the six thru holes on the bottom of the 1U+ module. This was modeled with fixed supports as shown in Figure 4.12, with the neon green sections highlighting the fixed locations.

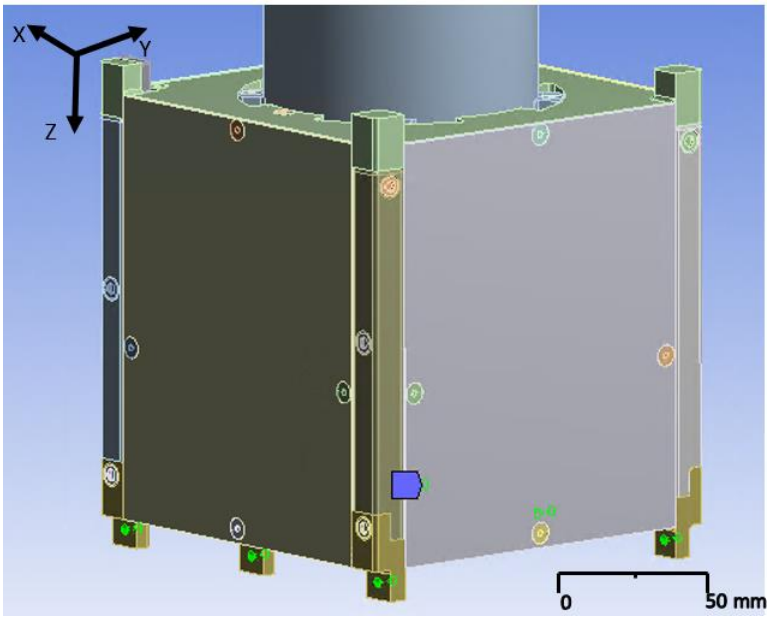

Figure 4.12: Fixed Supports for Vibrational Simulation, highlighted in neon green

In addition to the fixed support, remote displacements were utilized on the top as well as the sides of the railing. The remote displacements limited movement in the X, Y and Z directions, but allowed moments to be created around the X, Y, and Z axis. The remote displacement supports are shown in neon green Figure 4.13.

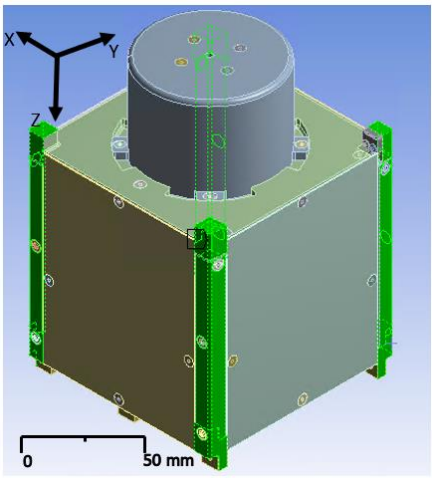

Figure 4.13: Remote Displacement supports highlighted in neon green

The mesh was then generated with Ansys meshing software (Figure 4.14), utilizing adaptive sizing of elements with coarse relevance and span angle centers. In the overall 1U+ model, there were 319,652 nodes with 176,641 elements.

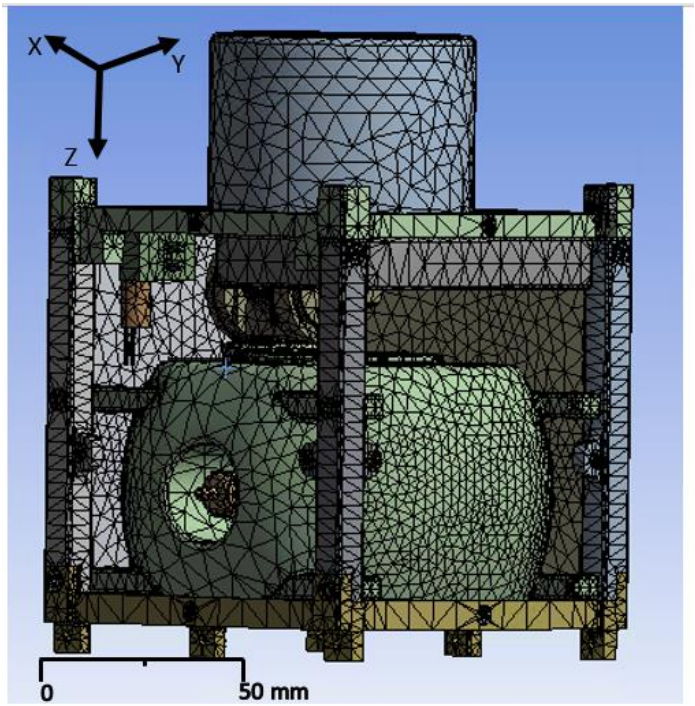

Figure 4.14: Propulsion Module vibrational simulation mesh

4.2.2 Random Vibrational Analysis Results

The random vibrational simulation was run in the X, Y and Z. Directional deformation and equivalent stress were then calculated in the X, Y and Z axis, for each random vibration simulation. Deformation was calculated along either the X, Y or Z axis, of each simulation at a 3-sigma scale factor as defined by NASA GEVS [59].

The maximum deformation throughout all the vibrational simulations was 0.0003 mm in the X direction during the X axis random vibrational analysis. A maximum deformation of 0.05 mm was determined to be the success criteria for the simulation, as movement of internal functional components could disrupt operation of the Propulsion Module. Therefore, the simulation shows that Propulsion Module design should be able to move forward with manufacture and then testing. The overall results for all three directions are shown in Figure 4.15 through Figure 4.17.

In the X-axis vibrational analysis, the maximum deformation occurs in the -X direction of the Propulsion Module. This makes sense, as the largest deformation should occur along the axis of vibration and farthest away from supporting structures. The same phenomenon occurs in both the Y axis, with the largest deformation also happening on the side paneling thin sections that are in the axis of vibration. The component with the largest deformation is the Side Paneling, which has a 2mm thickness in the axis of vibration, therefore it makes sense that a larger deformation would occur in the thinnest area of the assembly affect the part. In the Z-axis the largest deformation happens on the Tuna Can. The Tuna Can attaches to Pocket Rocket in the center of a thin walled aluminum structure, which causes a mass concentration and therefore, the largest deformation is likely to occur within the area. The magnitudes of deformation shown in the simulation results are within μm range, therefore while there are differences between each axis tested, it is unlikely that mechanical deformation will be measurable between physical tests.

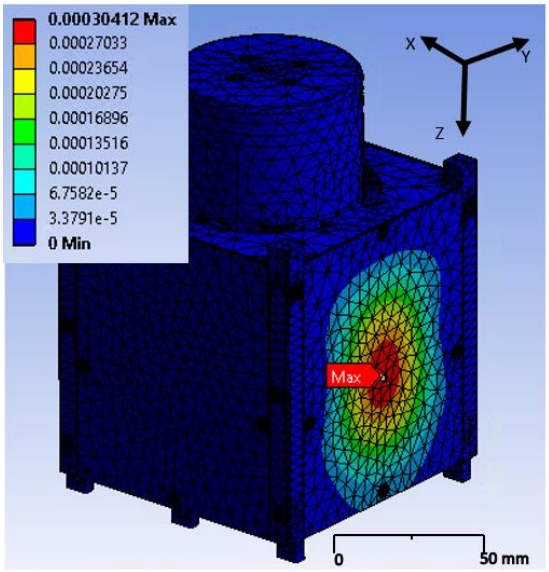

Figure 4.15: Random vibe results X-axis largest deformation (mm)

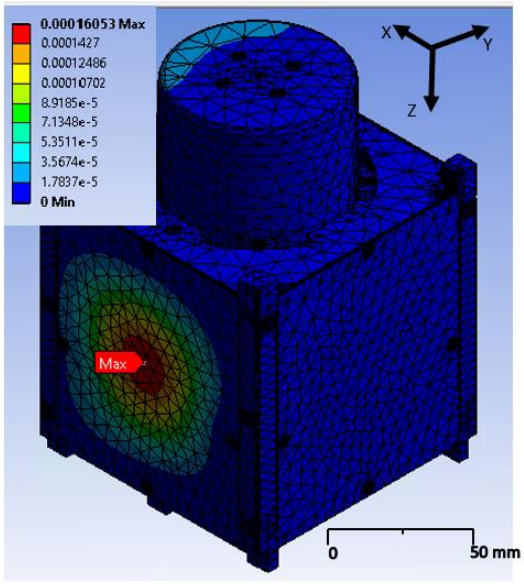

Figure 4.16: Random vibe results Y-axis largest deformation (mm)

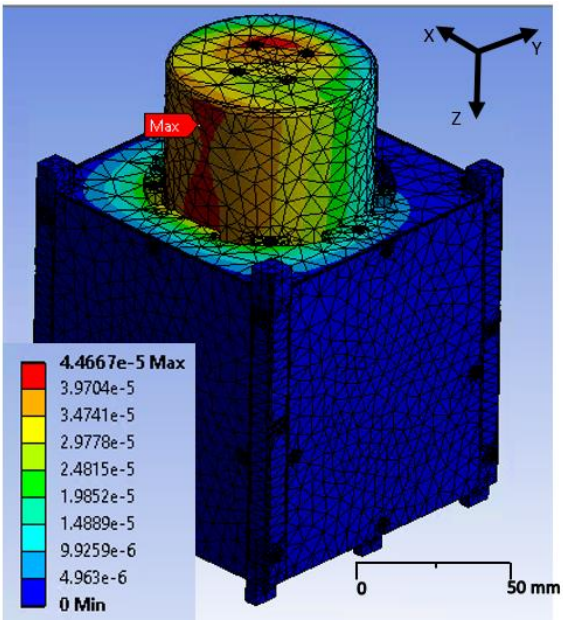

Figure 4.17: Random vibe results Z axis largest deformation (mm)

4.3 Thermal Environment Verification

In addition to the external heating environment, Pocket Rocket and the RF PCB generate excess heat during operation of the thruster that must be managed throughout the module design. Therefore, a thermal simulation was performed to characterize whether the Propulsion Module would be able to handle the heating environment during operation, ignition, and standby phases. The thermal simulation was utilized for verification by analysis that operational temperatures could be maintained for components within the 3U+ system.

After further development of the 3U+ system, and enhanced definition of the electrical components that constitute the 2U spacecraft is achieved. The thermal simulation should be updated with relevant internal heating environment changes, to ensure an accurate representation of what is to be expected in the operational orbit.

4.3.1 Simulation Setup

To simulate the operational temperature, Thermal Desktop and the AutoCAD suite were utilized to model the 3U+ spacecraft in an orbit deployed from the ISS with an orbital altitude of 402 km, and inclination of 52°. The Propulsion Module design, as well as a generic 2U with functional electrical components necessary to thruster operation were incorporated into the simulation. The thermal simulation was designed to run steady and transient state temperature analysis that would calculate the heating environment throughout the orbit, and then output spacecraft expected temperatures. The simulation considered external radiative heating environments such as solar, earth albedo, and earth infrared heating. Radiation between space, the earth, and spacecraft surfaces was considered, alongside the conduction between connecting components. Convection was ignored, because within a vacuum there are limited fluids for particles to travel through, thus convection is not a dominant heat transfer path [78].

The spacecraft was assumed to always be pointing the -Z face in the velocity vector direction, as if executing a burn. Further, solar panels and the +Y face of the 3U+ were oriented towards the Sun vector as power needs to be generated for the preliminary power budget and ConOps to be accomplished. The assumption that the solar panels are pointing towards the sun vector is appropriate, as energy storage and generation is critical to operation of the Propulsion Module and will minimize the waiting time between thruster operations, while also providing a worst-case hot temperature heating environment. Steady state temperature analysis was accomplished to determine the starting temperature for the transient analysis. For the transient analysis, the spacecraft was simulated for five total orbits to characterize the temperature range throughout the operation. The materials utilized in the simulation were: Aluminum 7075-T6, Arlon CLTE Microwave Circuit Board Substrate (PCB), Beryllium Copper, Lithium Ion, Macor, Silicon Solar Cells, SS 304, and SS 316L. If a component was not uniformly made of one material, the material that composed most of the structure or drove the thermal gradient was utilized. Material thermophysical properties can be seen in Table 4.5, with the respective components that utilized the material shown in Table 4.6.Optical properties from the simulation were chosen from NASA

technical publications, and the coatings utilized are: Alodyne Aluminum 6061-T2, Black Anodized Aluminum Oxide, Carbon Black Paint, Machined Stainless Steel, GSFC White Paint MS74, Plain Beryllium Copper, Polished Aluminum, Polished Stainless Steel, Silicon Wafer, Tedlar White Plastic, and TRW Solar Cells. Coating optical properties can be seen in Table 4.7 with respective components that utilize the coatings listed in Table 4.8. If an exact replica to the optical property was not available, assumptions based on the appearance were made such as with the modeling of Macor, which is a white ceramic whose optical properties were assumed to be similar to white paint. Similarly, the solenoid's optical properties were assumed to be primarily equivalent to white plastic.

Table 4.5: Thermophysical Properties of materials in TD simulation [70,73,74,76,77,79–82]

Material Type	Conductivity (W/mm/K)	Density (g/mm$^{3)}$	Cp (J/gK)
Aluminum 7075-T6	130.00E-3	2.81E-3	0.96
PCB	0.50E-3	2.38E-3	0.70
Beryllium Copper	118.00E-3	8.26E-3	0.42
Lithium Ion	3.40E-3	2.68E-3	1.28
Macor	1.46E-3	2.52E-3	0.80
Silicon Solar Cells	150.00E-3	2.32E-3	0.85
304SS	16.20E-3	7.99E-3	0.50
316LSS	16.20E-3	7.99E-3	0.50

Table 4.6: Thermophysical Properties by component

Material Type	Components Utilized
Aluminum 7075-T6	**Propulsion Module:** RFB Enclosure, Boot, Side Panels, Side Rails, Tuna Can, Pocket Rocket, PR Al Disk, Top Hat **2U:** ADCS, Side Panels, Solar Panel Structure
PCB	**Propulsion Module:** RF PCB, Solenoid, Deployment Switch **2U:** PIB board, CPCL radio
Beryllium Copper	**Propulsion Module:** PR Copper Disk
Lithium Ion	**2U**: Battery
Macor	**Propulsion Module:** PR Macor Inner Cup, PR Macor Outer Cup
Silicon Solar Cells	**2U:** Solar Cells
304SS	**Propulsion Module:** MN-1414, PRD3HP, MCB-1018
316LSS	**Propulsion Module**: Pressure Vessel

Table 4.7: Optical Properties in TD simulation [82]

Coating Name	Absorptivity	Emissivity
Alodyne Aluminum 6061-T2	0.44	0.14
Black Anodized Aluminum Oxide	0.67	0.84
Black Paint	0.96	0.88
Machined Stainless Steel	0.47	0.14
GSFC White Paint MS74	0.17	0.92
Plain Beryllium Copper	0.31	0.03
Polished Aluminum	0.14	0.03
Polished Stainless Steel	0.42	0.11
Silicon Wafer	0.57	0.56
Tedlar White Plastic	0.39	0.87
TRW Solar Cell	0.86	0.82

Table 4.8: Optical properties by component

Coating Name	Components Utilized
Alodyne Aluminum 6061-T2	**Propulsion Module:** RFB enclosure **2U:** ADCS, Solar Cell Backing
Black Anodized Aluminum Oxide	**Propulsion Module:** Boot, Side Panels, Side Rails, Tuna Can, Top Hat **2U:** Solar Panel Structure
Black Paint	**2U:** Battery, Deployment Switch, CPCL Radio
Machined Stainless Steel	**Propulsion Module:** Pressure Vessel
GSFC White Paint MS74	**Propulsion Module:** PR Macor Inner Cup, PR Macor Outer Cup
Plain Beryllium Copper	**Propulsion Module:** PR Copper Disk
Polished Aluminum	**Propulsion Module:** Pocket Rocket Thruster Body, PR Aluminum Disk
Polished Stainless Steel	**Propulsion Module:** MCB-1018, MN-1414, PRD3HP
Silicon Wafer	**Propulsion Module:** RFB PCB **2U:** PIB
Tedlar White Plastic	**Propulsion Module:** Solenoid Valve
TRW Solar Cell	**2U:** Solar Cells

After the thermophysical and optical properties were determined, the contact resistance that describes conduction interactions between the components waere established. The four types of contact resistances utilized in the simulation are presented in Table 4.9. Face contactors were utilized to represent connection points beyond components that would be touching in the Propulsion Module or 3U+ design. If the material contact resistance was not known, an assumed Aluminum to Aluminum contact resistance was utilized to simulate the worst case conductive environment.

Table 4.9: Contact Resistance utilized for TD simulation [78]

Contacting Material	Contact Resistance (W/mm^{2}K)	Contact Pressure (MPa)
Al 7075-T6 / Al 7075-T6	28.39E-4	0.34
Al / SS	32.93E-4	0.34
Copper (OFHC)	70.98E-4	0.34
SS 304 / SS 304	2.839E04	0.34

After initial mechanical, thermophysical and optical properties were characterized. The geometry of the Propulsion Module internal components was simplified by removing chamfers, filets, bolt holes and small features that increase the complexity of the mesh but do not drive thermal gradients. The model simplification is shown in Figure 4.18. The simplified model was then imported into thermal desktop to further develop the simulation.

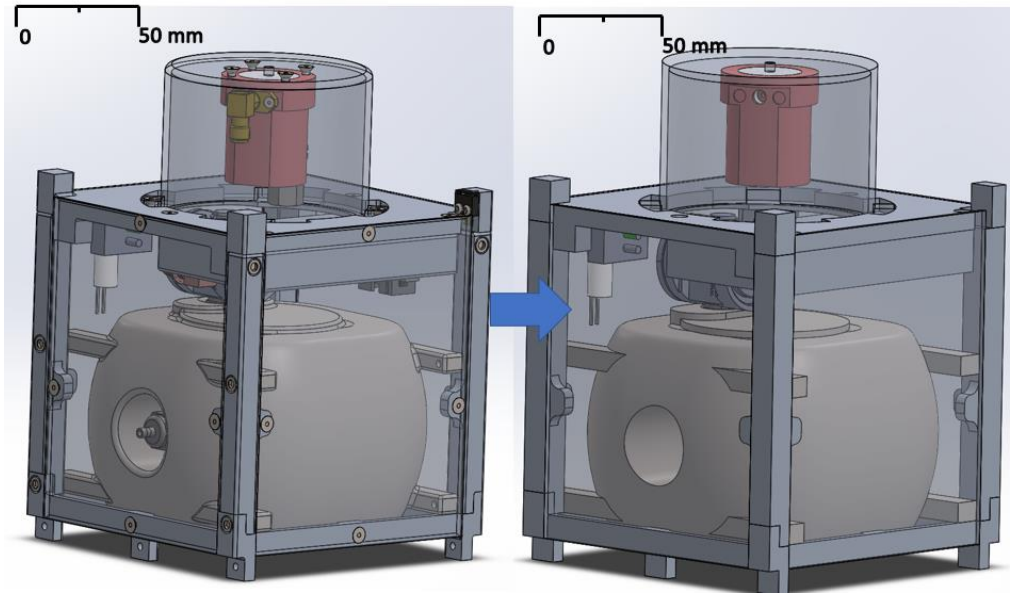

Figure 4.18: a) Propulsion Module with all components included and b) Simplification of Propulsion Module geometry for thermal simulation removing chambers, filets, bolt holes, and small features

Once imported into the software, the geometry was simplified into AutoCAD shapes with two separate approaches. The first of which utilized finite difference (FD) surfaces and solids to

mimic the shapes with non-complex geometries. The simplification was to ensure accurate representation of temperature gradients that can be modeled within the AutoCAD software, as well as to limit computation resources needed to run different cases. Multiple solids would be used to simplify complex geometry, and then the solids would be connected to each other as shown in Figure 4.20. The interface between the two components was then given an arbitrarily high conductance, to emulate the conductance within a single part instead of multiple part.

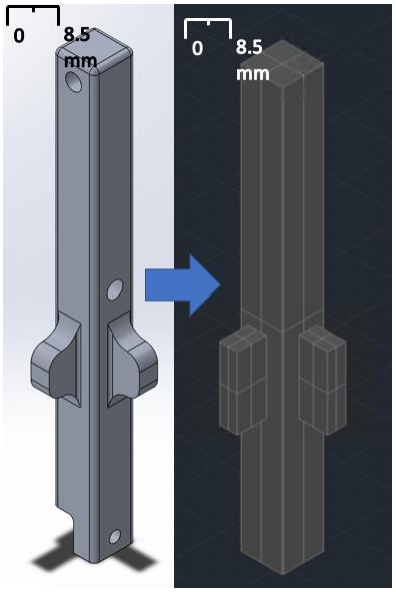

Figure 4.19: a) Side Rail Geometry with no simplifications and b) Side Rail geometry simplification into FD solids for TD simulation

Models with complex geometry that affected temperature gradients and would limit the ability to simplify to FD solids were meshed as separate parts. The meshing of the components with complex geometries was limited to components with shapes that would drive the radiative environment, due to computation limitations present at Cal Poly. Each meshed component utilized the TD meshing software to generate an element size that was 90% of the size of the maximum dimension for the part with a maximum turning angle of 45 degrees as shown in Figure 4.21. The components that necessitated complex meshing approaches, have simple flat face conducting interfaces but complex radiation environments, conduction is the dominant form of heat transfer in these components therefore the limited meshing size is justifiable. An overview of the entire Propulsion Module meshed in TD is shown below in Figure 4.21

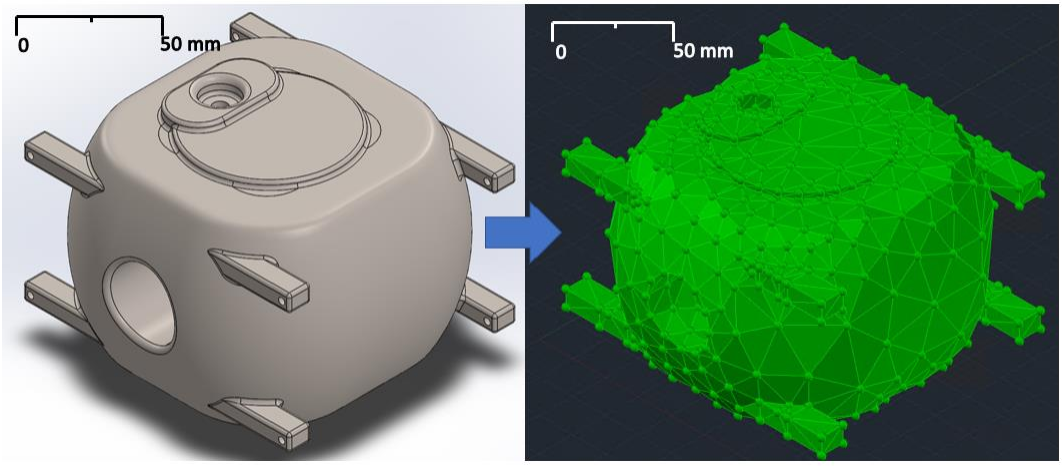

Figure 4.20: a) Pressure Vessel design with no simplification and b) Mesh generation of complex geometry within the Propulsion Module

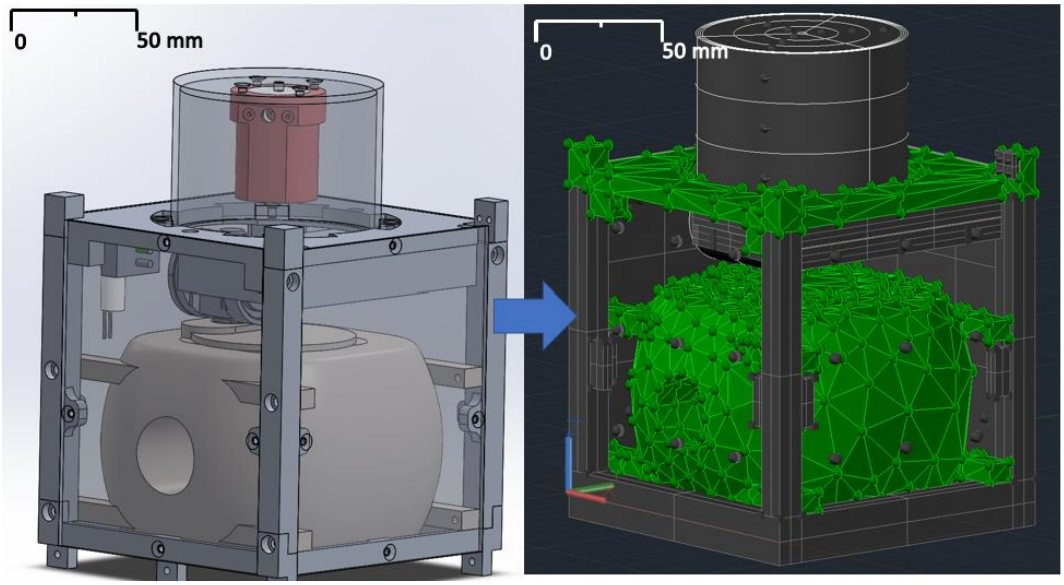

Figure 4.21: a) Propulsion Module simplified geometry and b)TD model of the Propulsion Module

After the geometry of the propulsion model, a generic 2U CubeSat that incorporated an ADCS system, battery, communications radio control, as well as deployable solar panels was incorporated into the simulation as shown in Figure 4.22. The generic 2U CubeSat geometries are based on the BCT XACT-15 ADCS system, CPCL Radio , CPCL batteries & PIB, and then BCT 3U deployable Solar Panels [61–63]. The components modeled were chosen based on the

effects they would have on the heating environments. Each component modeled utilizes or generates power and is assumed to operate during the firing of the Pocket Rocket thruster.

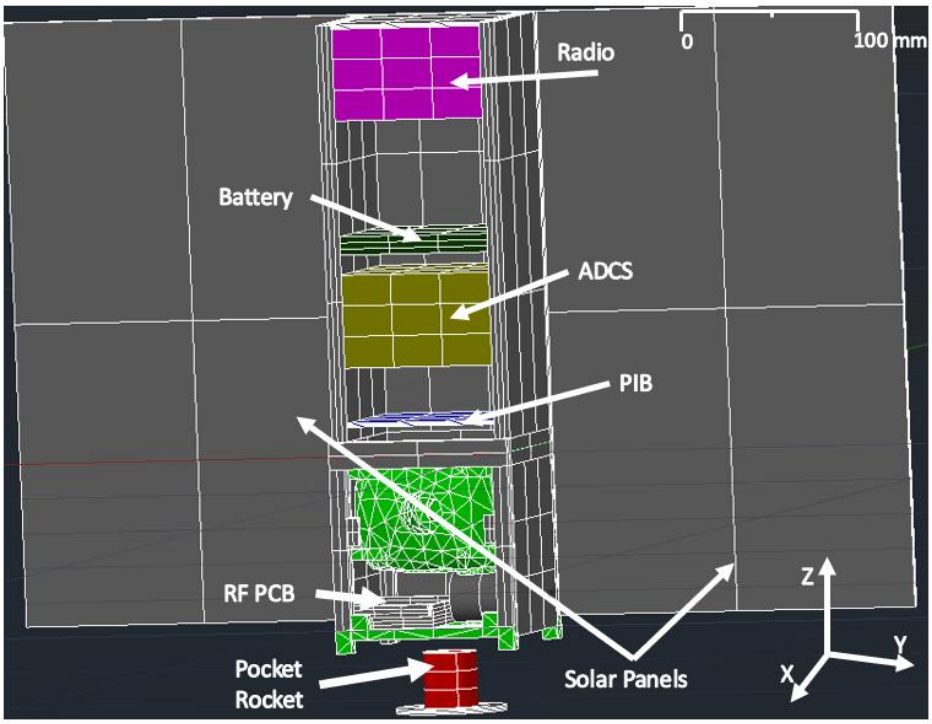

Figure 4.22: 2U Interfacing CubeSat generic geometry with Propulsion Module and Side Paneling removed

The final step in the setup of the thermal desktop simulation was incorporating the heating from the internal environments. The heat generated from the inefficiencies of the electrical components was modeled utilizing solid heat loads for each electrical component and for the copper disk within Pocket Rocket that heats the propellant. Efficiencies as well as heat generated during the phases of the orbit are shown in Table 4.10. The battery power draw as well as heat load were determined by operational phases and the sum of all power utilization within the system. Additionally, the heat generated at the RF PCB that is transferred to Pocket Rocket, was assumed to be 100% efficient in the transfer to the Pocket Rocket copper disk, as a worst-case temperature assumption. Heating removed from the CubeSat via the thruster plume is not simulated, to ensure a worst-case simulation of the temperature profiles. Based on the ConOps

shown in Figure 3.4 and Figure 3.5, the heat loads were varied throughout the orbital simulation to show the changing internal heating environment during the thruster operational phases.

Table 4.10: Internal heating loads generated by component

Component	Standby Heat Generated (W)	Thruster Startup Heat Generated (W)	Thruster Nominal Operations Heat Generated (W)	Electrical Efficiency (%)
ADCS	0.1	1.1	1.1	80.0
Battery	0.1	2.5	1.7	95.0
CPCL Radio	0.2	5.2	5.2	59.0
PIB	0.1	0.1	0.1	80.0
RF PCB	0.5	30.0	15.0	50.0
Solenoid	0.0	0.2	0.2	80.0
PR Copper Disk	0.5	30.0	15.0	N/A

4.3.2 Steady State Results

Steady state temperature was used to calculate a starting temperature for every node within each component. The steady state temperature was utilized as a tool to gauge the temperature range of the system, before running a longer transient analysis. Steady state results were also utilized when changing settings to increase the computational speed of the simulation to ensure that the system still accurately reflected the outcome prior to changes. The steady state results are shown in Figure 4.23 and Figure 4.24.

The steady state results make sense, as the external radiative heating environments should dominate the overall heating of a CubeSat, that only utilizes passive thermal management techniques. The areas that see the largest amount of the sun are at temperatures higher than components completely internal to the CubeSat. The internal component temperatures that are

closer to the surfaces that face the sun, are at a higher temperature then the components on the other side of the CubeSat as expected.

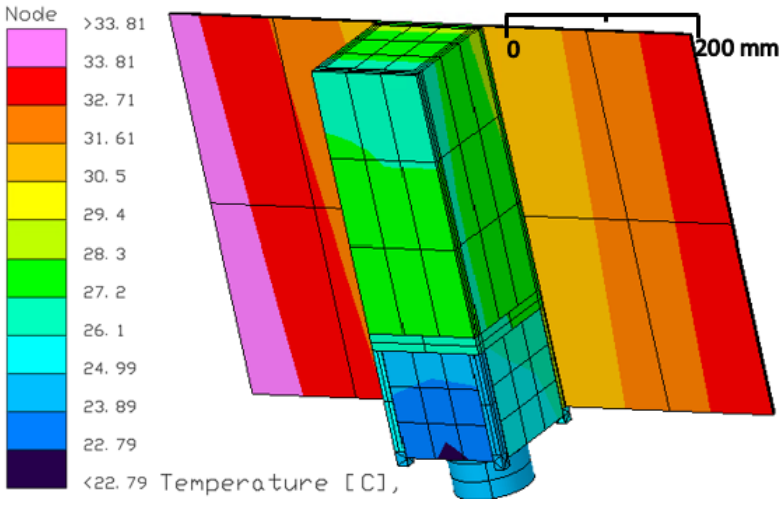

Figure 4.23: Steady State Results for 3U+ system

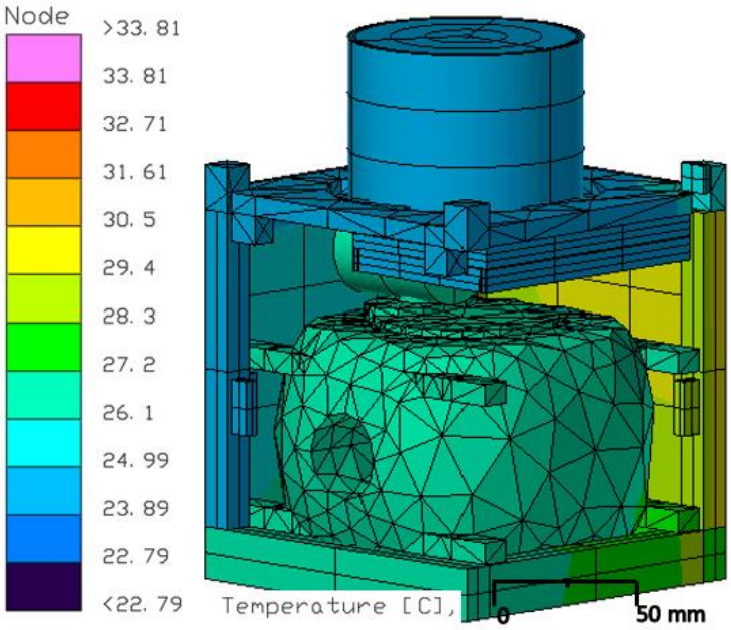

Figure 4.24: Steady State results for the Propulsion Module with Side Panels removed

4.3.3 Transient Results

To characterize the response over the simulated time steps, a transient state simulation was executed. The temperature at every time step was calculated and stored to allow for closure of the thermal budget for critical subsystems. The critical subsystems for operation of the Propulsion Module include the RF PCB, PIB, as well as Battery, ADCS, and CPCL Radio. The operational temperatures were maintained as the change in temperature cyclically changed over the course of the orbit. There was no need for active thermal control, and passive control was the primary means of accomplishing the thermal control.

Table 4.11: Component Operational Temperature ranges

Component Name	Operational Temperature (°C)	Analysis Temperature Range (°C)
RF PCB	-40 - +100	+11 - +40
PIB	-20 - +80	+11 - + 41
Battery	+10 - +45	+11 - + 41
ADCS	-20 - +50	+11 - + 41
CPCL Radio	-20 - +50	+11 - +41

The transient temperatures for the critical components are shown in Figure 4.25. The average temperature of all nodes for each component was averaged to produce a single representative trendline. Raw data for all transient cases can be found in Appendix H. Overviews of the Propulsion Module temperature as well as 2U temperature can be seen in Figure 4.27 through Figure 4.32

The transient heat results make sense as the trend is cyclical, and in LEO the CubeSat should be entering and exiting eclipse once per orbit. In eclipse the environment should be much cooler, so the drop seen every orbit as the spacecraft is in eclipse makes sense. The internal component temperatures follow the same external heating environment trends, as in the simulation insulation material was not applied between the CubeSat structure and each individual component.

The simulated temperature ranges of the battery, radio, as well as ADCS system highlighted in Table 4.11 are within a few degrees of the operational temperature ranges. Temperatures for these components should be higher in the simulation as compared to the physical environment, as the current mechanical layout of the 2U is unknown and increased amounts of aluminum are simulated. Aluminum conducts heat at a faster rate then plastic, silicon, and other materials that should be apart of the 2U mechanical layout. Therefore, the simulation overcompensates for the conduction between components, and creates an environment that is warmer.

The simulation presented should be iterated upon, after an advanced understanding of the mechanical layout and components within the 2U is established. The seconds version of the thermal testing should maintain critical components within 15 degrees of the coldest allowable temperature and 10 degrees within the warmest allowable temperature. The simulation and physical testing of the CubeSat do not have to be identical, simplifications made to the geometry and components will vary the heating environment as compared to the actual CubeSat, but the temperature ranges can still be acceptable for showcasing that the CubeSat could survive the thermal environment. However, if it is determined that the system cannot maintain temperature limits after the second version is developed then, investigation into different passive and active thermal mitigation techniques should be explored.

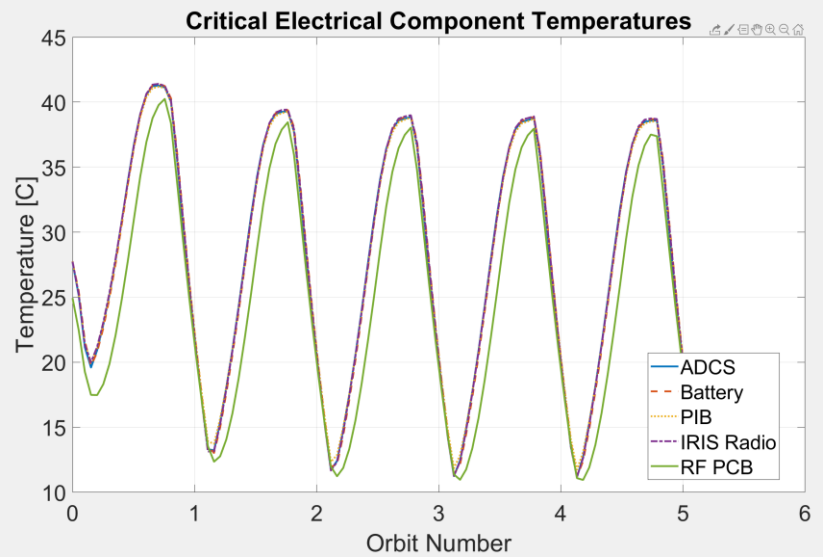

Figure 4.25: Transient Temperature results for critical components

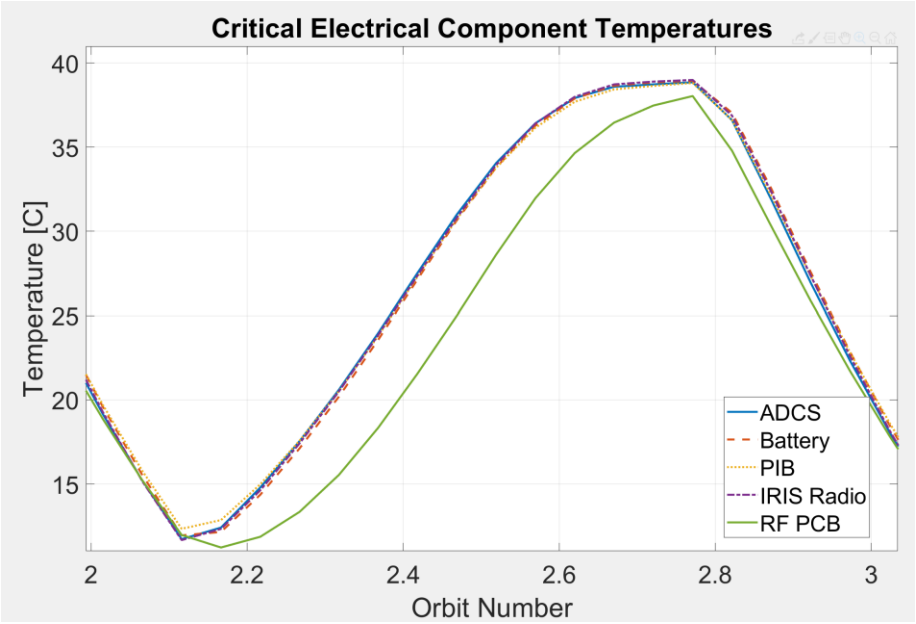

Figure 4.26: Transient temperature results for critical components zoomed in on orbit 2 - 3

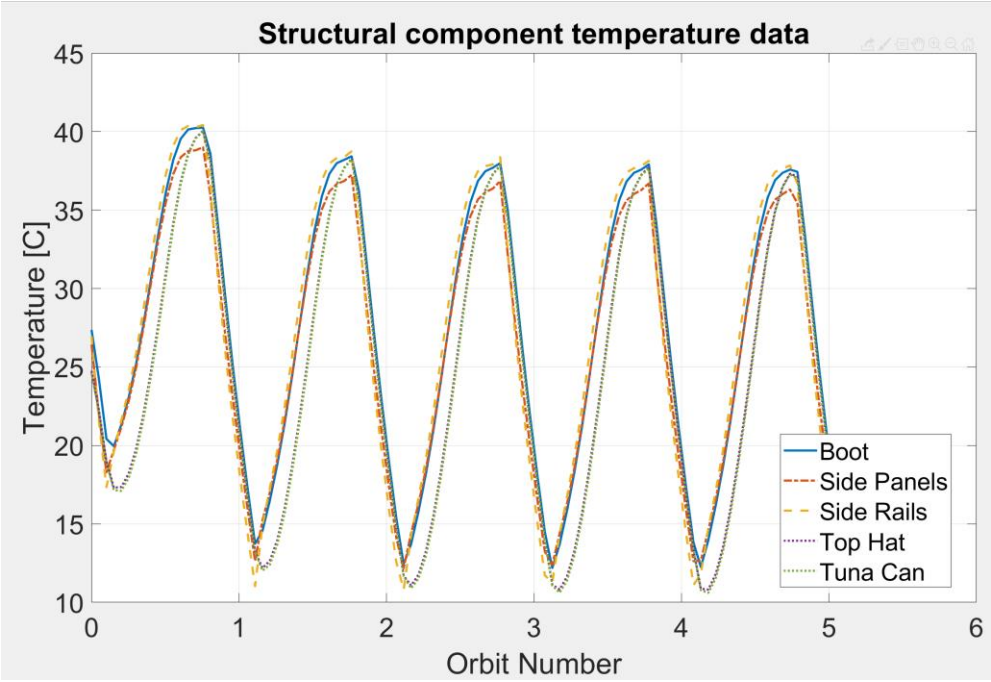

Figure 4.27: Propulsion Module structural component transient data

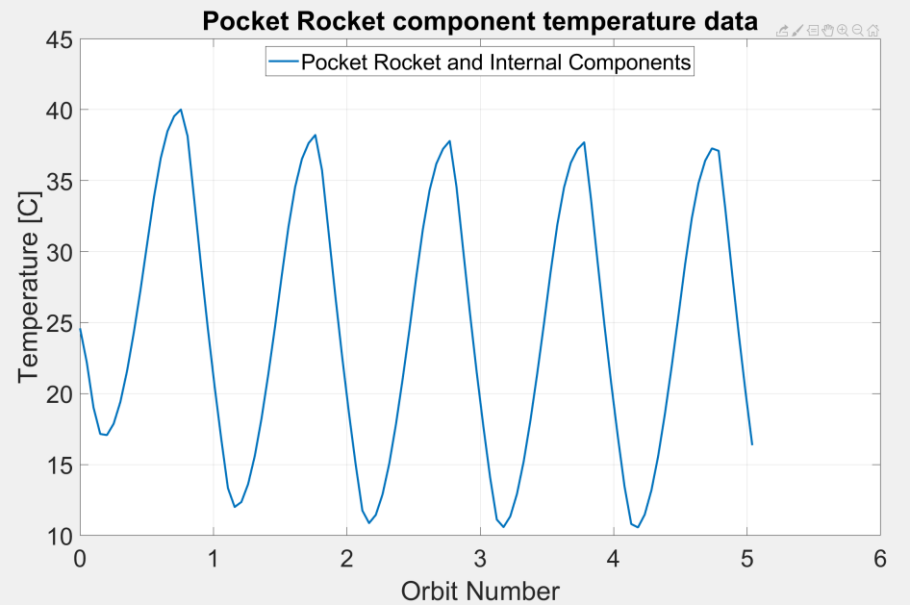

Figure 4.28: Propulsion Module transient temperature data for Pocket Rocket and internal components

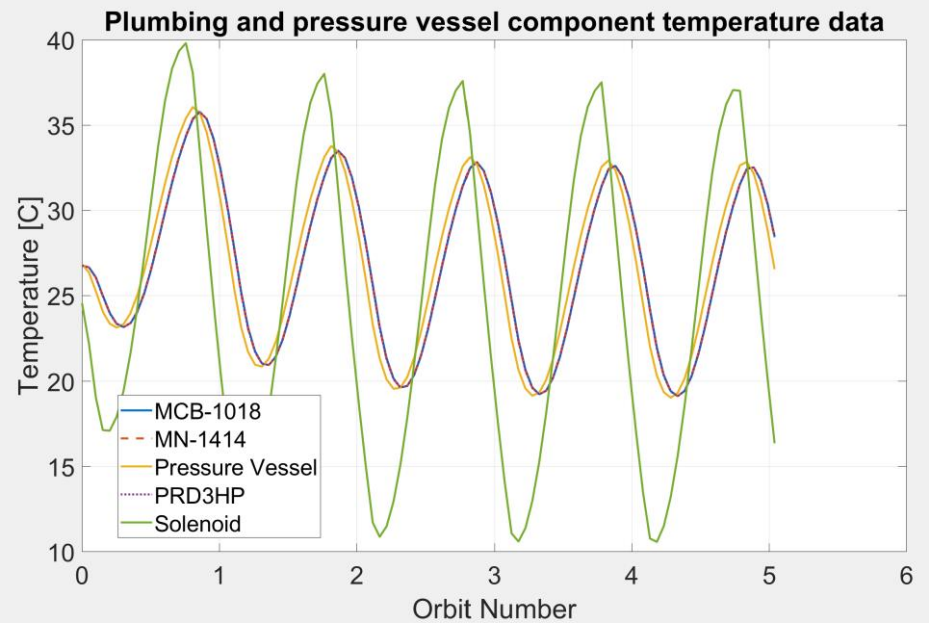

Figure 4.29: Propulsion Module plumbing system component transient data

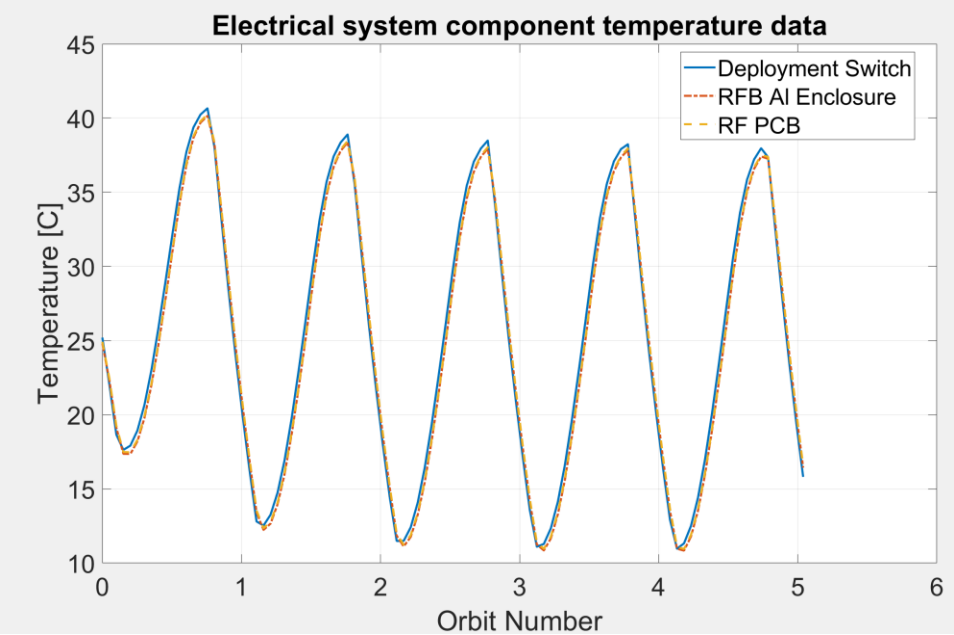

Figure 4.30: Propulsion Module electrical system component transient data

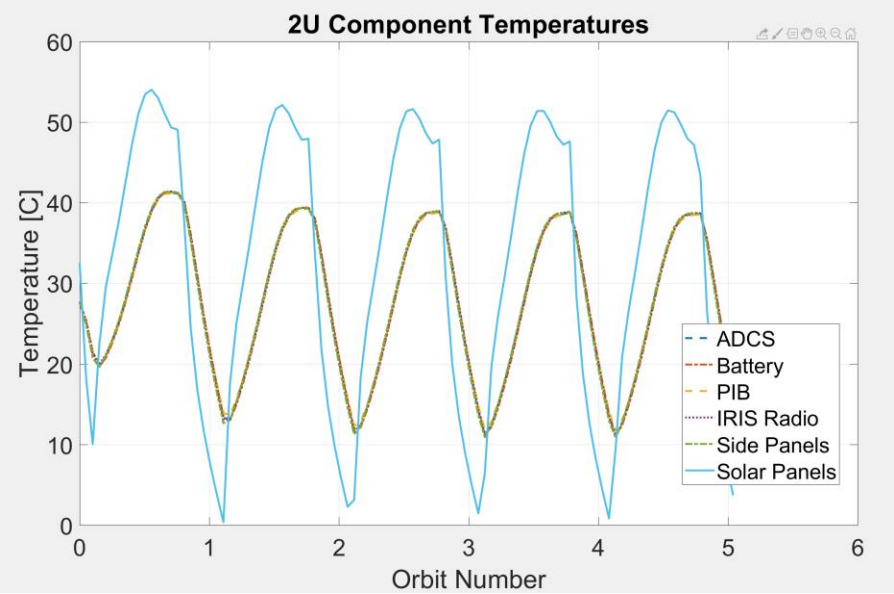

Figure 4.31: 2U CubeSat transient temperature data

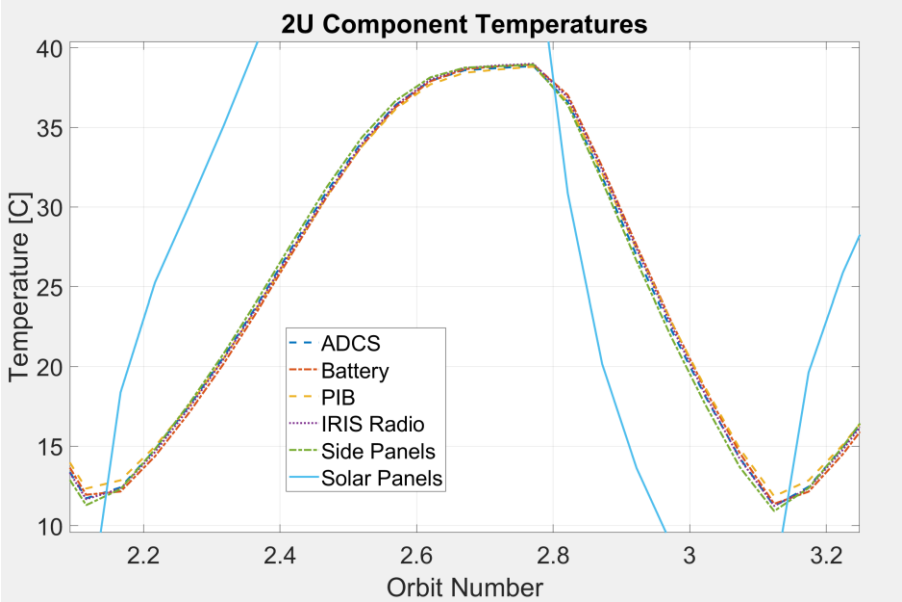

Figure 4.32: 2U CubeSat transient temperature data zoomed in on Orbit 2-3

4.4 Cost Analysis

Estimates for the overall cost were created to gauge the resources necessary to accomplish the manufacture, testing, and integration of the Propulsion Module. The driving cost factors for the development of the propulsion system are the pressure vessel manufacture and subsequent required testing. The pressure vessel including the structure and supports systems requires about 2 kg of 316L stainless steel powder, which can cost around $600 dollars. Utilizing the 3D printer at Cal Poly for the time needed to print the pressure vessel, including student time can cost upwards of $150 dollars, bringing the total cost of the pressure vessel to $730.

Welding of the pressure vessel can also be expensive, with EB welding costing $3,100 dollars per weld joint, or TIG welding that could be accomplished at CPCL. After manufacture, the pressure vessel must undergo multiple safety tests such as proof of pressure acceptance, random vibration, cycle, and burst testing as shown in Figure 2.2. These tests can further drive up the price of the Propulsion Module by $5,000+. The testing required for qualification of the pressure vessel would necessitate a minimum of two pressure vessels to be printed, as one of the structures would need to be tested to failure. The overall estimated cost with most of the labor accomplished through CPCL members, is expected to be about $17,500 for two Propulsion

Modules. The cost breakdown is detailed in Table 4.12. The cost could further increase depending on the range safety requirements around requiring additional testing for the system before enabling the system to launch as a secondary payload. Managing the cost of the pressure vessel will be the most difficult aspect of the design due to the testing needed to qualify new pressure vessels. An alternative approach would be to explore options for industry partnerships to either develop a commercial pressure vessel alternative that can fit within the confines of the Propulsion Module or explore a testing plan that would accomplish proof of pressure acceptance, random vibration, cycle and burst testing for the pressure vessel at Cal Poly.

Table 4.12: Cost Analysis Breakdown

Part Name	Manufacturer	Quantity	Price/unit	Total Cost
MCB-1018	Busek Engineering	1	$4.90	$4.90
MCBL-1018	Busek Engineering	1	$10.20	$10.20
MN-1414	Busek Engineering	1	$5.30	$5.30
MTT-1018 (Plastic Tubing 100 ft)	Busek Engineering	1	$2.00	$2.00
PRD3HP	Busek Engineering	1	$190.00	$190.00
Pocket Rocket	CPCL	1	$20.00	$20.00
Mini Service Valve	Cobham	1	$150.00	$150.00
LHDA - Solenoid Valve Assy	Lee Co	1	$100.00	$100.00
RF PCB (Include Components)	CPCL/Digikey	1	$200.00	$200.00
SMA-F Connector	Digikey	1	$5.43	$5.43
Single Conductor Cabling (3 ft)	Digikey	3	$0.67	$2.01
Ribbon Cabling (1 ft)	Digikey	1	$94.39	$94.39
Deployment Switch	CPCL	1	$15.00	$15.00
Coaxial Cabling (1 ft)	Digikey	1	$79.77	$79.77
Pressure Vessel Printing Material (Assumption of $3.58 /cm3 * Volume)	CPCL	2	$730.00	$1,460.00
Welding of Pressure Vessel	EB Industries	2	$3,090.00	$6,180.00
Stock Aluminum 7075-T6 for machining of most parts?	Online Metals	1	$750.00	$750.00
Assorted Screws	McMaster	1	$100.00	$100.00
Labor				
Student Time (5 Students, 3% benefit and 35 % overhead)	CPCL	160	$83.43	$13,348.80
Engineer (59% benefits 50/hr and 35 % overhead)	CPCL	80	$107.33	$8,586.00
External Site Testing Related Fees	CPCL & Launch Providers	1	$5,000.00	$5,000.00
Total Costs			**$36,303.80**	
Total Costs + 20 % Margin			**$43,564.56**	

4.5 Orbital Regulatory Concerns

One consideration that was not incorporated into the mission design of the 3U+ CubeSat is regulatory concerns related to operation in an orbit nearby the ISS. The current ConOps dictates that the Propulsion Module will fire once an orbit every orbit, which will compensate for drag incurred in that timeframe and increase the orbital altitude of the 3U+ CubeSat over the course of the thruster demonstration mission. The orbital altitude increase is dictated by two separate factors, the pointing budget, and the ConOps of the CubeSat. The ConOps dictates firing once an orbit outside of eclipse if enough energy storage is accomplished until the Propulsion Module has used all propellant stored. The operation schedule in combination with the current pointing budget of ± 43 degree could increase the orbital altitude 40 – 70 km. The variance in altitude increase is dictated by the amount of delta-V imparted in the velocity vector direction and assumes a Hohmann transfer that ignores orbital plane changes. An increase in 40 – 70 km from an ISS deployed orbit assumed for this research, could have the orbit of the 3U+ CubeSat intersecting with the ISS. Therefore, if this is determined to be a regulatory issue, the ConOps, deployment orbit, or pointing budget could be changed to reflect regulatory guidelines.

Chapter 5

CONCLUSIONS, FUTURE WORK AND LESSONS LEARNED

5.1 Conclusion

The research presented the design and analytical verification of a 1U+ Propulsion Module that utilizes the Pocket Rocket thruster. Previous iterations of the Propulsion Module design were analyzed, and mission objectives were established and developed into three main mission level requirements.

- The Propulsion Module system shall demonstrate 20 ± 3 m/s of delta-V for a CubeSat propulsion system aligned with the velocity vector
- Pocket Rocket TRL shall increase from 5 to 9
- Cal Poly CubeSat Laboratory shall operate the 3U+ CubeSat

A target deployment from the ISS, as well mission ConOps was defined to show how the Propulsion Module would fulfill the derived requirements and accomplish the mission objectives of the technology demonstration mission. System power, pointing, and mass budgets were created that aligned with the system ConOps, and further guided the detailed design of the Propulsion Module. Xenon was chosen as the propellant for this mission through a trade study, and targets for a system pressure of 20.68 MPa (3000 PSI), as well as a storage volume of 220 cm^3 were establsihed. The pressure vessel was designed, for a MEOP of 20.68 MPa (3000 PSI), with a safety factor greater than 1.5, to comply with AFSCMAN91-710, and enable launch as a secondary payload on US based rocket launches. The design of the plumbing system was established to control the flow of propellant and regulate the inlet pressure for Pocket Rocket from 20.68 MPa (3000 PSI) to between 0.26 – 0.62 kPa (0.03 – 0.09 PSI). The electrical systems were designed to interface with the 2U spacecraft and accommodate the RF generation and amplification necessary for Pocket Rocket operation. Mechanical and electrical interfaces were defined between Propulsion Module components as well as the 2U spacecraft to enable operation of the Pocket Rocket thruster, and fulfillment of derived requirements. The changes

made to the Propulsion Module design in this research demonstrate that the system can achieve 20 ± 3 m/s of delta-V for use in drag compensation or orbital maneuvers.

Afterwards analytical verification of the pressure vessel safety factor was accomplished. A static structural simulation was created to ensure that pressure vessel design maintained a minimum safety factor of 1.5 throughout the structure. A random vibration simulation was developed to ensure that the components internal to the Propulsion Module would not deform more than 0.05 mm and ensure that the system would survive the launch environment, without compromising operational capabilities. Critical electrical components temperature ranges were established, and a thermal environment simulation of the ISS based 402 km, 51° inclination orbit was performed. Operational temperatures for critical electrical components were shown to be maintained throughout the operation of the Propulsion Module, utilizing steady state and transient analysis. Finally, a rough project budget was created, that defined the aspects that drive the cost of the project to around $17,500.

With the increase in demand of CubeSat mission capabilities, and demand for micro-propulsive technologies as one solution, the need for experience with development of CubeSat propulsion technologies could increase. Therefore, with the development of a Propulsion Module design, CPCL can increase the TRL level of Pocket Rocket, as well as demonstrate the capability to operate, manufacture, test and integrate a CubeSat propulsion system. Introduction of a flight capable CubeSat Propulsion Module could further the hands-on experiences of students, faculty, and professors as well as enable educational outreach for the CPCL

5.2 Future Work

There are several key aspects that would benefit from further analysis to support the assumptions made in this research. The development of the 2U CubeSat design is of critical importance for the further advancement of the Propulsion Module Design. Clear definition in the design of the 2U CubeSat should allow for iteration on system budgets. The pointing budget could be improved with enhanced knowledge of the moment of inertia matrix, as well as center of

mass of the 3U+ system. A detailed design of the ADCS components could be established to ensure that the 3U+ system is still able to maintain pointing necessary for mission success. Additionally, enhanced knowledge of the 2U CubeSat power draw would allow for a more concrete understanding of the system power draw during all phases of the CubeSats operation. Internal component selections established by further 2U development could ensure enhanced definition of electrical and mechanical interfaces between the 2U and Propulsion Module. Finally, simulations that provide analytical verification would have to be updated to account for enhanced design definition from the 2U system. Random vibrational, as well as thermal simulations would need to be updated with relevant information to ensure that the simulation still accurately represents the spacecraft operational environment.

Development of the PIB, as well as RF PCB must also be explored in the future. The RF PCB, component layout must be established and finalized to allow for iteration on routing instructions developed for the Propulsion Module. Calibration of the RF PCB for operation with xenon must be accomplished, as well as characterization of electrical efficiency once board design is finalized. Before, the Propulsion Module is flight capable, characterization of RF leak within the CubeSat must be accomplished via acoustic testing of a flight model. The acoustic testing allows for determination of RF shielding within the system, and assurance that the flight configuration will not interfere with another spacecraft or RF frequency as per the World Radiocommunication Conference.

Exploration of alternate manufacturing techniques for the Pressure vessel design should be beneficial to the overall development of the Propulsion Module. Development of a new pressure vessel can cost upwards of $7,000. Therefore, exploring aluminum casting or traditional manufacturing practices for the manufacture of the pressure vessel could reduce the overall cost needed, as well as the weight of the system.

Regulatory concerns regarding operation in a near ISS orbit should be investigated further. Operational changes to the 3U+ CubeSat should be accomplished if it is determined that the current ConOps and/or pointing budget would interfere with the ISS operational orbit. The ConOps could be changed by varying the operation schedule of Pocket Rocket to maintain an

orbital altitude range that would ensure no interference with the ISS. Further, the pointing budget could also be refined to ensure that with an updated ConOps, the CubeSat would remain within a dictated orbital altitude range.

Finally, exploration into the necessity of incorporating a GPS receiver for increased accuracy Iin delta-V measurements should be accomplished. If NORAD data is deemed insufficient for mission timeline, a GPS receiver integrated into the 2U spacecraft or Propulsion Module could provide increased accuracy at shorter time intervals then relying on the NORAD tracking data.

5.3 Lessons Learned

During this research, several key lessons were learned, and improvements implemented.

- **Importance of Accurate Boundary Conditions**

  Creation of multiple structural simulations was accomplished via the use of Ansys software. Boundary conditions played a critical role in ensuring the accuracy of the simulation and not over constraining the analysis. Overuse of boundary conditions can lead to generation of infinite stiffness areas that in turn do not reflect the true mechanical behavior of the system. Therefore, it is critical to understand which fixtures, and mechanical interfaces are critical to an accurate representation of the structural response. The use of remote boundary conditions that allow for restriction of translation as well as rotation in the X, Y, and Z axis, is key to representing a vibrational fixture for a CubeSat or mechanical interfaces between two parts. Overuse of fixed supports, that restrict translation as well as rotation in all axis, can lead to inaccurate results that do not reflect the overall mechanical behavior of the system. Accurate usage and understanding of what each support does is key to creating a simulation that is accurate to the actual configuration, as well as valid to the mechanical response.

- **Thermal Desktop Computational Speed**

  When a thermal desktop model is created, in some circumstances' filets, chamfers and some bolt holes can be removed to reduce the computation power needed to run the

simulation within AutoCad. To ensure accurate representation of heat transfer pathways, steady state analysis should be accomplished before and after major geometry simplifications. However, implementation of complex geometry is sometimes necessary and can cause increases in run time, especially when working remote. The easiest way to solve this issue is to simplify your model via built in AutoCad shapes. The accuracy of the model simplification can then be determined by simulating the steady state temperatures before and after to see if there are major changes to the temperatures. This enables simplifications to occur that can speed up the run time of transient analysis and maintain accurate heat transfer pathways. When complex geometry unable to be simplified with normal AutoCad shapes are required, TD Mesh is a powerful tool that can create the necessary shape from a STEP file. TD mesh generates thousands of nodes and should be used sparingly when computational resources are limited.

In addition to computational speed improvements due to geometry simplification, improvements with the speed of nodal calculations can be investigated. CSGmin is a factor that characterizes the sum of conductors within the thermal desktop simulation. A model with a small and/or large conductor will slow down transient analysis simulations. Each time step of transient analysis is dictated by 1000 times the smallest CSGmin value nominally. Therefore, if transient analysis is running slowly, you can improve the speed of the simulation significantly by changing the calculation method for nodes with a smaller CSGmin. Instead of the default nodal calculation, selection of an arithmetic calculation will increase computational speed.

BIBLIOGRAPHY

[1] How New Business Models Will Disrupt Old Space Industry. https://noosphereventures.com/how-new-business-models-will-disrupt-old-space-industry/. Accessed Apr. 4, 2020.

[2] Sputnik. https://history.nasa.gov/sputnik/. Accessed Apr. 4, 2020.

[3] How Satellites Work. *HowStuffWorks*. https://science.howstuffworks.com/satellite.htm.Accessed Nov. 14, 2019.

[4] SSL. SSL 1300 Spacecraft Bus for RSDO Applications. *https://rsdo.gsfc.nasa.gov/images/201608/Rapid-III-NNG16VW08B-Spacecraft-Data-Package-SSL.pdf*. https://rsdo.gsfc.nasa.gov/images/201608/Rapid-III-NNG16VW08B-Spacecraft-Data-Package-SSL.pdf. Accessed Nov. 14, 2019.

[5] Community, 65 Authors from the Astronautics. *Space Mission Engineering: The New SMAD*. Microcosm Press, Hawthorne, CA, 2011.

[6] Mabrouk, E. What are SmallSats and CubeSats? *NASA*. http://www.nasa.gov/content/what-are-smallsats-and-cubesats. Accessed Nov. 5, 2019.

[7] Mehrparvar, A. *CubeSat Design Specification, Revision 13*. The CubeSat Program, California Polytechnic State University: San Luis Obispo, 2014.

[8] Esionwu, C. C. “CubeSat Market Analysis and Cost Breakdown.”

[9] MarCO. *NASA Solar System Exploration*. https://solarsystem.nasa.gov/missions/mars-cube-one/in-depth. Accessed Nov. 21, 2019.

[10] Poghosyan, A., and Golkar, A. “CubeSat Evolution: Analyzing CubeSat Capabilities for Conducting Science Missions.” *Progress in Aerospace Sciences*, Vol. 88, 2017, pp. 59–83. https://doi.org/10.1016/j.paerosci.2016.11.002.

[11] Bouwmeester, J., and Guo, J. “Survey of Worldwide Pico- and Nanosatellite Missions, Distributions and Subsystem Technology.” *Acta Astronautica*, Vol. 67, No. 7, 2010, pp. 854–862. https://doi.org/10.1016/j.actaastro.2010.06.004.

[12] Krejci, D., and Lozano, P. “Space Propulsion Technology for Small Spacecraft.” *Proceedings of the IEEE*, Vol. 106, No. 3, 2018, pp. 362–378. https://doi.org/10.1109/JPROC.2017.2778747.

[13] Ideas Lab: Cross-Cutting Initiative in CubeSat Innovations (Nsf19530) | NSF - National Science Foundation. https://www.nsf.gov/pubs/2019/nsf19530/nsf19530.htm. Accessed Nov. 14, 2019.

[14] Hall, L. Pathfinder Technology Demonstrator. *NASA*. http://www.nasa.gov/directorates/spacetech/small_spacecraft/ptd.html. Accessed Nov. 14, 2019.

[15] HQ, T. T. : N. Cubesat Proximity Operations Demonstration (CPOD). *NASA*. http://www.nasa.gov/directorates/spacetech/small_spacecraft/cpod_project.html. Accessed Nov. 14, 2019.

[16] NSPIRES - Solicitations Summary. https://nspires.nasaprs.com/external/solicitations/summary!init.do?solId={A2654B9F-4E54-79D5-ED0A-8144DE40D4F3}&path=open. Accessed Nov. 14, 2019.

[17] Tummala, A. R., and Dutta, A. “An Overview of Cube-Satellite Propulsion Technologies and Trends.” *Aerospace*, Vol. 4, No. 4, 2017, p. 58. https://doi.org/10.3390/aerospace4040058.

[18] Sutton, G. P., and Biblarz, O. Rocket Propulsion Elements Seventh Edition. 2007.

[19] In-Space Rocket Engines | Aerojet Rocketdyne. https://www.rocket.com/space/space-power-propulsion/monopropellant-rocket-engines. Accessed Nov. 14, 2019.

[20] Polk, J. “Demonstration of the NSTAR Ion Propulsion System on the Deep Space One Mission.” p. 25.

[21] National Research Council. *A Review of United States Air Force and Department Of Defense Aerospace Propulsion Needs*. 2006.

[22] Air Force Space Command. RANGE SAFETY USER REQUIREMENTS MANUAL VOLUME

3 – LAUNCH VEHICLES, PAYLOADS, AND GROUND SUPPORT SYSTEMS REQUIREMENTS. https://static.e-publishing.af.mil/production/1/afspc/publication/afspcman91-710v3/afspcman91-710v3.pdf.
[23] Lemmer, K. “Propulsion for CubeSats.” *Acta Astronautica*, Vol. 134, 2017, pp. 231–243. https://doi.org/10.1016/j.actaastro.2017.01.048.
[24] Mueller, J., Hofer, R., Parker, M., and Ziemer, J. “SURVEY OF PROPULSION OPTIONS FOR CUBESATS.” p. 56.
[25] Bonin, G. R., Roth, N., Armitage, S., Newman, J., Risi, B., and Zee, R. E. CanX–4 and CanX–5 Precision Formation Flight: Mission Accomplished! 2015.
[26] Mauthe, S., Pranajaya, F. M., and Zee, R. E. The Design and Test of a Compact Propulsion System for CanX Nanosatellite Formation Flying. 2005.
[27] Kolbeck, J., Lukas, J., Teel, G., Keidar, M., Hanlon, E., Pittman, J., Lange, M., and Kang, J. “MCAT Micro-Propulsion Solution for Autonomous Mobile On-Orbit Diagnostic System.” p. 6.
[28] Williams, D. D. Propulsion Solutions for CubeSats and Applications. Logan, Utah, Aug 12, 2012.
[29] Gnagy, S. L., Henken, A., and Greig Amelia. CubeSat Electrothermal Plasma Micro-Thruster: System Development and Integration. 2018.
[30] Wu, S.-F., Chen, W., and Chao, C. The STU-2 CubeSat Mission and In-Orbit Test Results. 2016.
[31] ELFIN - EoPortal Directory - Satellite Missions. https://directory.eoportal.org/web/eoportal/satellite-missions/e/elfin. Accessed Jun. 8, 2020.
[32] Wright, W. P., and Ferrer, P. “Electric Micropropulsion Systems.” *Progress in Aerospace Sciences*, Vol. 74, 2015, pp. 48–61. https://doi.org/10.1016/j.paerosci.2014.10.003.
[33] Hejmanowski, N. J., Woodruff, C. A., Burton, R. L., Carrol, D. L., and Cardin, J. M. CubeSat High Impulse Propulsion System (CHIPS). Presented at the 62nd JANNAF Propulsion Meeting (7th Spacecraft Propulsion), Nashcille, TN, 2015.
[34] Davis, S., Fite, N., Mosleh, E., and Malphrus, B. “3D Printing and MEMS Propulsion for the RAMPART 2U CUBESAT.”
[35] Carroll, D. L., Cardin, J. M., Burton, R. L., Benavides, G. F., Hejmanowski, N., Woodruff, C., Bassett, K., King, D., Laystrom-Woodard, J., Richardson, L., Day, C., Hageman, K., and Bhandari, R. “PROPULSION UNIT FOR CUBESATS (PUC).” p. 18.
[36] Nanosatellite & CubeSat Database | Nanosats Database. https://www.nanosats.eu/database. Accessed Nov. 17, 2019.
[37] Van Ness, P., Ramirez, G., Gnagy, S., Diamantopoulous, S., and Greig, A. Pressurized 1U CubeSat Propulsion Unit.
[38] “NASA Strategic Plan 2018.” p. 64.
[39] Jackson, S. NASA’s CubeSat Launch Initiative. *NASA*. https://www.nasa.gov/directorates/heo/home/CubeSats_initiative. Accessed Oct. 12, 2019.
[40] Past Launches. *CubeSat*. http://www.cubesat.org/past-launches. Accessed Nov. 17, 2019.
[41] Burton, R., Eden, G., Park, S.-J., Yoon, J. K., Chadenedes, M., Garrett, S., Raja, L. Sitaraman, H., Woodard, J., Benavides, G., and Carrol, D. Initial Development of the Microcavity Discharge Thruster. Presented at the 31st International Electric Propulsion Conference, University of Michigan - Ann Arbor, Michigan, 2009.
[42] Chadenedes, M. L. D. “PROPULSION PERFORMANCE OF A MICROCAVITY DISCHARGE DEVICE.” p. 80.
[43] CU Aerospace. Propulsion System Performance Matrices | CU Aerospace | Small-Satellite Propulsion Unit for CubeSats (PUC). https://www.cuaerospace.com/Portals/2/SiteContent/pdfs/datasheets/CUA-Propulsion-Systems-v21.pdf. Accessed Nov. 20, 2019.
[44] ChEMS, V. “VACCO Micro Propulsion Systems.” p. 16.
[45] Micci, M. M., Bilén, S. G., and Clemens, D. E. History and Current Status of the Microwave

Electrothermal Thruster. Presented at the Progress in Propulsion Physics, Brussels, Belgium, 2009.
[46] Abaimov, M., Sinha, S., Bilén, S., and Micci, M. CubeSat Microwave Electrothermal Thruster (CμMET). 2013.
[47] Gallucci, S., Micci, M., and Bilén, S. Design of a Water-Propellant 17.8-GHz Microwave Electrothermal Thruster. Presented at the 35th International Electric Propulsion Conference, 2017.
[48] Hopkins, J., Micci, M., and Bilén, S. Design and Testing of Low Power Radio-Frequency Electrothermal Thruster. Presented at the 31st International Electric Propulsion Conference, 2009.
[49] Greig, A. *Pocket Rocket: An Electrothermal Plasma Micro-Thruster*. 2015.
[50] Greig, A., Charles, C., and Boswell, R. "Spatiotemporal Study of Gas Heating Mechanisms in a Radio-Frequency Electrothermal Plasma Micro-Thruster." *Frontiers in Physics*, Vol. 3, 2015. https://doi.org/10.3389/fphy.2015.00084.
[51] White, J., Holemans, W., and Huang, D. A. "Make Your Cubesat Overnight and Put It in Any Orbit (Well… Almost)." p. 30.
[52] Rutledge, T., Micci, M., and Bilén, S. Design and Initial Tests of a Low Power Radio-Frequency Electrothermal Thruster. Presented at the 44th AIAA/ASME/SAE/ASEE Joint Propulsion Conference & Exhibit, Hartford, CT, 2008.
[53] Reyes, B. *Thermal Control Handbook*.
[54] Claricoats, J., and Dakka, S. M. "Design of Power, Propulsion, and Thermal Sub-Systems for a 3U CubeSat Measuring Earth's Radiation Imbalance." *Aerospace*, Vol. 5, No. 2, 2018, p. 63. https://doi.org/10.3390/aerospace5020063.
[55] State of the Art of Small Spacecraft Technology 2018. https://sst-soa.arc.nasa.gov/. Accessed Sep. 29, 2019.
[56] Corpino, S., Caldera, M., Nichele, F., Masoero, M., and Viola, N. "Thermal Design and Analysis of a Nanosatellite in Low Earth Orbit." *Acta Astronautica*, Vol. 115, 2015, pp. 247–261. https://doi.org/10.1016/j.actaastro.2015.05.012.
[57] Reiss, P., Hager, P., Macdonald, M., and Lucking, C. "NEW METHODOLOGIES FOR THE THERMAL MODELLING OF CUBESATS." p. 12.
[58] "CubeSat 101: Basic Concepts and Processes for First-Time CubeSat Developers." p. 96.
[59] GSFC-STD-7000 | NASA Technical Standards System (NTSS). *General Environmental Verification Standard*. https://standards.nasa.gov/standard/gsfc/gsfc-std-7000. Accessed Mar. 17, 2020.
[60] Drewry, S. Miniaturized Plasma Microthruster RF Amplifier. Cal Poly: College of Engineering, Sep, 2019.
[61] Blue Canyon Technologies. https://bluecanyontech.com/components. Accessed Apr. 17, 2020.
[62] Hegel, D. "FlexCore: Low-Cost Attitude Determination and Control Enabling High-Performance Small Spacecraft." *Small Satellite Conference*, 2016.
[63] NASA. Iris V2.1 CubeSat Deep Space Transponder. *www.jpl.nasa.gov*. https://www.jpl.nasa.gov/cubesat/pdf/Brochure_IrisV2.1_201611-URS_Approved_CL16-5469.pdf. Accessed Apr. 22, 2020.
[64] Charles, C., Boswell, R. W., Bish, A., Khayms, V., and Scholz, E. F. "Direct Measurement of Axial Momentum Imparted by an Electrothermal Radiofrequency Plasma Micro-Thruster." *Frontiers in Physics*, Vol. 4, 2016. https://doi.org/10.3389/fphy.2016.00019.
[65] Charles, C., and Boswell, R. W. "Measurement and Modelling of a Radiofrequency Micro-Thruster." *Plasma Sources Science and Technology*, Vol. 21, No. 2, 2012, p. 022002. https://doi.org/10.1088/0963-0252/21/2/022002.
[66] PRD3HP. *Beswick Engineering*. https://www.beswick.com/catalog/product-detail/PRD3HP?grandparentName=Regulators&grandparentSlug=regulators. Accessed Apr. 25, 2020.
[67] Face Mount. *The Lee Company*. https://www.theleeco.com/products/electro-fluidic-systems/solenoid-valves/control-valves/lhd-series/2-port/face-mount/. Accessed Apr. 25, 2020.
[68] Cobham Plc, Space Propulsion Systems, Service Valves.

https://www.cobham.com/mission-systems/space-propulsion-systems/service-valves/. Accessed Apr. 25, 2020.

[69] Carpenter Additive. Technical Data Sheet CT 316L E Powder. *CarpenterAdditive*.https://cdn2.hubspot.net/hubfs/6205315/carpenter_additive/image/Resources/Datasheets/CT%20PowderRange%20316L%20E.pdf. Accessed May 3, 2020.
[70] AK Steel 316L Austenitic Stainless Steel. http://www.matweb.com/search/DataSheet.aspx?MatGUID=9e9ab696974044cab4a7fd83687934eb. Accessed May 3, 2020.
[71] Bednar, H. *Pressure Vessel Design Handbook*. Krieger Pub Co, Malabar, Fla, 1991.
[72] Wright, M. “Flight Systems Integration & Test.” p. 81.
[73] Aluminum 7075-T6; 7075-T651. http://www.matweb.com/search/DataSheet.aspx?MatGUID=4f19a42be94546b686bbf43f79c51b7d&ckck=1. Accessed May 4, 2020.
[74] Beryllium Copper, UNS C17000. http://www.matweb.com/search/DataSheet.aspx?MatGUID=9b159fd901454263b8a90c22a66f1988. Accessed May 4, 2020.
[75] Material Properties of Thermoset Glass Epoxy - G-10, FR4 and G-11. Dielectric Manufacturing.
[76] Macor| Macor Grinding | Ceramic Macor | Macor Properties. http://www.ferroceramic.com/macor_table.htm. Accessed May 4, 2020.
[77] 304 Stainless Steel. http://www.matweb.com/search/DataSheet.aspx?MatGUID=abc4415b0f8b490387e3c922237098da. Accessed May 4, 2020.
[78] Rohsenow, W. M., and Hartnett, J. R. “HANDBOOK OF HEAT TRANSFER.” p. 12.
[79] Maleki, H., Al-Hallaj, S., Selman, J., Dinwiddie, R., and Wang, H. “Thermal Properties of Lithium-Ion Battery and Components.” *Journal of The Electrochemical Society*, Vol. 146, 1999, pp. 947–954. https://doi.org/10.1149/1.1391704.
[80] Thurber, Mattis, Liu, and Filliben. The Relationship Between Resistivity and Dopant Density for Phosphorus- and Boron-Doped Silicon.
[81] Silicon, Si. http://www.matweb.com/search/DataSheet.aspx?MatGUID=7d1b56e9e0c54ac5bb9cd433a0991e27. Accessed May 4, 2020.
[82] Kauder, L. “Spacecraft Thermal Control Coatings Reference.” *NASA/ Goddard Space Flight Center*, No. TP-2005-212792, 2005.

APPENDICES

A. Delta-V calculation assumptions

For delta-V calculations, the mass of the satellite was assumed to be a total of 5 kg. The area affected by drag for the satellite was assumed constant 0.03 m^2, which is equivalent to one side of the 3U CubeSat. The perturbations included were J2, atmospheric drag, solar radiation pressure, and n body effects of the sun and moon. Delta-V was assumed to be imparted instantaneously. The orbital TLE's utilized for calculations were of the IOD-1 GEMS deployed 7-08-2019, the orbital COE's are listed below in Table A.0.1.

Table A.0.1: Orbital COE's for ISS based orbit

Eccentricity	Semi-Major Axis (km)	Inclination (°)	Right Angle of Ascending Node (°)	Argument of Perigee (°)
0.0	6781.1 km	51.6	252.5	316.8

Drag compensation burns were assumed to occur after losing 10 km of altitude and impart a delta-V to return the CubeSat to the original unperturbed circular orbit. Drag would be able to be compensated 10 km at a time for a maximum of 6.9 times during the mission, imparting 3.4 m/s of delta-V each burn. The drag compensation burns utilized a Hohmann transfer that ignored plane changes, between the perturbed orbit after 10 km of altitude loss, and the initial non-perturbed orbital altitude

Rendezvous delta-V estimates were assumed to encompass constellation deployment as well as formation flight. Rendezvous calculations utilized the CW equations, which assumes the target is in a circular orbit, there are no external forces on the chaser spacecraft, and delta-V is impulsive. For the range of delta-V needed to accomplish constellation deployment as well as formation flight, an assumption that the chaser spacecraft was 2 – 6 km behind in the vbar direction was utilized. The relative speeds of each spacecraft were assumed to be equal.

A Hohmann transfer was utilized to create a range of delta-V values for orbital corrections and maneuvers. The Hohmann transfer assumes instantaneous impart of delta-V and each CubeSat is in a circular orbit. Plane changes were ignored to create a range of delta-V values.

The range incorporated, a transfer from an ISS 402 km orbit to a 506 km orbit, a 402 km orbit to a 450 km orbit, and a 450 km orbit to a 506 km orbit.

B. Propulsion Module RAS

The file for the RAS sheet for the Pocket Rocket Propulsion Module is called Pocket Rocket RAS Rev 1.8.xlsx. The sheet contains requirements, rationale, as well as verification methods for the Propulsion Module.

C. SWaP & System Budgets

The file for the SWaP as well as system budgets for the Pocket Rocket Propulsion Module is called Pocket Rocket SWaP and System Budgets.xlsx. The sheet contains the SWaP of the Propulsion module, cost budget, Power budget, and pointing budget calculations

D. Propulsion Module ICD

The file for the ICD for the Pocket Rocket Propulsion Module is called Pocket Rocket ICD Rev 1.3.xlsx. The sheet contains an overview of the system internal and external components, mechanical interfaces, thru hole spacing, 2U interface info, modes of operation and interactions as well as electrical and plumbing component information.

E. Propulsion Module Propellant Trade Study

The file for the trade study for the propellant choice of Pocket Rocket is called System Trade Studies.xlsx. The sheet contains a trade study with rationale reference data, as well as scoring criteria for the propellant choice trade study.

F. Propulsion Module Assembly Instructions

The file for the Propulsion Module Assembly Instructions is called Pocket Rocket 1U+ Assembly Guide.pptx. The file incorporates rough assembly instructions for all the components of the Propulsion Module.

G. Propulsion Module Routing Instructions

The File for the Propulsion Module Routing Instructions is called Propulsion Module 1U+ Routing Instructions.pptx. The file incorporates the electrical as well as plumbing routing instructions for the Propulsion Module.

H. Thermal Desktop Transient Simulation Raw Data

The file for the transient simulation raw data from Thermal Desktop is Transient Data for Thermal Simulation.xlsx. The raw data file has the temperature information for all the applicable nodes of the simulation